Using Machine Learning to Predict Facies Associations from Wireline Logs for the Carboniferous in the Southern North Sea

By

Deema Albeesh

in partial fulfilment of the requirements for the degree of

Master of Science
in Applied Earth Sciences

at the Delft University of Technology,
to be defended publicly on Thursday July 1, 2021 at 9:00 AM.

Supervisor:	Assist. Prof. Dr. H.A. Abels	TU Delft
Thesis committee:	Prof. Dr. A.W. Martinius,	TU Delft
	Assoc. Prof. Dr. A. Barnhoorn,	TU Delft
	T.F. Baars, MSc,	TU Delft
	E. Cecchetti, MSc.	TU Delft

An electronic version of this thesis is available at http://repository.tudelft.nl/.

Contents

Abstract

The use of wireline facies associations can alleviate core data shortage during facies prediction by providing a more extensive input dataset. Wintershall has assigned wireline facies associations directly on cored and un-cored wells in the Carboniferous of the Sothern North Sea. Conducting facies prediction using these wireline facies associations as an input can help with tapping into the remaining exploration and development potential of the area. However, the accuracy of this input must be evaluated using core data before machine learning algorithms are applied. This was quantified as 71% for 9 cored wells, where the background floodplain and braided channel facies had the highest accuracies of 88% and 81% respectively, and the mouth bars and marine shales facies could not be adequately validated due to their insufficient core sampling. Consequently, when using wireline facies associations for training facies prediction algorithms, this input's intrinsic uncertainty should be accounted for while examining the outputs, especially for facies that are not sufficiently validated by cores. Applying facies prediction with Support Vector Machine (SVM), Multilayer Perceptron Neural Network (MLP) and Recurrent Neural Network (RNN), showed that RNN can achieve the highest overall accuracy of 80.9%, due to the highest F1 scores for braided channel (0.88), point bars (0.60) and coal (0.53). The class imbalance problem is apparent for this dataset where the majority classes of background floodplain, braided channel, point bar and coal, are more predicted than the minority classes of crevasse splay sands, mouth bars, and marine shale. Applying RNN on the Westphalian A, B and C separately served as a form of imbalance correcting technique that increased the F1 scores of underrepresented facies. Future work can further refine the results by exploring imbalance correcting techniques through under-sampling the background floodplain and over-sampling the crevasse splay, mouth bar and marine shale facies.

Acknowledgements

I would like to thank my thesis advisor Dr. Hemmo Abels for providing me with vital guidance and feedback throughout this project to make it possible. I would also like to thank Dr. Allard Martinius for his invaluable input, and Dr. Auke Barnhoorn for his kind support. I am grateful to PhD candidates Timothy Baars and Emilio Cecchetti for their consistent and generous help and advice, which made the project smoother and more enjoyable. Finally, I would like to thank Wintershall for the opportunity to work with their data and their interest in the project.

1 Introduction

1.1 Literature Review

More than twenty significant gas discoveries have been made in the Carboniferous of the southern North Sea since 1984 [1]. The British Geological Survey (BGS) has determined that there still remains a wealth of untapped potential in the exploration of undrilled prospects and the development of existing discoveries [1]. Building a high integrity geomodel indicating the distribution of facies in the subsurface is an essential part of exploration and development.

It is typical for the availability of wireline logs to surpass that of rock cores for monetary reasons. Information derived from the limited lengths of cored intervals, such as lithofacies and facies associations, gives spatially restricted knowledge about the architecture of an entire field. As a result, efforts have been dedicated to developing methods for predicting lithofacies from wireline log measurements that extrapolate core observations to be supplemented into the geomodel. The limited availability of cores as input for facies prediction can hinder the effectiveness of the process or make it impossible. Wintershall has manually assigned wireline facies associations directly on wireline logs for a number of cored and un-cored wells in the Carboniferous of the Southern North Sea. This is accomplished by tying extensive knowledge of the Carboniferous basin with wireline log signatures. These wireline facies associations can potentially provide a more extensive input dataset for facies predictions compared to core data alone.

The oldest facies prediction method relies on applying cutoffs to a well log histogram, which usually generates results that conflict with core data [2]. This is because a single log is insufficient for discriminating between facies where measured properties overlap due to the insufficient log sensitivity, noise, and measurement errors. Geological interpretation of well log data can be challenging because each log measures a different rock property and has a different depth of investigation and sensitivity. Prior to use, well logs should be corrected for environmental and hole conditions and normalized for the effect of different tool generations and vendors [2].

More advanced methods use multiple well logs to apply statistical and artificial intelligence approaches to reduce ambiguities. A plethora of unsupervised and supervised facies prediction methods using multivariate statistics are available. In unsupervised methods, such as k-mean and hierarchical clustering, no prior geological distribution model is supplied, and data-driven log trends are detected and assigned a geological meaning [3]. The number of facies to be interpreted can be decided upon using methods such as the Bayesian and Akaike criteria, in combination with geological knowledge [2]. The results from these methods are electrofacies that are characterized by log responses linked to geological attributes which distinguish one layer from another. These electrofacies are not always the same as facies, but they can be calibrated to facies identified in cores. Unsupervised methods can be advantageous because they can reveal associations with useful information to the geologic model. However, these methods are at the risk of creating unrealistic or geologically unmeaningful results, especially in complex lithologies [3]. For this reason, this project opted to focus on supervised methods.

In supervised methods, such as support vector machine and neural networks, facies schemes are pre-defined using core data and existing geological knowledge. The goal of these types of methods is to find the best function to classify the data into the pre-defined facies in the scheme. This is done by conditioning the algorithm to link the pre-defined facies with the log data [3]. Some facies will have a clear log signature in one or more wireline log, while others are harder to discern. Some facies can be completely discrete while others gradually blend into one another. These non-discrete facies have a higher likelihood of being misclassified. Facies that are commonly difficult to differentiate in logs, due to similarities in properties and petrophysical signatures, are sometimes grouped together [2]. Unknown observations are classified according to their likelihood of membership to one category or the other [3].

1.2 Research Question

Wireline facies associations are assigned directly on wireline data, which are a measured property of the rock, compared to core facies associations which are assigned directly on the rocks. Consequently, this thesis targets the questions: How accurate are the southern North Sea's Carboniferous wireline facies associations compared to core facies associations? And, when these wireline facies association are used as a machine learning input, what supervised multivariate statistical method gives the best facies prediction results?

Determining the accuracy of wireline facies associations compared to core data can help in understanding their effectiveness in alleviating core data shortage for facies prediction. Conducting facies prediction for the Carboniferous of the southern North Sea can contribute to tapping into the exploration and development potential of the area. Facies prediction provides an enhanced understanding of the distribution of facies beyond the location of cored wells and thus understanding the architecture, quality and behavior of reservoirs by providing inputs to geomodels. It also enables better predictions of volumes and fluid flow.

1.3 Approach

This thesis project aims to achieve the following:

- Evaluate the accuracy of the wireline facies associations that have been picked on the wireline logs using core data.
- Apply and compare three supervised machine learning facies prediction methods: Support Vector Machine, Multilayer Perceptron Neural Network (MLP) and Recurrent Neural Network (RNN).
- Suggest a workflow and provide recommendations for facies prediction with the use of wireline facies associations as an input for the southern North Sea's Carboniferous.

1.4 Geologic Background

The sediments of interest are of the Late Carboniferous (Westphalian) age in the southern North Sea, which are preserved in the UK quadrants 43-53 and Netherlands quadrants D-S [4]. These deposits can be divided into the Westphalian A (Langsettian), Wesphalian B (Duckmantian) and Westphalian C/D (Bolsovian) and are topped by the base Permian unconformity [1] (Figure 1). In the southern part of the area lies the major northwest-southeast oriented Murdoch anticline. On either side of the anticline, Westphalian C/D can be found, while Westphalian A and B are found on the crest of the anticline and in the northern part of the area [5].

The Westphalian is comprised of minor delta system crevasse splays, prograding into predominantly lacustrine interdistributary bay and floodplain areas, resulting in coarsening upwards and shallowing upwards fills. This is topped by meandering channels or coal seams, and by scattered braided channels. The sediment supply was primarily from the north and flowed on a south to southwestern historic slope resulting in a decrease in the amount of sand in the south. In the north, the difference in sand content found in wells suggests that syn-depositional faulting might have concentrated the major distributary channels. Overall, the thickness of the succession increases from north to south due to an increase in subsidence and proximity to the shoreline [5].

The Late Carboniferous in the southern North Sea has been extensively drilled and logged, and it contain gas discoveries. The most productive of these Carboniferous reservoirs are the Westphalian C/D, also known as the Ketch Member or the red beds, followed by the early Westphalian B Caister Sandstone unit, then the Namurain to early Westphalian A sandstones of the Millstone Grit

Formation. The Westphalian B to early Westphalian C's Westoe Coal Formation have no significant gas yields [6].

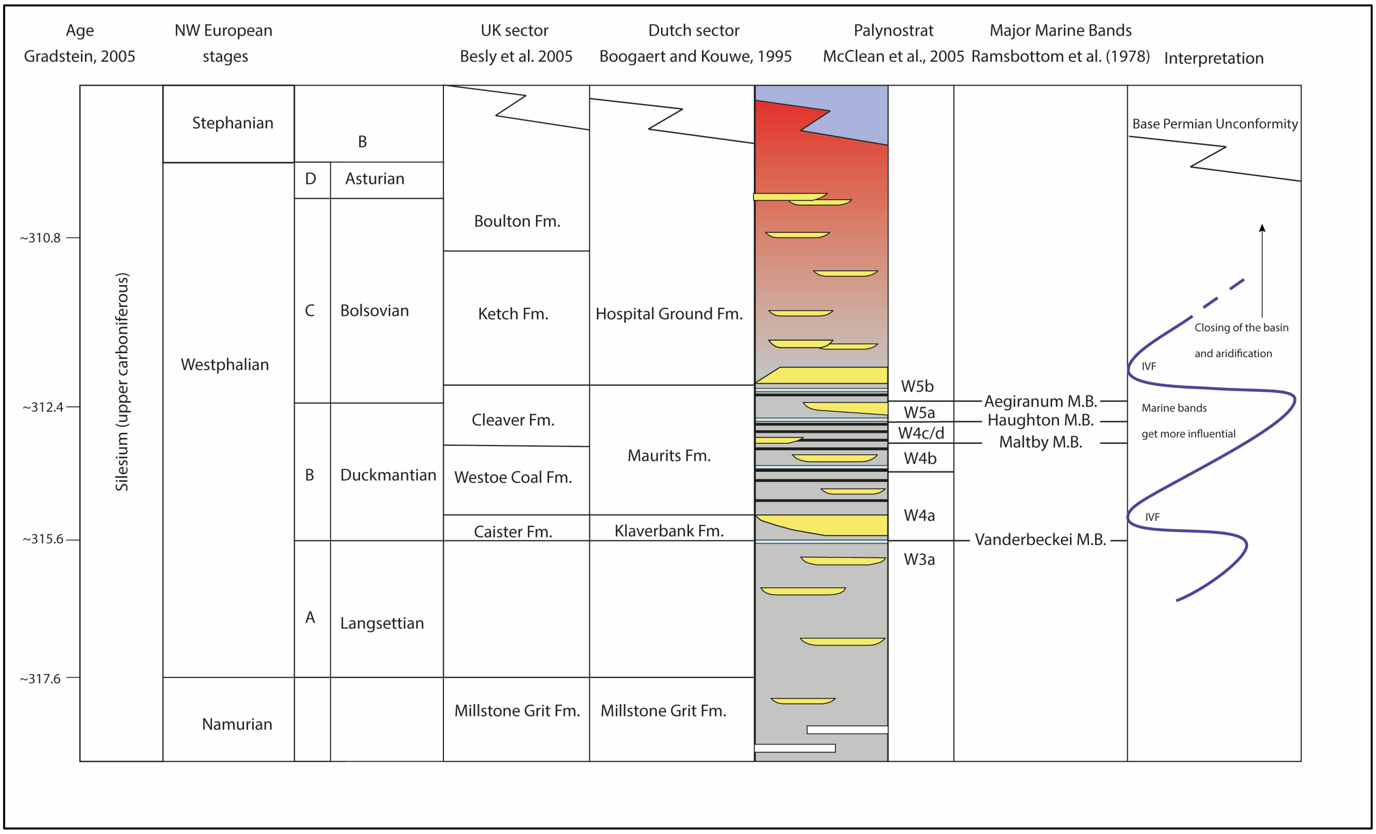

Figure 1. Stratigraphic column of the Upper Carboniferous, courtesy of PhD candidate Timothy Baars.

2 Methods

The project followed the workflow summarized in Figure 2, to first evaluate the validity of the wireline facies associations as a machine learning facies prediction input. Then, determine whether SVM, MLP or RNN yields the best facies prediction results for the Carboniferous in the southern North Sea. The workflow starts with selecting wells with good quality wireline logs, some of which are cored. After that, the dataset was explored with the use of cross-plots, histograms and violin plots to understand the distribution and signatures of the inputted wireline logs and their facies associations. Next, the accuracy of the wireline facies associations was evaluated with the use of cores.

The wells are separated into a training set used to build classifiers and a smaller validation set to conduct blind tests. Machine learning estimators require that the dataset be standardized. A number of data scalers and transformers were tested to find the one that was the best fit for this project's data. Once the data is standardized, SVM, MLP and RNN were applied on the dataset as a whole, and the results of the three methods are compared. The method that yields the best result is then applied to each Westphalian A, B, C unit separately to observe how the stratigraphic separation would affect the algorithm's performance. The details for the steps in the workflow are described below.

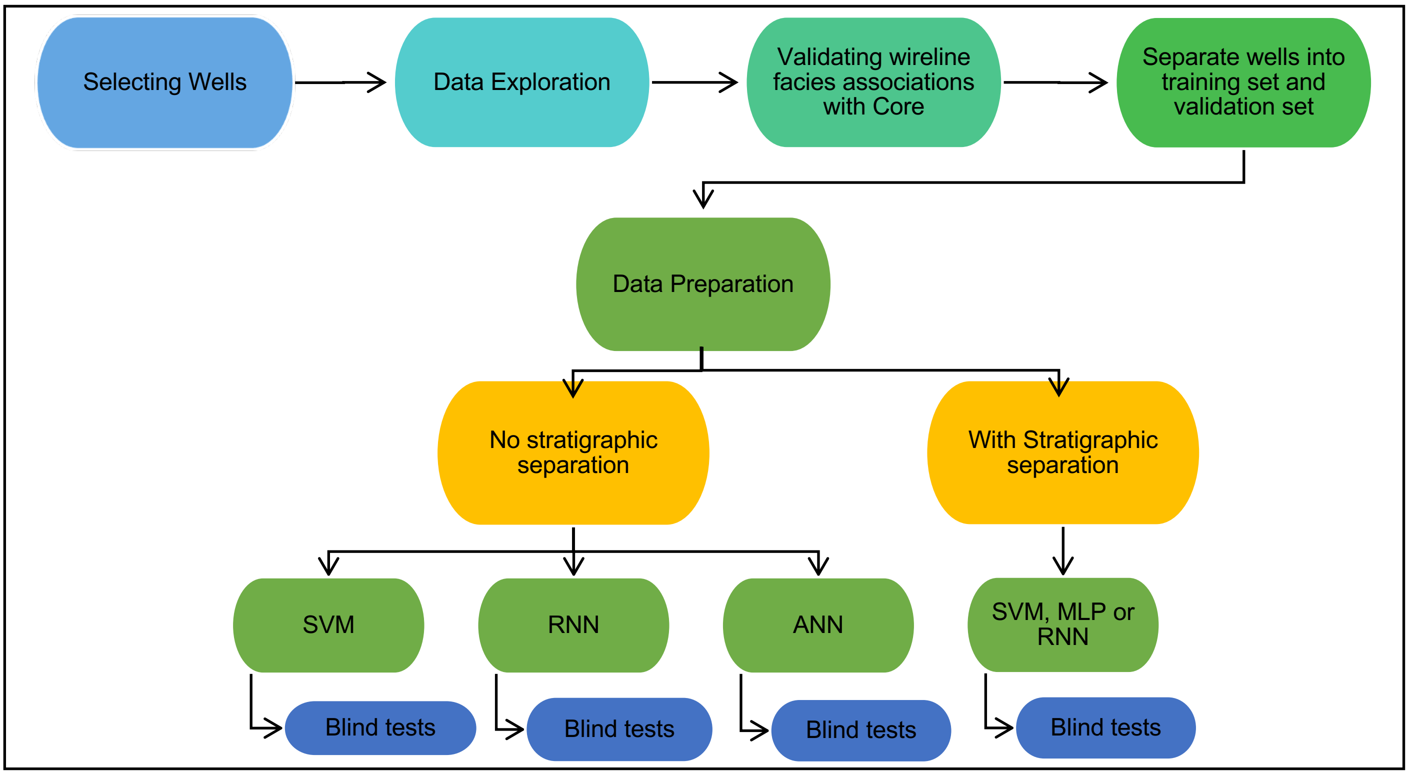

Figure 2. Flow chart showing the project workflow.

2.1 Dataset Description

The project is using a data set supplied by Wintershall from the UK Quadrants 44 and 49 and Dutch blocks D and E in the southern North Sea (Figure 3). A total of 17 wells targeting the Westphalian A, B and C of the Carboniferous were selected, 9 of which are cored (Table 1). Wells were selected based on log quality and core recovery. Since log coverage is always more extensive than core coverage, the total length of core being used represents 10% of the total length of logs being facilitated (Table 2).

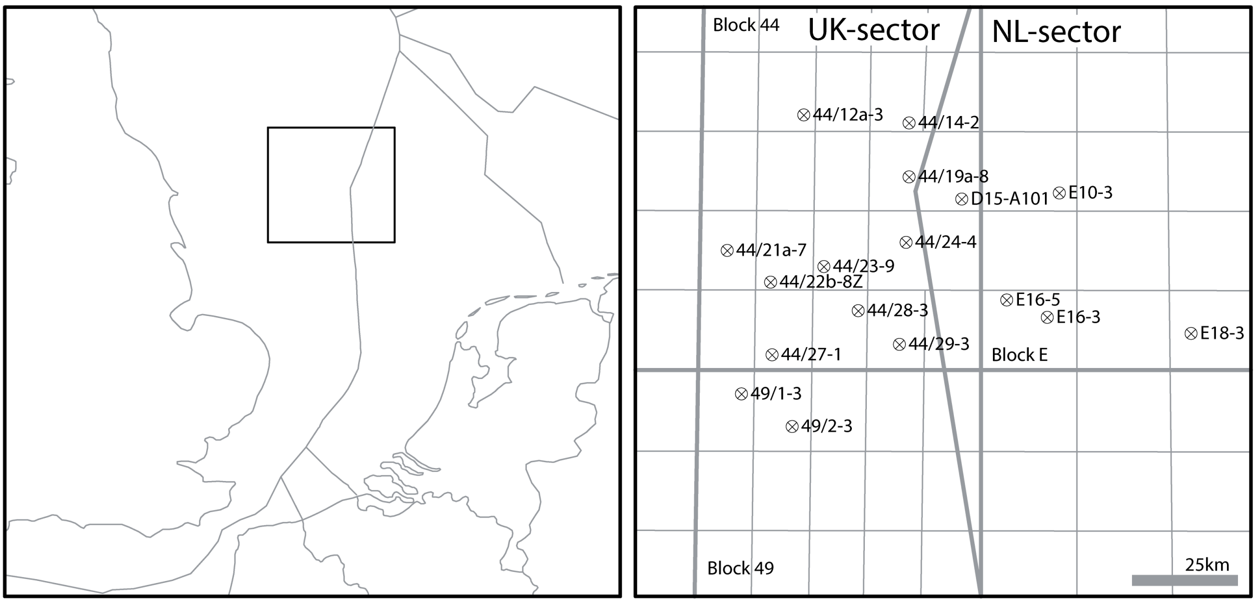

Figure 3. Map of the study area showing the wells being used in the project, courtesy of PhD candidate Timothy Baars.

Table 1. List of the selected 17 wells and indication of core description availability and logged intervals.

Well Name	Available Core Description	Logged Intervals (Westphalian)
44/12a-3	Yes	A, B, C
44/14-2	No	C, B
44/19a-8	Yes	A, B, C
44/21a-7	Yes	A, B, C
44/22b-8Z	No	A, B
44/23-9	Yes	A, B
44/24-4	No	A, B, C
44/27-1	Yes	A, B, C
44/28-3	No	A, B
49/1-3	Yes	B, C
49/2-3	No	A, B, C
E16-3	No	B, C
E16-5	No	A, B, C
E18-3	No	A, B, C
E10-3	Yes	A, B, C
D15-A101	Yes	B, C
44/29-3	Yes	B, C

Table 2. Data description summary.

Total Number of Wells	17
Number of Cored Wells	9
Total Log Length	9181 m
Total Core Length	936 m
% Core Coverage of Total Log Length	10%
Total Number of Wireline Facies Associations	7

A sedimentary facies scheme was developed based on published and unpublished sedimentological information on different parts of the Carboniferous basin in addition to extensive onshore field work by authors in the East Midland and Yorkshire [4]. The scheme is based on sediment grain size, body geometry, upper and lower boundaries and sedimentary structures. The wireline log characteristics of each facies has been identified [4]. All 17 wells being used in this project have gamma ray, density, neutron, sonic and resistivity logs, while some have spectral gamma ray logs. Wireline facies associations have been manually assigned to these wells by Wintershall following the same aforementioned facies scheme (Table 3). The well logs and the wireline facies associations logs are used as the input data for the supervised machine learning algorithms.

Table 3. Geological description and log signature of the Wintershall wireline facies associations [5][4]. Log signature examples are taken from the wells used in this project.

Wireline facies association	Geological Description					Log Signature	
	Lithology	Grain Size	Sorting	Thickness	Sedimentary Structures		
Background Floodplain (FP)	Mudstones, siltstones and fine-grained sandstones. May contain siderite or pyrite nodules.	Clay and silt sized, with some fine-grained sand.	-	-	Usually structureless due to rootlet disturbances and bioturbations.	High gamma ray. The presence of ironstone nodules would cause relatively lower responses.	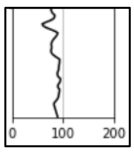
Braided Channel (BC)	Mainly clean sandstones with an erosive base and sharp top.	Varies widely from fine to very coarse and conglomeritic within a body. Overall fining upwards.	Range from well sorted to poorly sorted as grain sized increases.	Typically 20-30 meters and can locally be up to 50-60 m.	Well-developed cross-beddings.	Blocky and consistent gamma ray with pronounced top and bottom inflexions. Finer grains	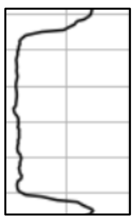

						can cause localized fluctuations.	
Point Bar (PB)	Meandering or high sinuosity channel deposits. Argillaceous sandstone with local mudstone interclasts deposited by high sinuosity channels. Have an erosive base and a gradational top.	Mostly fine and very fine.	Well sorted.	Maximum thickness of 20-25 m.	Commonly contain epsilon cross bedding and small-scale cross bedding, ripple cross lamination, and parallel laminations.	Sharp gamma ray base inflexion, but the top can be either sharp or gradational depending on the body’s lithology.	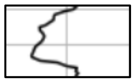
Crevasse Splay Sands (CSS)	Argillaceous sandstone with interbedded siltstones.	Very fine to fine. Typically have a gradational base and coarsening upwards. Occasionally have an erosional base and fine upwards.	Well sorted.	Typically 2-5 m.	Convolute and ripple cross laminations, discontinuous parallel laminations and small-scale trough cross bedding.	Upward decreasing gamma with sharp upper contact inflexion. Can also be bell-shaped upward increasing Logs are internally erratic corresponding to the interbedding of lithologies.	 
Coal (Co)	Result of compacted peat swamps.	-	-	On average 2-3 m.	-	Very distinctive spikes of low gamma, low density, and high neutron and sonic.	GR 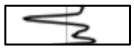 RHOB 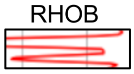 NPHI 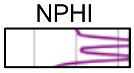 DT 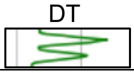
Mouth Bar (MB)	Fairly clean sandstone unit overlying a mudstone or siltstone.	Usually coarsening upwards from very fine to fine, but can be locally coarse and fining upwards.	Sand unit is well sorted.	Mud/siltstone unit is typically 10-15 m thick.	Sandstones: ripple cross laminations at the base and trough cross bedding at the top. Mud/ siltstones: parallel laminations or homogenized by bioturbations.	Gamma ray and sonic gradually decreases upwards with a sharp upper inflexion.	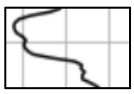
Marine Shale (MS)	Condensed dark mudstone .	Clay sized grains.	-	-	Presence of macrofauna such as goniatites and micro-gastropods.	Gamma ray as high as 150 API.	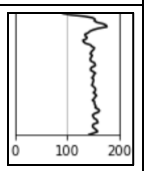

When facies were being picked by Wintershall on the well logs, the braided channels, point bars, crevasse splays, coals, mouth bars and marine shales are recognized by their log signatures (Table 3), then any depth interval that has not been identified as one of these 6 facies was assigned as a background floodplain. This makes the background floodplain inclusive of the lake, marine bay and interdistributary bay deposits. Marine shale bands have been characterized as being difficult to identify with certainty in offshore wells, especially when it comes to correlating them to key onshore bands [5][4].

2.2 Dataset Exploration

A combination of histograms, cross plots and violin plots can be used to explore the dataset. Histograms can be used to view the distribution of facies in the wells for all Westphalian as a whole and each of the A, B and C units separately. A cross plot matrix can be used to visualize the relationship between the variables in the data set and the overlap or separability of the data. To understand the statistical distribution of each facies with respect to each wireline log, violin plots can be used, where the probability density, modality, range, median and interquartile range of each facies can be viewed and compared for all eight wireline logs.

2.3 Validation of Wireline Facies Associations with Core Data

In order to determine the quality of the machine learning inputs it is important to evaluate how accurately the provided facies associations are. Since the wireline facies associations are assigned using log data only, core validation is needed. To validate this, 9 of the 17 selected wells were cored wells with good quality cores and core descriptions containing core facies associations. There are several challenges accompanying this validation process. Each core has been described by a different company or a different individual and descriptions date between 1992 and 2016. This can introduce discrepancies such as those related to conventions and use of nomenclature. Another shortcoming of this process is that core coverage is always shorter than log coverage and cores usually target reservoir sand sections. Consequently, only limited sections of each well can be validated and some facies can be validated more than others.

For each of the nine cores, the facies associations and their core descriptions were linked to their wireline log response and in turn their comparable wireline facies association. The result is a facies classification that is unified for all the cores which follows the classification of the wireline facies associations (Table 3). The facies from the core descriptions were digitized, depth shifted and plotted using the unified code. Then, the accuracy from the match between the wireline and the core facies associations was calculated.

The total depth shift applied to each core reflects that which has been applied by the core loggers in addition to adjustments made when the digitized core facies associations were plotted next to the logs and wireline facies associations (table 4). This additional depth shift was applied using clear markers such as the top and bottom of braided channel sand bodies where the gamma ray has clear sharp inflexions.

2.4 Data Preparation and Preprocessing

2.4.1 Data Preparation

Many machine learning algorithms are design for input data with values close to zero and with comparable scales. Metric-based and gradient-based estimators require a dataset that is centered and with a unit variance, i.e. a standardized dataset. Using unscaled data as input can slow down or prevent the convergence of estimators [7]. A total of five scalers and transformers were explored and their effectiveness is observed. Scalers are linear, while transformers differ in the way in which they estimate the parameters used for scaling.

2.4.1.1 Standard Scaler

In this scaling method, the mean is removed and the data is scaled to a unit variance. This method is sensitive to the presence of outliers when the empirical mean and standard deviation are calculated, and thus it does not guarantee the output of balanced feature scales [7].

2.4.1.2 Min-Max Scaler

Each feature is rescaled individually with this scaler such that all values fit in the range [0,1]. Similar to the standard scaler, the min max scaler is also sensitive to outliers [7].

2.4.1.3 Robust Scaler

With this method, the median is removed and the data is scaled according to the interquartile range, i.e. the range between the first (25^{th} quantile) and the 3^{rd} quartile (75^{th} quantile). This is done independently on each feature. Since percentiles are used for centering and scaling, this method is not sensitive to vary large marginal outliers. This can lead to better results compared to outlier sensitive scalers, but can also create comparatively larger ranges for the scaled features [7].

2.4.1.4 Power Transformer (Yeo-Johnson)

This is a non-linear, parametric, monotonic transformation where data is mapped to a normal Gaussian-like distribution in order to minimize the skewness and stabilize the variance by applying a zero-mean unit variance normalization [7].

2.4.1.5 Quantile Transformer (Uniform and Gaussian Output)

This is a non-linear transformation that shrinks the distance between outliers and inliers by mapping the probability density function of each feature to either a uniform distribution or a Gaussian distribution within the range [0,1]. Similar to the Robust Scalar, this method is less sensitive to the addition or removal of outliers. However, outliers are collapsed into the predefine range, which can lead to saturation artifacts for extreme values [7].

2.4.2 Data Preprocessing

The Westphalian formations have all been deposited as continuous successions, thus a unified facies scheme is applicable for all three units. However, there are differences in which facies are more occurrent in each of the Westphalians [4]. This difference is also apparent in the histogram distributions of the input data (Figure 7). As a result, each machine learning method detailed below has been applied twice, once on the data as a whole with Westphalian A, B and C grouped together, and once after stratigraphically separating the data into three Westphalian formations. The result of applying this stratigraphic separation is then observed and compared to those of the lumped data.

2.5 Facies Prediction

Three machine learning facies prediction methods are applied in this project: Support Vector Machine (SVM), Multilayer Perceptron Neural Networks (MLP), and Recurrent Neural Networks (RNN). All three methods start with separating the input data, which is in the form of well logs with facies associations, into a training set and a smaller validation set. The training set is used for the algorithm to discover features and trends and build a classifier accordingly.

Often times, a subset is separated from the training set and used for cross-validation of the developed classifier. Cross-validation is used to tune the parameters of the model. This is done by creating a series of models with different combinations of parameters to find the optimal choice of parameters. The model with the lowest cross-validation is the one used as a classifier to train the training set. Instead of the exhaustive process of model parameter selection, which can make classifiers more complex and take longer to train, this project opted for using recommended guidelines for the choice of parameters and focus on comparing the efficacy of different methods [4][1].

The validation set has been separated from the initial data set so that it can be used to evaluate the accuracy of the classifier by comparing the predicted and the assigned wireline facies associations. This is known as a blind test. In the blind test, precision, recall and confusion matrices are used to evaluate the performance of the classifier. Precision is the probability that a sample actually belongs to the class it was assigned to, while recall is the probability that a sample will be classified into the correct class. These two criteria are combined into the F1 score for each facies association, and for the classifier overall [4]. During this process, it is important to differentiate between facies associations with high prediction success rate and those difficult to discern. Once a satisfactory validation is reached, the classification method can be applied to wells that have no facies associations [3].

2.5.1 Support Vector Machine (SVM)

Support vector machine is commonly used for regression and classification objectives. The input for the algorithm is called a feature vector. In the case of facies prediction, the feature vector is the set of measurements at each depth interval that can be comprised of log measurements and indicator variables. Each feature vector is associated with a class which represents the facies type. For data that is not linearly separable, as shown in the cross-plot matrix (Figure 8), the goal of the algorithm is to project the data into the N-dimensional space, with N equal to the number of features, where it can find a hyperplane that can separate the data (Figure 4). This is done during the training step with the use of a kernel function. The position and orientation of the hyperplane is influenced by the data points closest to it. Different kernel functions can be used for this purpose [11].

The advantages of this method lie in its effectiveness in high dimensional spaces, its use of support vectors that represent subsets of the training points that make it memory efficient, and its versatility where a common or customized kernel function can be used. The disadvantages are that there is a risk of over-fitting the data if the number of features is much greater than the number of samples, and that this method does not directly provide probability.

To apply SVM, the code developed by Enthought's Brendon Hall was facilitated [4]. The code uses the SVM open-source Python implementation in scikit-learn. The SVM classifier is built and tuned by using cross-validation for model parameter selection. The Radial Basis Function (RBF) kernel is used, which takes two parameters: C and gamma [4]. The C parameter is common for all kernel functions. It determines the tradeoff between allowable misclassification and the simplicity of the decision surface. A low C value gives a smooth surface with higher room for misclassification, which might make the model unable to classify outlier and result in larger errors. A high C has a less smooth surface but aims at more correct classification, which might lead to overfitting, making a classifier unable to generalize when applied on new data. The gamma parameter is specific to the RBF kernel. It represents the inverse of the radius of influence of a sample in the feature space, with low values meaning higher distances and high values meaning closer distances. The trained and optimized model can then be applied on blind wells for further validation, after which the classifier is ready to be applied to wells with no facies assignment. After several experiments with the model parameter selection step with this project's dataset, it was observed that the recommended default parameters [4] yielded the best results. Thus, the cross-validation step was not incorporated in the final results.

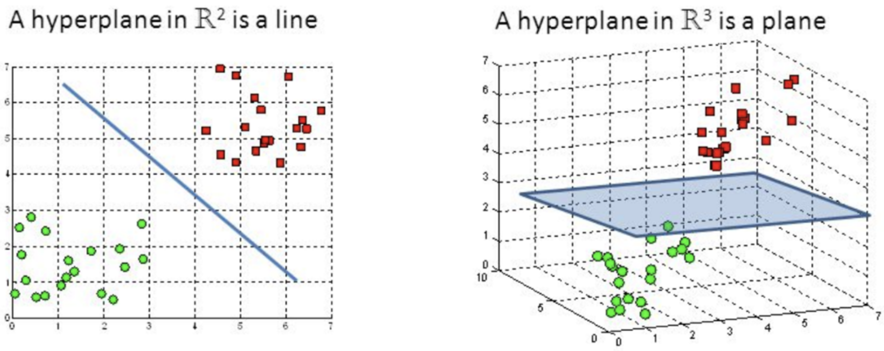

Figure 4. Example of hyperplanes in 2D and 3D [12].

2.5.2 Multilayer Perceptron Neural Networks (MLP)

The theory for artificial neural networks (ANN) stems from neuroscience research on the structure and function of the brain. Limitations of ANNs include their inability to generate physical interpretations and the tendency to create facies clusters with similar proportions, which can be compensated for by integrating geologic knowledge [2]. There are three main classes of neural networks, two of which have been implemented in this project: Multilayer perceptron (MLP) and recurrent neural networks (RNN).

MLP is the classical type of neural networks. A conventional MLP neural network is comprised of a hierarchy of layers in which nodes are connected by arcs (Figure 5). Every node is arithmetically equivalent to the sum of the proceeding nodes, where each is multiplied by the weight of the connecting arc. A basic network contains three layers: an input layer, a hidden layer and an output layer. As the name suggests, the input layer contains the input data or features. The hidden layer transforms values from the input neurons with a weighted linear summation followed by a non-linear activation function. The output transforms the values received from the hidden layer to output values. While training the network, a set of patterns are repeated, and arc weights are modified to obtain a better match between the output and the desired result. Training is conducted by backpropagating errors through the network. The difference between the output and desired results is used as incremental adjustments to the interconnection weights in an iterative manner. A trained network is achieved when the weights converge to an equilibrium setting [3].

Even though it is possible to make a neural network training set complex enough with many hidden layers and nodes per layer to produce nearly perfect results, doing so is undesirable and unnecessary. That is because doing so would increase the likelihood that the network would memorize associations in the training set and loose the ability to generalize leading it to perform worse when new observations are used to generate predictions. A generalizing network is capable of filtering out localized and random errors and absorbing systematic trends linking observations [3][1]. The advantages of MLPs include their ability to learn non-linear models in real time. The disadvantages include: First is that the hidden layers have a non-convex loss function where more than one minimum exist, which means that different initial random weights can result in different levels of accuracy; Second, that the network requires the tuning of the number of neurons, layers and iterations; Third, the network is sensitive to feature scaling [14].

To apply this method, the code provided by SEG was utilized. Similar to the SVM execution, this code also uses the scikit-learn Python package to apply MLP [15]. A parameter optimization step was not applied. Instead, the complexity of the network was kept at a minimum by following two rules for choosing the number of hidden layers and neurons. The first rule is that one hidden layer is used, since that is considered sufficient for the majority of problems. The second rule is that the number of hidden neurons should be between the number of input and output neurons, or the mean of the sizes of the input and output layers [1].

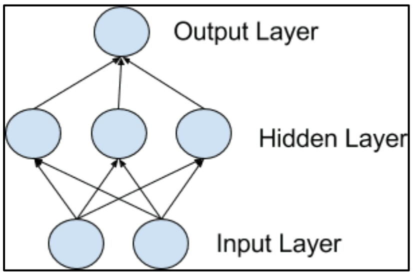

Figure 5. Model of a simple neural network [16].

2.5.3 Recurrent Neural Networks (RNN)

Recurrent Neural Networks, compared to Multilayer Perceptrons, have additional connections that add memory to the network allowing it to learn broader abstractions. These additional loops and architecture allow signals to not only be passed forward from one layer to another, but also laterally between neurons of a layer, and to feedback the output as input [17] (Figure 6).

A successful RNN needs to address two issues, backpropagation training and the prevention of gradient vanishing or exploding. Backpropagation of error is used in typical networks to update its weights. However, this breaks down in RNN because of the loop connections. This issue is solved with unrolling an RNN network by creating copies of neurons that have recurrent connections. When backpropagation is used on unrolled networks, gradients that are calculated to update weights can become unstable. They can either *explode* by become very large or *vanish* by becoming very small. This problem is addressed in RNNs with the use of architecture known as Long Short-Term Memory Networks (LSTM) [17].

LSTM networks use memory blocks with several components and a memory instead of neurons. Each block contains gates that manage its state and output with a sigmoid activation function. There are three types of gates: A forget gate that conditionally determines which information is discarded from a block; An Input gate that conditionally determines which input values to update; An output gate that conditionally determines what to output based on the input and the memory of the block. Each gate has a weight that is learned and updated during the training [17]. To apply this method, the keras Python package was used to apply a facies classification with RNN and the Gated Recurrent Units (GRU) gating mechanism [18]. GRUs are similar to LSTM but without an output gate [19].

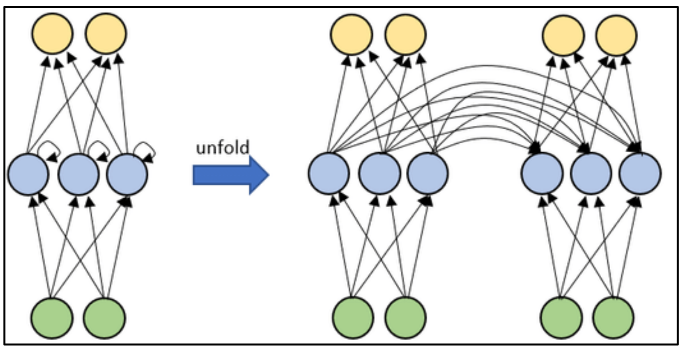

Figure 6. Diagram of a basic recurrent neural network [20].

3 Results

3.1 Dataset Exploration

Since the facies were predominantly picked based on the gamma ray log signatures, the gamma ray violin plot shows the most variation in the distribution of the facies (Figure 10.a), followed by the density and neutron (Figure 10.b, c). Appendix A shows tables summarizing the count, mean, standard deviation, minimum value, maximum value and 25th, 50th and 75th percentiles for the logs of each facies.

The distribution of facies in the wells used in this project shows that there is a significant difference in the sampling of each facies, where the floodplain facies makes up for 66% of the dataset (Figure 7.d). Westphalian A covers 14% of the dataset, and the Westphalian B and C cover 62% and 24%. All 7 facies have been identified in the Westphalian A sections of the wells. However, no marine shales were identified in the Westphalian B and C, and no coals occur in the Westphalian C (Figure 7.a, b, c).

A cross plot matrix can be used to visualize the relationship between the variables in the data set (Figure 8 and Figure 9). These cross plots demonstrate that the data of all facies overlap and cannot be linearly separable, making it necessary to apply advanced methods to achieve classifications for facies prediction.

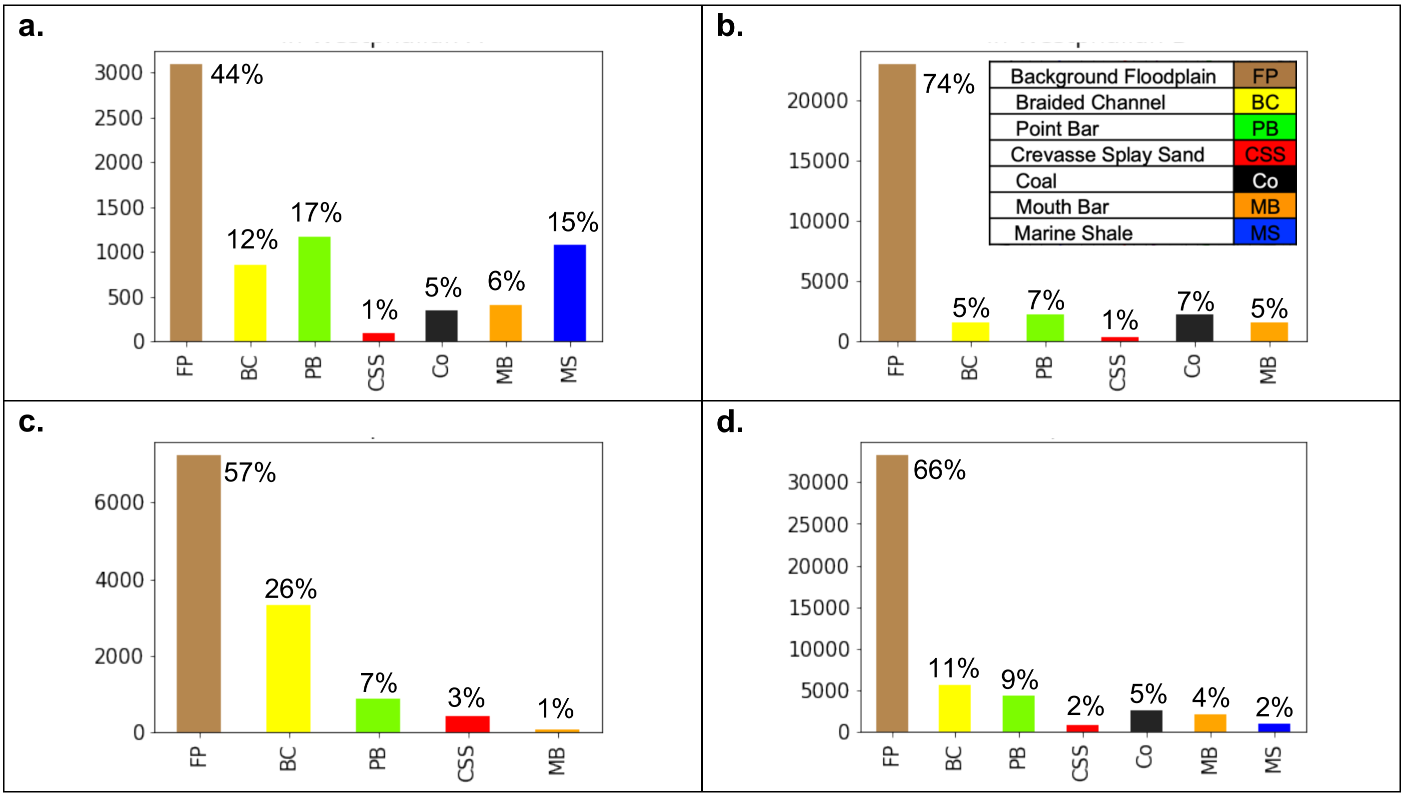

Figure 7. Distribution of the data by facies in (a) Westphalian A only, (b) Westphalian B only, (c) Westphalian C only, (d) Westphalian A, B and C Combined. Note that the background floodplain facies occurs significantly more than any other facies.

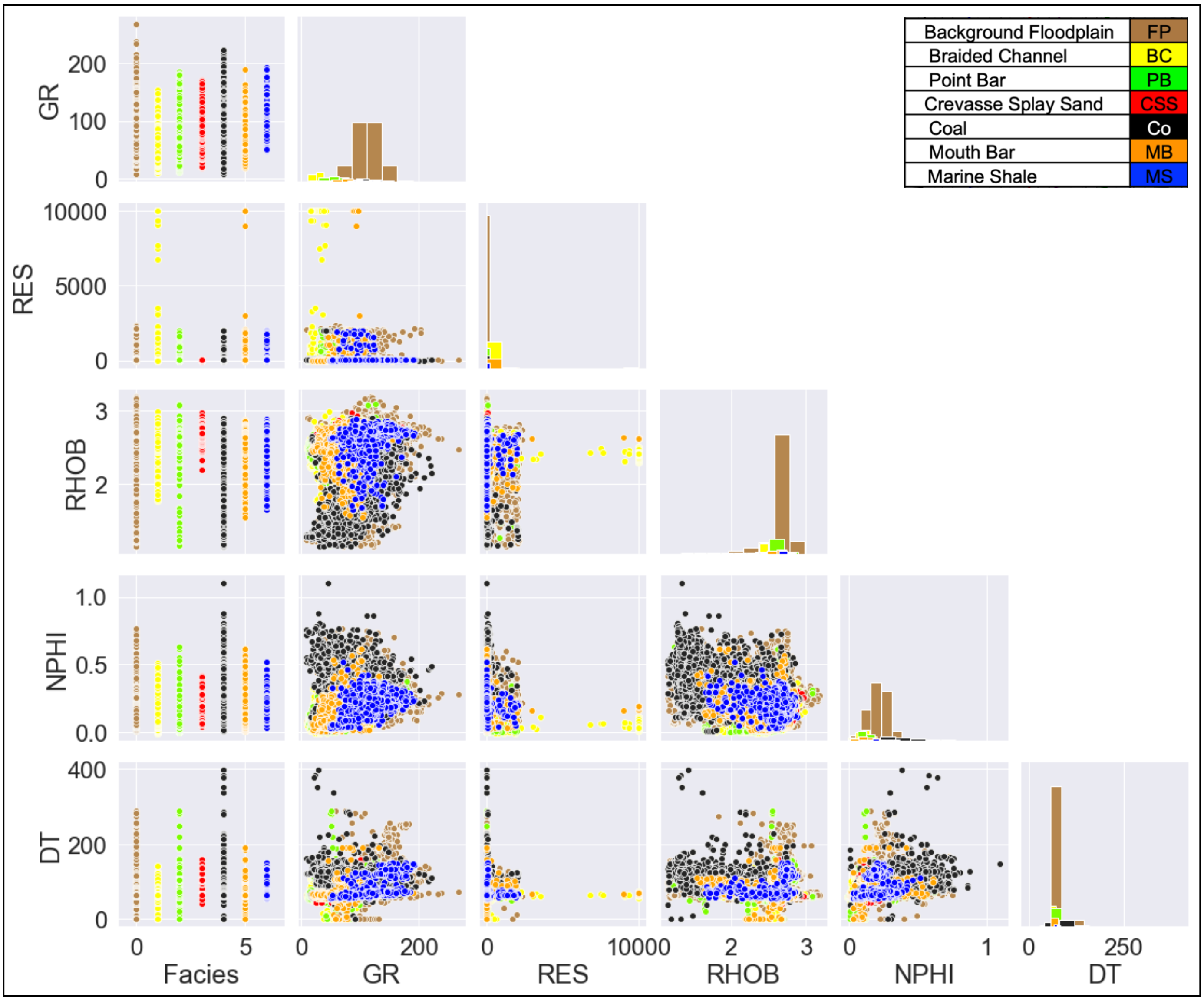

Figure 8. Cross plot matrix with histograms showing the variation of wireline measurements sorted by facies. Note that the data of all facies heavily overlap, and large outliers are present.

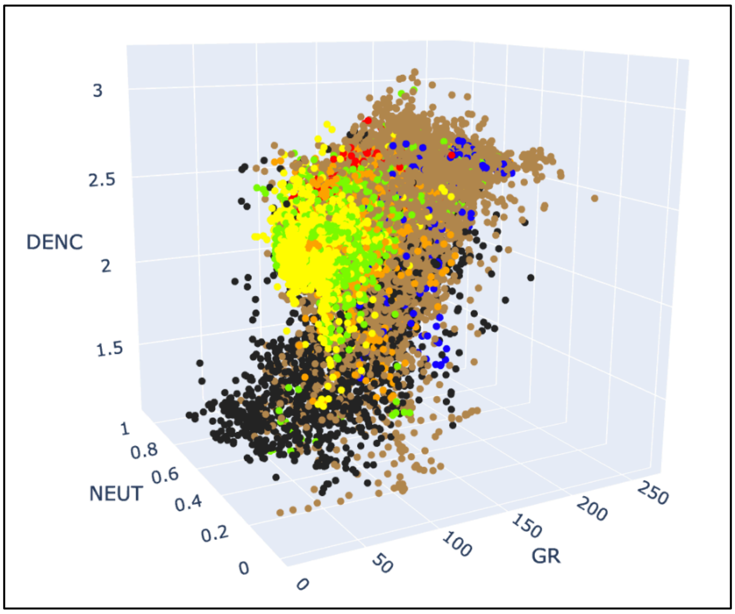

Figure 9. 3D plot of the gamma ray, density and neutron logs sorted by facies. Note that the data of all facies still heavily overlap as observed in 2D cross plots.

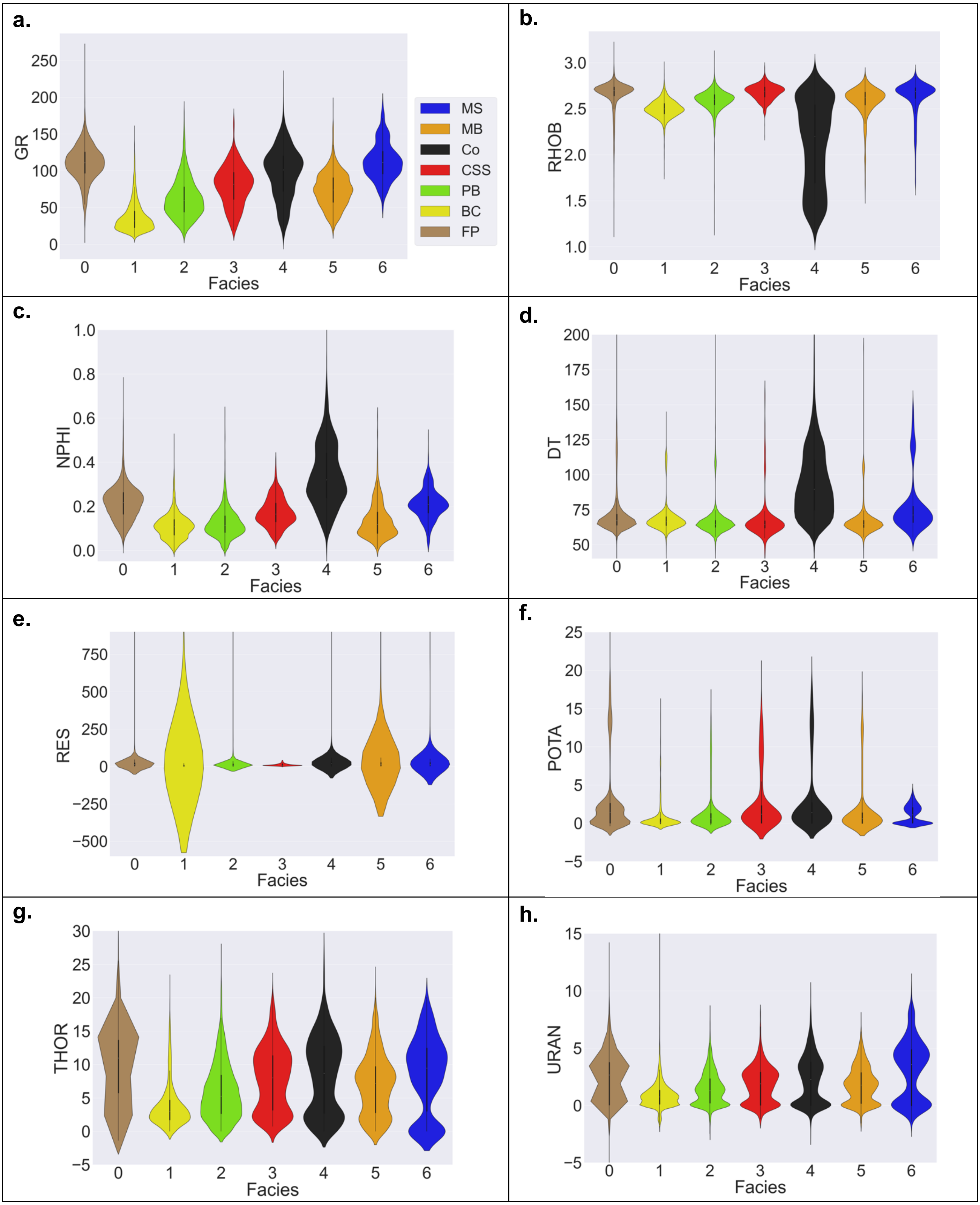

Figure 10. Violin plots showing the statistical distribution of each facies with respect to each wireline log: (a) gamma ray, (b) density, (c) neutron, (d) sonic, (e) resistivity, (f) potassium (g) thorium and (h) uranium. The gamma ray shows the most difference between the facies, followed by the neutron and density.

3.2 Validation of Wireline Associated Facies with Core Data

The calculated overall accuracy of all 9 wells is 71% (Table 4) (appendix B - D). Table 5 breaks down the core by facies and shows the percentage of presence of each facies in the cores, and the percentage of which that has been correctly identified by wireline facies associations. Coring operations target reservoir units, and thus braided channels are more sampled than other facies, making it an easier facies to validate. This also means that other facies are under sampled and less validated.

The marine shale facies has not appeared in these offshore cores, and in some instances, what was identified as marine shale in the logs corresponded to background floodplain in the cores. Consequently, the validity of marine shale in the wireline facies association is unknown. As mentioned above in the data description and exploration section, this facies is difficult to recognized in the wireline data of the offshore realm. Extensive coring and sidewall coring is necessary to identify the marine macrofauna characteristic of this facies. For these reasons, marine shale and background floodplain can possibly be treated as non-discrete facies.

In the examined core descriptions, mouth bar was only identified in one interval in well 49/1-3 (figure 6D appendix D). The mouth bar facies association in the wireline logs often correspond to crevasse splay sands in the core. Since mouth bars are part of the crevasse splay system, these two facies can be considered as adjacent and non-discrete, similar to the marine shale and background floodplain facies.

The three wells with accuracy lower than 70%: 44/27-1, D15-FA101 and 44/29-3, were excluded from the training set and used for the blind tests, along with the well 44/19a-8 which has the highest accuracy of 89%. This means that a total of five cored wells with a total accuracy of 76% are being used as part of the training set, and 4 cored wells are being used for the blind tests. For the 3 wells with the lowest accuracy, part of the blind test evaluation would be to determine whether the machine learning algorithm can predict facies with a higher match to the core facies associations than the match between the core and wireline facies associations.

Table 4. Amount of depth shift applied to each core and the percent match between the wireline and the core facies associations.

Well Name	Total Depth Shift [m]	Percent Match between Wireline and Core Facies Association
44/12a-3	+4.0	81%
44/19a-8	+0.0	89%
44/23-9	+3.0	70%
44/24-4	+6.2	79%
44/27-1	+4.0	69%
49/1-3	+9.0	85%
E10-3	+2.0	72%
D15-A101	+6.0	54%
44/29-3	+0.0	47%
	Overall Accuracy	**71%**
	Accuracy of Training Wells Only	**76%**

Table 5. Percent presence of each facies in the core and percent match with the wireline facies associations.

Core Facies Associations	% of Core	Correctly Identified by Wireline Facies Associations
Background Floodplain (FP)	39.4%	88%
Braided Channel (BC)	39.1%	81%
Point Bar (PB)	3.2%	47%
Crevasse Splay Sands (CSS)	16.3%	16%
Coal (Co)	1.8%	29%
Mouth Bar (MB)	0.2%	100%
Marine Shale (MS)	0%	0%

3.3 Data Preparation

The input features of the dataset have very different scales and large outliers makes it difficult to visualize the data and can degrade the performance of machine learning algorithms. The five input wireline logs: Gamma ray, density, neutron, sonic and resistivity have scales thar are very dissimilar and large outlier are present (Figure 8), making the data preparation for machine learning more challenging. This is particularly more apparent with the resistivity log, which has a range of [0, 10,000] with large outliers especially from the braided channel facies, and the sonic log, which has a range of [0, 400] with the largest outliers from the coal facies (Figure 11).

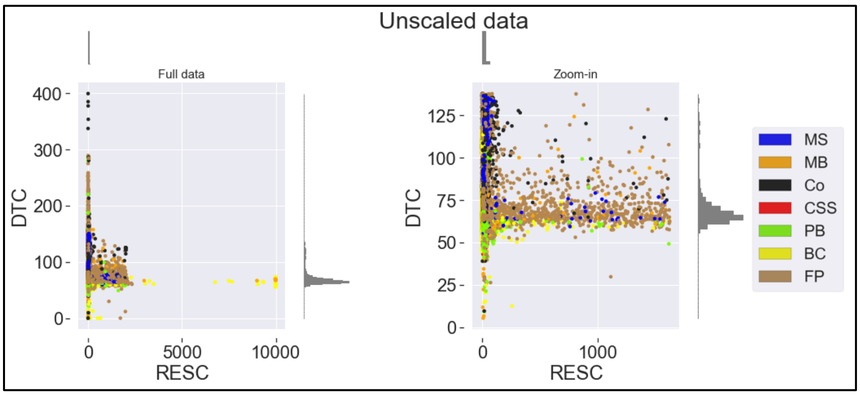

Figure 11. Cross plot of resistivity versus sonic before scaling showing large outliers.

Out of the five scalers and transformers applied, the Yeo-Johnson power transformation and the quantile transform appear to be the most effective because they were able to produce centered data with comparable scales despite outliers. The standard scaling method resulted in features with different spreads: [-2.5,5] for gamma ray, [-5, 2.5] for density, [-2.5,10] for neutron, and [0,15] for resistivity and sonic (Figure 12). With the min-max scaler, even though all features have been fit into the predefined range of [0,1], the inliers for the resistivity data are compressed in the range [0, 0.25], and the inlier for the sonic data are compressed between [0, 0.5] because of the outliers in these two features (Figure 13). For the robust sacler, since the input features have very different scales and this scaler is applied independently on each feature, the resulting ranges are not comparable (Figure 14).

The Yeo-Johnson power transform performed comparatively better than the three scalers above. The results show a range of [-2.5, 2.5] for resistivity, neutron and the inliers of density, and [-2.5, 7.5] for the inliers of gamma ray and sonic (Figure 15). This transformer achieves a normal distribution centered around zero for all features including the resistivity and sonic data (Figure 16). The quantile transforms, with both uniform (Figure 17 and Figure 18) and gaussian (Figure 19 and Figure 20) distribution, has been the most effective in standardizing the data set by centering it and achieving perfectly comparable scales for all input features. The quantile transforms' rescaling of outliers introduces the risk of artifacts. For this reason, the three machine learning methods have been tested using data that has been transformed by the Yeo-Johnson power transform, quantile transform with uniform distribution, and quantile transform with Gaussian distribution.

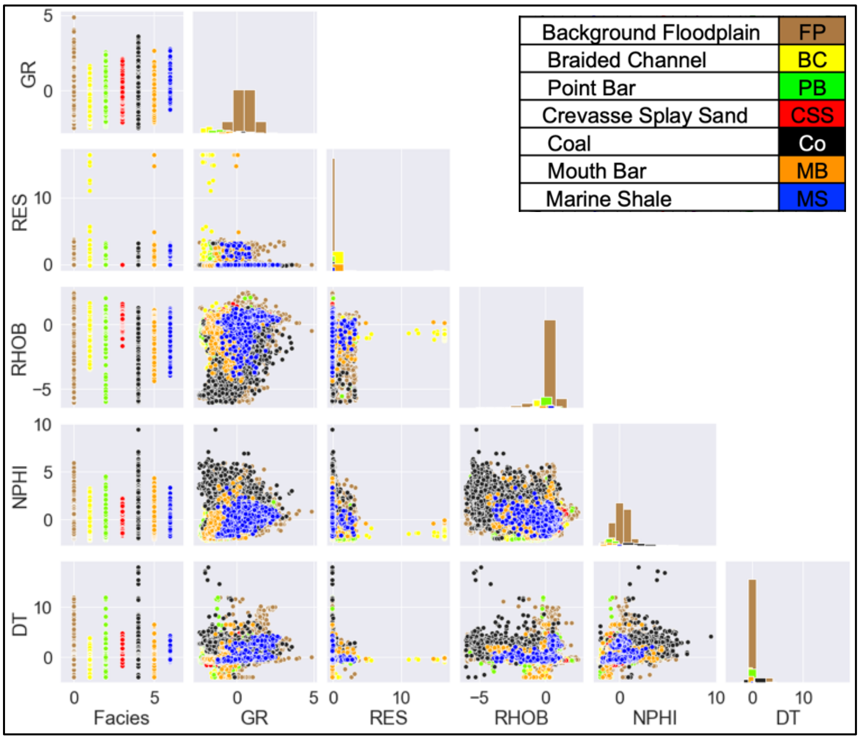

Figure 12. Cross plot matrix with histograms showing the variation of wireline measurements sorted by facies after standard scaling. Comparable scales for all logs were not achieved.

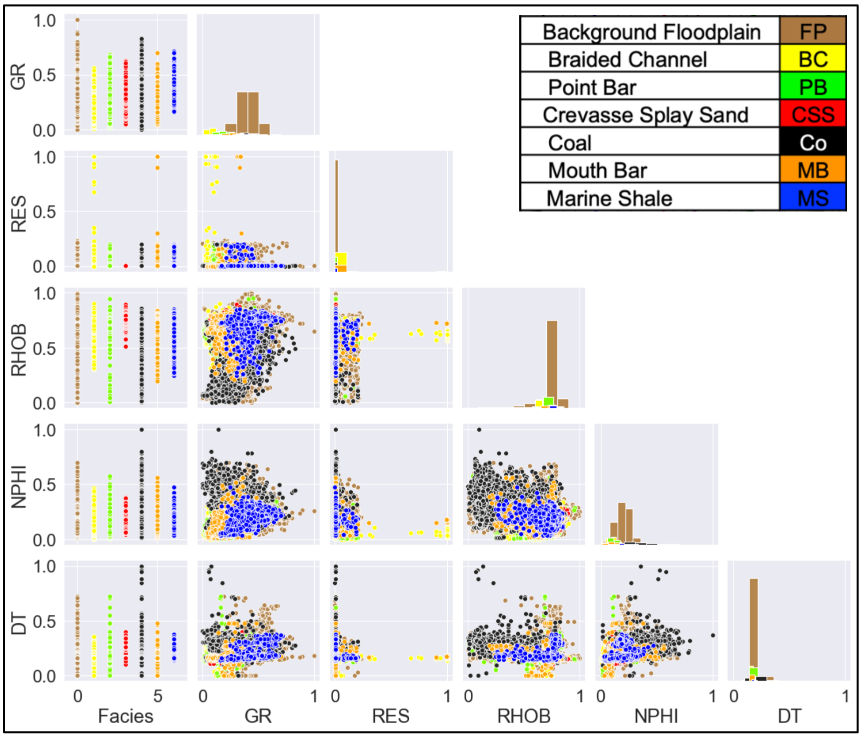

Figure 13. Cross plot matrix with histograms showing the variation of wireline measurements sorted by facies after min-max scaling. Comparable scales for all logs were achieved, but the inlier of the resistivity and sonic are compressed into small ranges due to outliers.

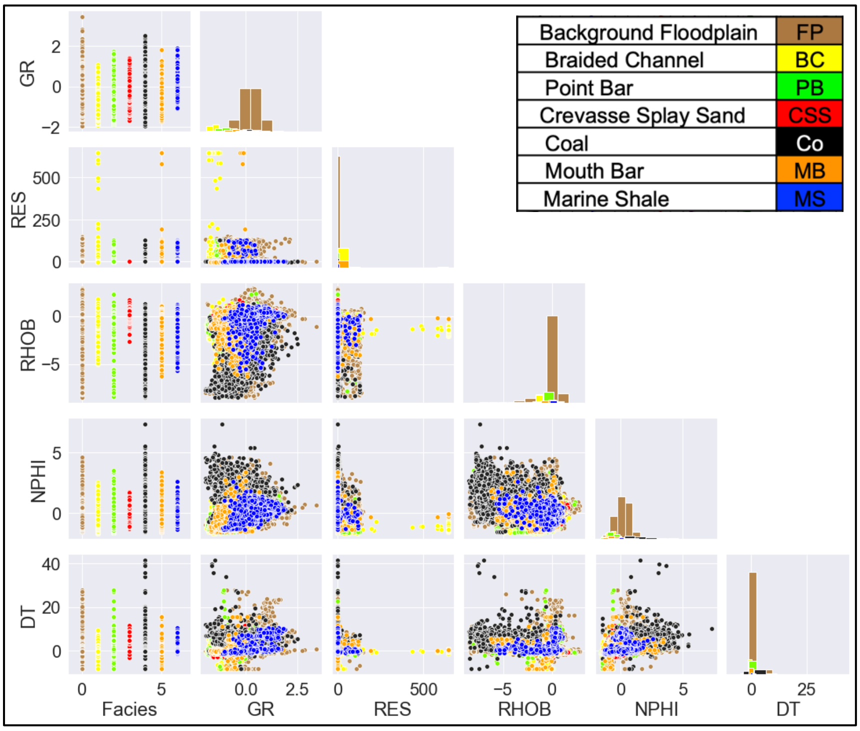

Figure 14. Cross plot matrix with histograms showing the variation of wireline measurements sorted by facies after robust scaling. Comparable scales were not achieved.

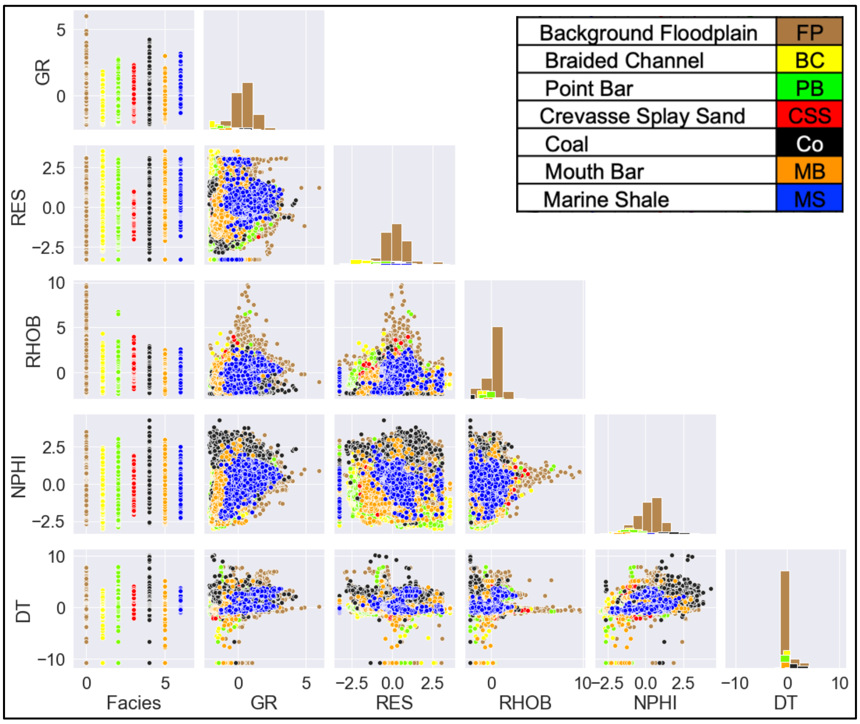

Figure 15. Cross plot matrix with histograms showing the variation of wireline measurements sorted by facies after power transformation (Yeo-Johnson). A normal distribution centered around zero was achieved for all logs with comparable scales for resistivity, neutron and the inliers of density, and comparable scales for the inliers of gamma ray and sonic.

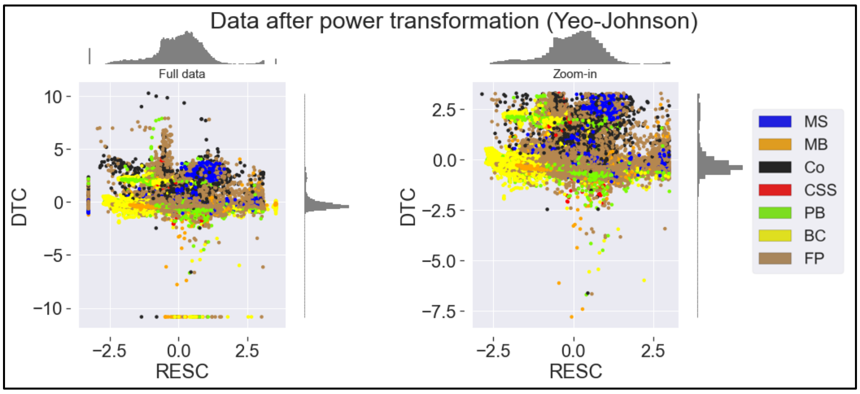

Figure 16. Cross plot of resistivity versus sonic after power transformation (Yeo-Johnson).

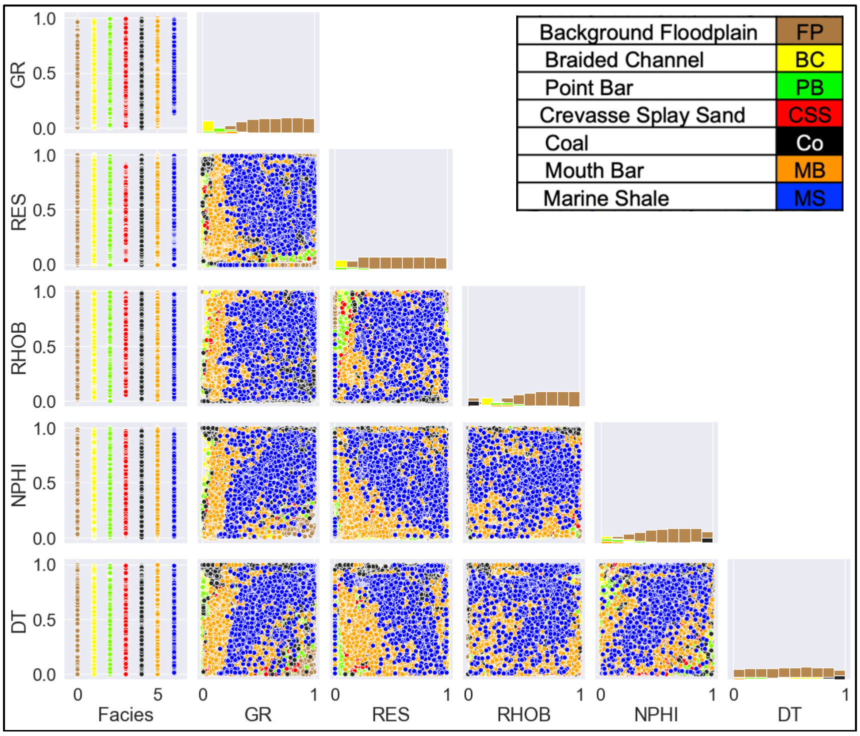

Figure 17. Cross plot matrix with histograms showing the variation of wireline measurements sorted by facies after quantile transformation (uniform pdf). All scales are comparable for all logs.

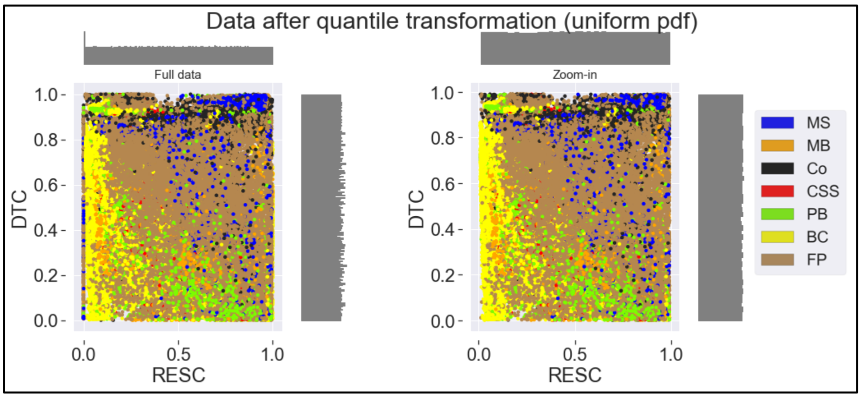

Figure 18. Cross plot of resistivity versus sonic after quantile transformation with normal distribution showing that outliers have been eliminated by rescaling.

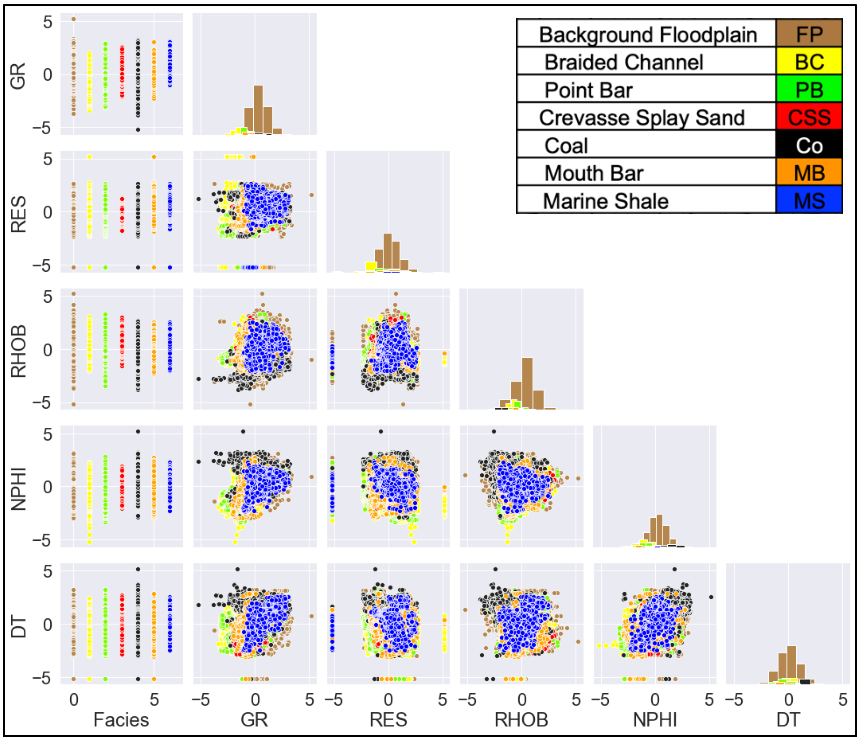

Figure 19. Cross plot matrix with histograms showing the variation of wireline measurements sorted by facies after quantile transformation (gaussian pdf). The scales for all logs are comparable with a normal distribution centered around zero.

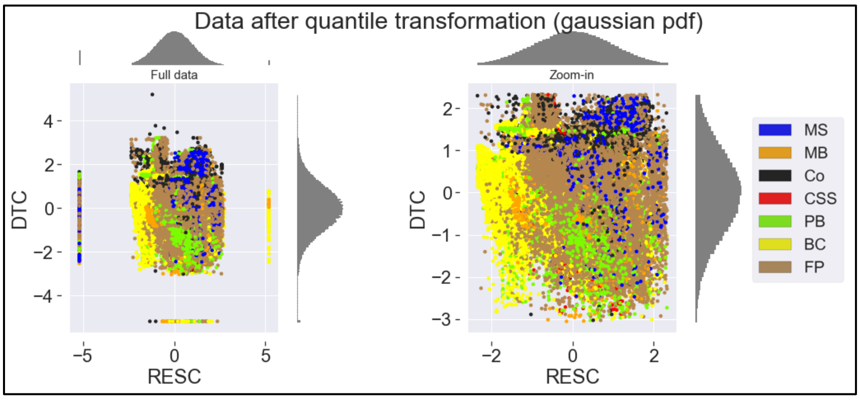

Figure 20. Cross plot of resistivity versus sonic after quantile transformation with gaussian distribution showing that outliers have been rescaled.

3.4 Facies Prediction

In all three machine learning methods, the quantile transform with Gaussian distribution achieves the highest blind test accuracy (Table 6). The confusion matrices show that the F1 score, which reflects the balance between precision and recall, for the background floodplain remained within the same range of 0.88-0.90 for all trials. However, the F1 score of the other facies was lowest for the power transformed data and highest for the quantile transformed data with a Gaussian distribution (Table 7 – Table 9 and appendix E).

When SVM, MLP and RNN were applied to the training data as a whole without stratigraphic separation of the Westphalian units, none of the three methods made predictions for all seven predefined facies (Figure 21). The SVM classifier did not make any predictions for the crevasse splay sands nor marine shale facies. The MLP classifier did not make any predictions for the mouth bar facies. The RNN classifier made no predictions for the marine shale facies. For all three methods, facies with higher occurrence (Figure 7d), which are the background floodplain, braided channel, point bar and coal, were more likely to be predicted compared to facies with lower occurrence, which are crevasse splays, mouth bars and marine shale (Figure 22 - Figure 25).

Three of the four blind wells, 44/27-1, D15-FA101 and 44/29-3, have a core validation accuracy less than 70% (Table 4). These wells were used to test whether using the wells with higher accuracy for training would result in predictions with a higher match to the core facies associations compared to the match between core and wireline facies associations. An example of an interval where that has occurred is in well 44/29-3 around 3675 meters, where all three machine learning algorithms correctly identifies an interval as a braided channel that has been erroneously identified as a point bar in the wireline facies associations (Figure 23). However, overall, the predicted facies match the wireline facies association logs more than the core.

The recurrent neural network (RNN) has achieved the highest overall accuracy of 80.9% from the three methods (Table 6). Confusion matrices for blind well 44/19a-8 (Table 7 -
Table ***9***) show that all three methods achieve a comparable F1 score of 0.88 or 0.89 for the background floodplain facies (FP), but that the higher overall accuracy of the RNN is attributed to the higher F1 scores for the braided channel (BC), point bars (PB) and coal (Co) facies, which increased by 5-6%, 25%, 26-36% respectively from the SVM and MLP to the RNN (Table 7 - Table 9). These improvements can be visually observed in the prediction logs where the RNN more accurately predicted solid intervals of point bars or braided channels, and it made less erroneous coal predictions (Figure 22).

The data set was stratigraphically separated into Westphalian A, B, and C, and RNN was applied on each Westphalian unit independently. The results were then concatenated (Figure 22 - Figure 25). This approach has achieved a lower overall accuracy of 75.6%. This decrease in overall accuracy is because the F1 score of the background floodplain, braided channel and point bar facies decreased, which can be due to the decrease in the number of samples in each of these facies once they have been separated into different Westphalian units (Table 10). However, compared to the classifiers that have been applied to the data as a whole without stratigraphic separation, this approach made predictions for all seven facies (figure 22 k-o), and the F1 score of the mouth bar facies increased from zero to 0.10 and that of the marine shale increased from zero to 0.17 (Table 10).

The overall accuracy of the blind test for the stratigraphically separated data increases to 78.6% when adjacent facies are considered. Adjacent facies groups crevasse splays and mouth bars as non-discrete facies, and background floodplain with marine shale. With this arrangement of facies, the F1 score of crevasse splays increases to 0.03, and that of marine shale to 0.84 (Table 11).

For both RNN methods with and without stratigraphic separation, the statistical distribution of the predicted background floodplain and braided channels have the highest match to that of the input (Figure 26). Without the stratigraphic separation RNN was unable to make marine shale predictions. However, with the stratigraphic separation, the statistical distribution of the marine shale highly matches that of the input.

Table 6. Accuracy of blind test on 44/19a-8 with SVM, MLP and RNN using different transformers. Quantile transform with a Gaussian performs best in all three, and RNN has the highest accuracy.

	Power Transform	Quantile Transform Uniform PDF	Quantile Transform Gaussian PDF
Support Vector Machine (SVM)	76.3%	78.7%	78.9%
Multilayer Perceptron (MLP)	77.5%	78.1%	78.4%
Recurrent Neural Network (RNN)	78.7%	80.3%	80.9%
RNN with Stratigraphic Separation	-	-	75.6%
RNN with Stratigraphic Separation for Adjacent Facies	-	-	78.6%

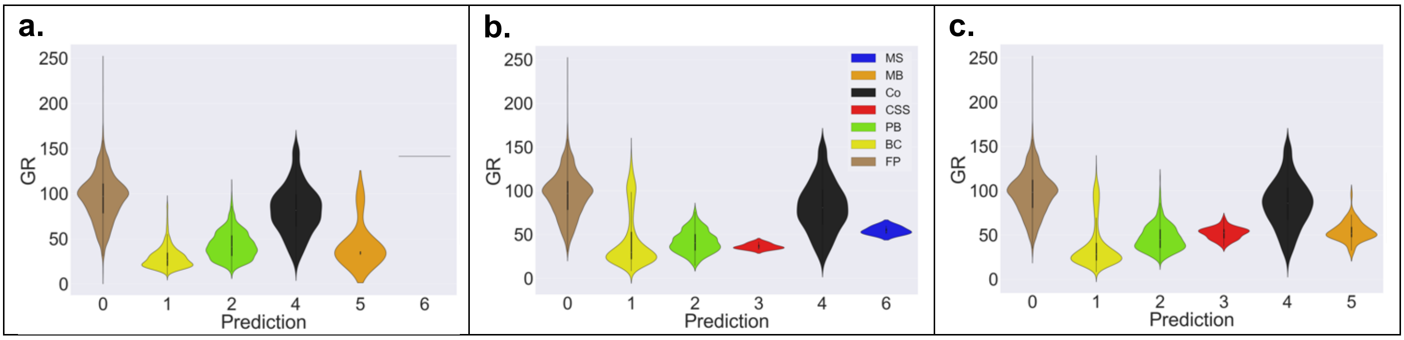

Figure 21. Violin plots showing the statistical distribution of each facies with respect to each wireline log as predicted by the blind tests with (a) SVM, (b) MLP, (c) RNN all of which after quantile transform with a Gaussian distribution. None of the three methods made predictions for all seven facies.

Table 7. Confusion matrix of SVM blind test on well 44/19a-8 after quantile transformation (Gaussian PDF).

True \ Prediction	FP	BC	PB	CSS	Co	MB	MS	Total
Background Floodplain (FP)	1752	3	36		11			1802
Braided Channel (BC)	30	453	38		18			539
Point Bar (PB)	72	84	124					280
Crevasse Splay Sands (CSS)	94		16					110
Coal (Co)	50		2		26			78
Mouth Bar (MB)	83		25		2			110
Marine Shale (MS)	64							64
Precision	0.82	0.84	0.51	0.00	0.46	0.00	0.00	0.71
Recall	0.97	0.84	0.44	0.00	0.33	0.00	0.00	0.79
F1	0.89	0.84	0.48	0.00	0.39	0.00	0.00	0.74

Table 8. Confusion matrix of MLP blind test on well 44/19a-8 after quantile transformation (Gaussian PDF).

True \ Prediction	FP	BC	PB	CSS	Co	MB	MS	Total
Background Floodplain (FP)	1752	2	34		14			1802
Braided Channel (BC)	37	432	49		21			539
Point Bar (PB)	87	67	125		1			280
Crevasse Splay Sands (CSS)	99		11					110
Coal (Co)	43		4		31			78
Mouth Bar (MB)	86		21		3			110
Marine Shale (MS)	64							64
Precision	0.81	0.86	0.51	0.00	0.44	0.00	0.00	0.70
Recall	0.97	0.80	0.45	0.00	0.40	0.00	0.00	0.78
F1	0.88	0.83	0.48	0.00	0.42	0.00	0.00	0.74

Table 9. Confusion matrix of RNN blind test on well 44/19a-8 after quantile transformation (Gaussian PDF). Higher F1 scores are achieved for braided channels (BC), point bars (PB) and coal (Co).

Prediction / True	FP	BC	PB	CSS	Co	MB	MS	Total
Background Floodplain (FP)	1740	5	42		14	1		1802
Braided Channel (BC)	22	462	37		18			539
Point Bar (PB)	64	45	170		1			280
Crevasse Splay Sands (CSS)	95		15					110
Coal (Co)	37		1		40			78
Mouth Bar (MB)	88	1	20		1			110
Marine Shale (MS)	64							64
Precision	0.83	0.90	0.60	0.00	0.54	0.00	0.00	0.73
Recall	0.97	0.86	0.61	0.00	0.51	0.00	0.00	0.81
F1	0.89	0.88	0.60	0.00	0.53	0.00	0.00	0.77

Table 10. Confusion matrix of RNN blind test on 44/19a-8 after quantile transformation (Gaussian PDF) using stratigraphic separation. The F1 score increases for mouth bars (MB) and marine shale (MS), but decreases for background floodplain (FP), braided channels (BC) and point bars (PB).

Prediction / True	FP	BC	PB	CSS	Co	MB	MS	Total
Background Floodplain (FP)	1631	36	47	4	28	7	49	1802
Braided Channel (BC)	28	433	59		11	6	2	539
Point Bar (PB)	81	59	130		3	7		280
Crevasse Splay Sands (CSS)	106		2			2		110
Coal (Co)	30		3		43	2		78
Mouth Bar (MB)	77	8	13		3	7	2	110
Marine Shale (MS)	38		14			1	11	64
Precision	0.82	0.81	0.49	0.00	0.49	0.22	0.17	0.71
Recall	0.91	0.80	0.46	0.00	0.55	0.06	0.17	0.76
F1	0.86↓	0.81↓	0.47↓	0.00	0.52	0.10↑	0.17↑	0.73

Table 11. Confusion matrix of RNN blind test on 44/19a-8 after quantile transformation (Gaussian PDF) using stratigraphic separation while considering crevasse splas sands (CSS) and mouth bars (MB) as adjacent facies, and floodplain (FP) and marines shale (MS) as adjacent facies. The overall accuracy is 0.785. Note the increase in F1 score of crevasse splays marine shales.

Prediction / True	FP	BC	PB	CSS	Co	MB	MS	Total
Background Floodplain (FP)	1680	36	47	4	28	7		1802
Braided Channel (BC)	28	433	59		11	6	2	539
Point Bar (PB)	81	59	130		3	7		280
Crevasse Splay Sands (CSS)	106		2	2				110
Coal (Co)	30		3		43	2		78
Mouth Bar (MB)	77	8	13		3	7	2	110
Marine Shale (MS)			14			1	49	64
Precision	0.84	0.81	0.49	0.33	0.49	0.23	0.93	0.75
Recall	0.93	0.80	0.46	0.02	0.55	0.06	0.77	0.79
F1	0.88	0.81	0.47	0.03↑	0.52	0.10	0.84↑	0.76

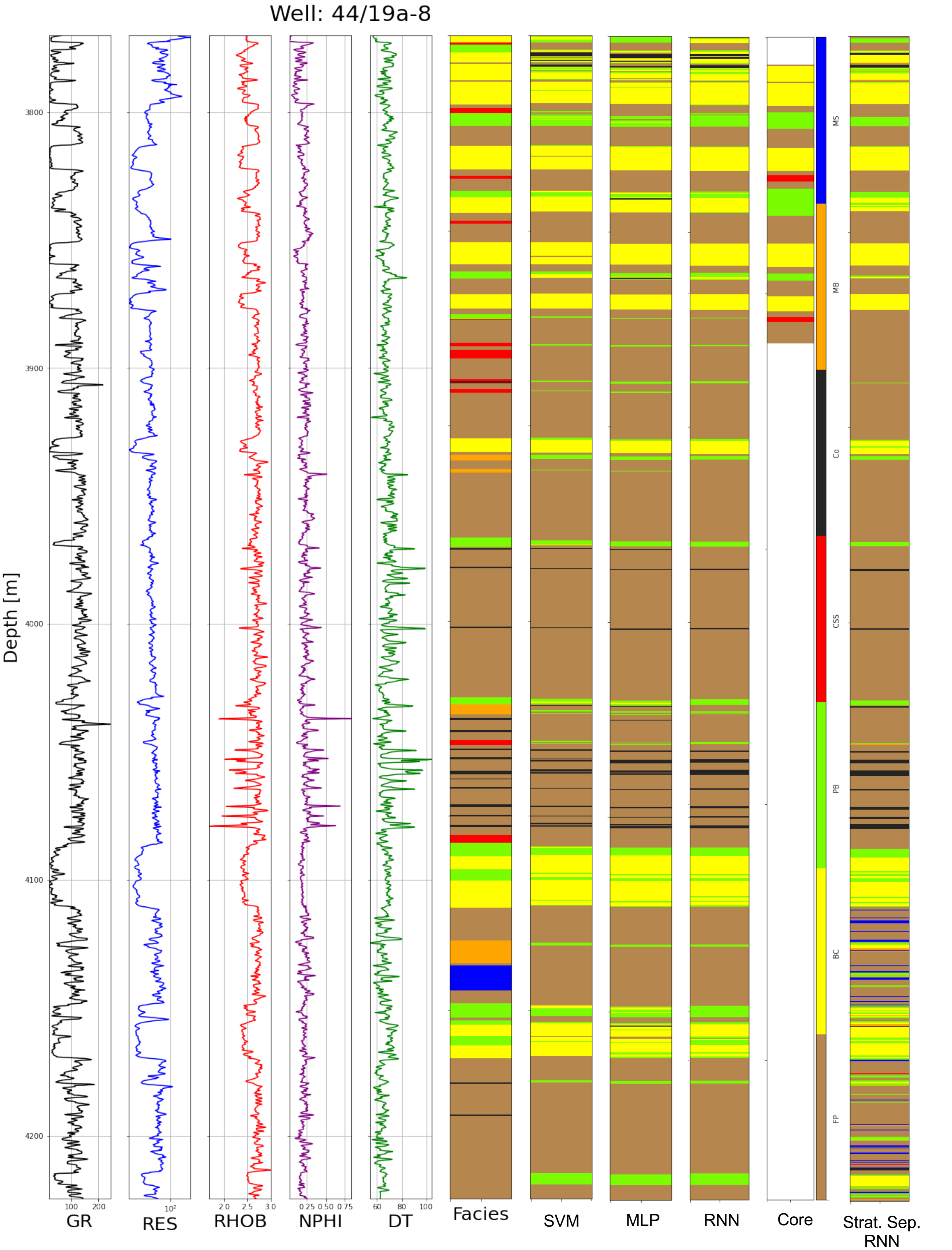

Figure 22. Blind test results for well 44/19a-8 using SVM and MLP without stratigraphic separation and using RNN without and with stratigraphic separation. The RNN shows better overall accuracy.

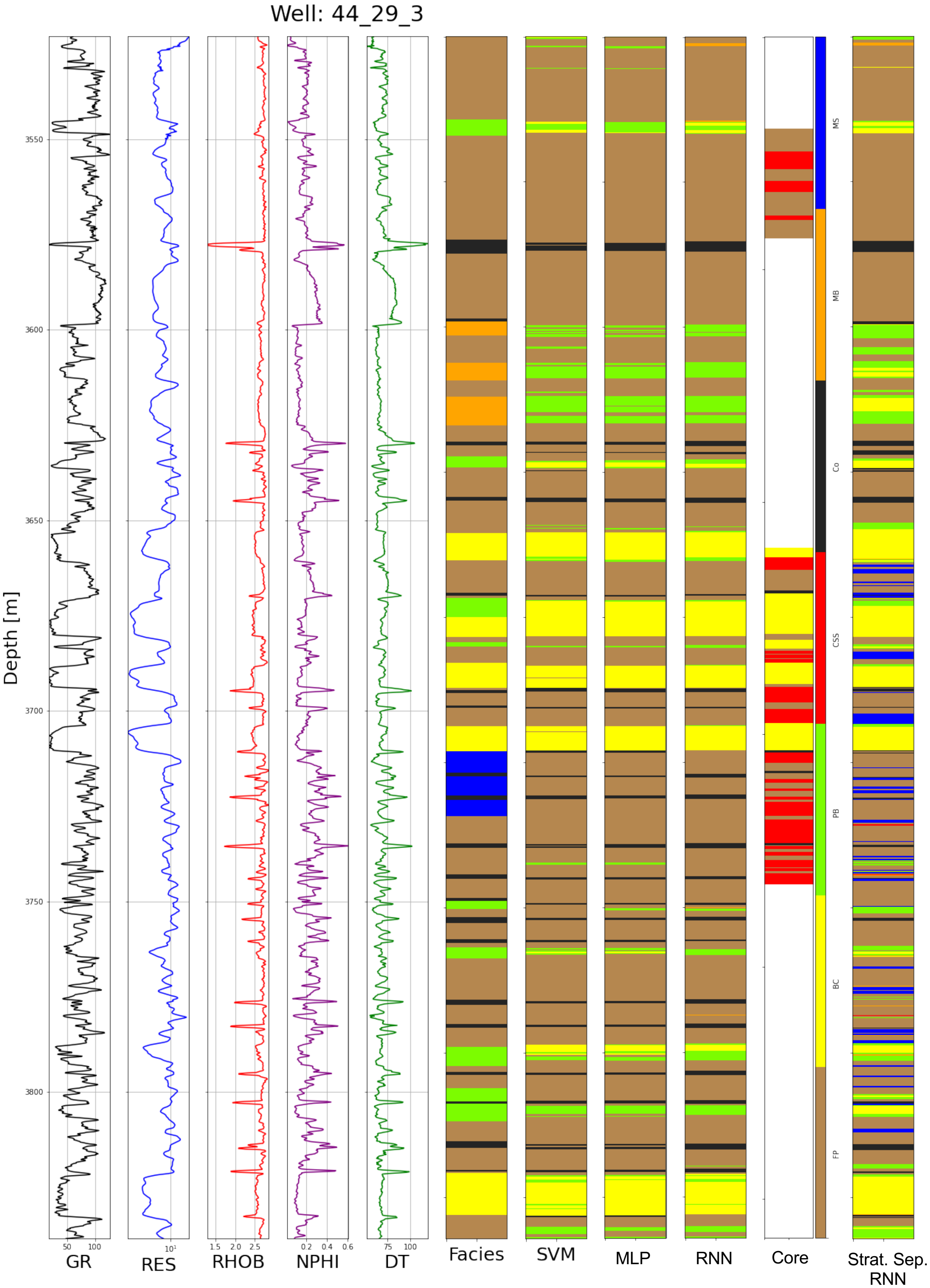

Figure 23. Blind test results for well 44/29-3 using SVM and MLP without stratigraphic separation and using RNN without and with stratigraphic separation. At 3675 m machine learning correctly identified a braided channel unit that has been inaccurately interpreted as a point bar in the wireline facies associations

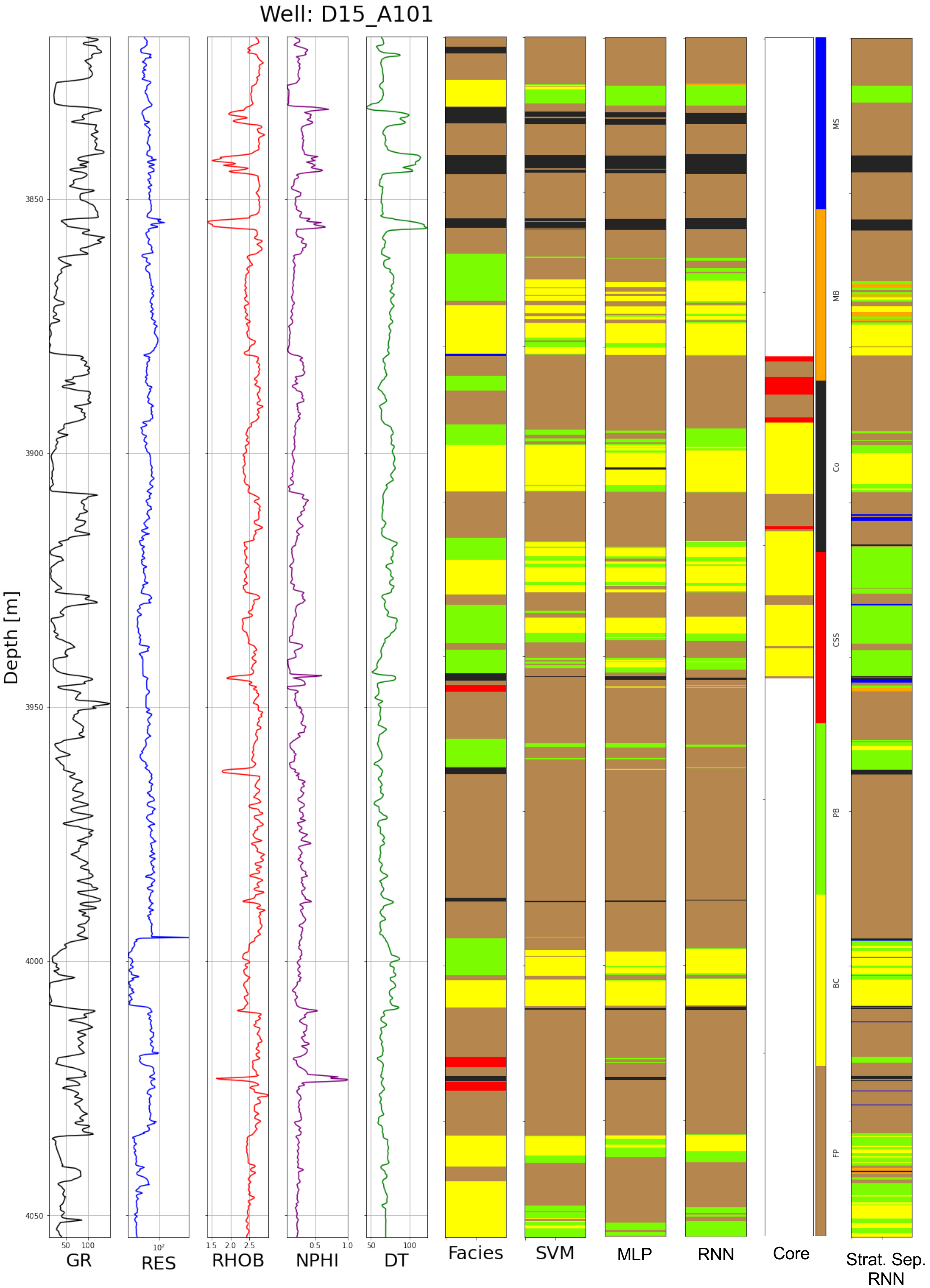

Figure 24. Blind test results for well D15-A101 using SVM and MLP without stratigraphic separation and using RNN without and with stratigraphic separation.

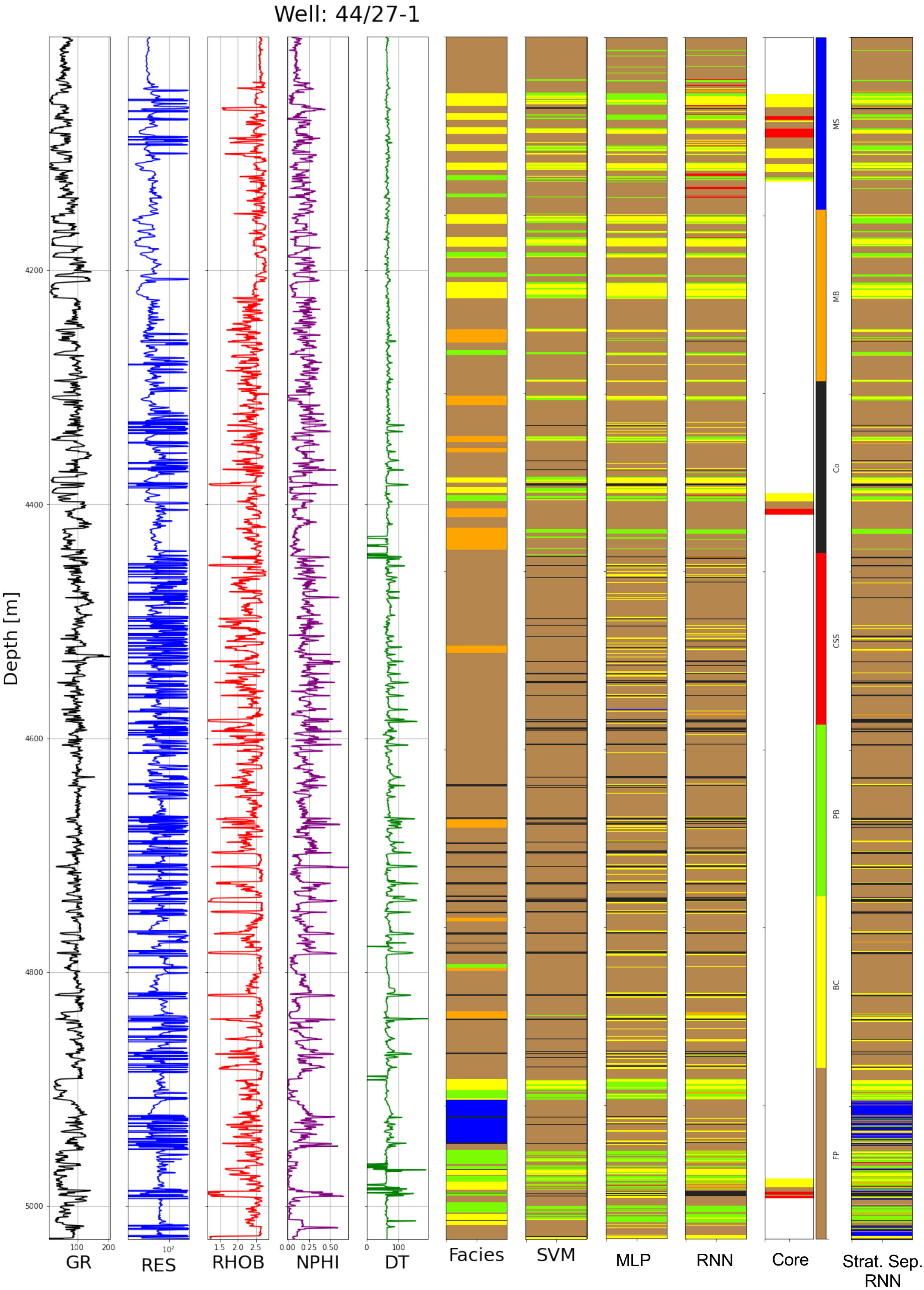

Figure 25. Blind test results for well 44/27-1 using SVM and MLP without stratigraphic separation and using RNN without and with stratigraphic separation.

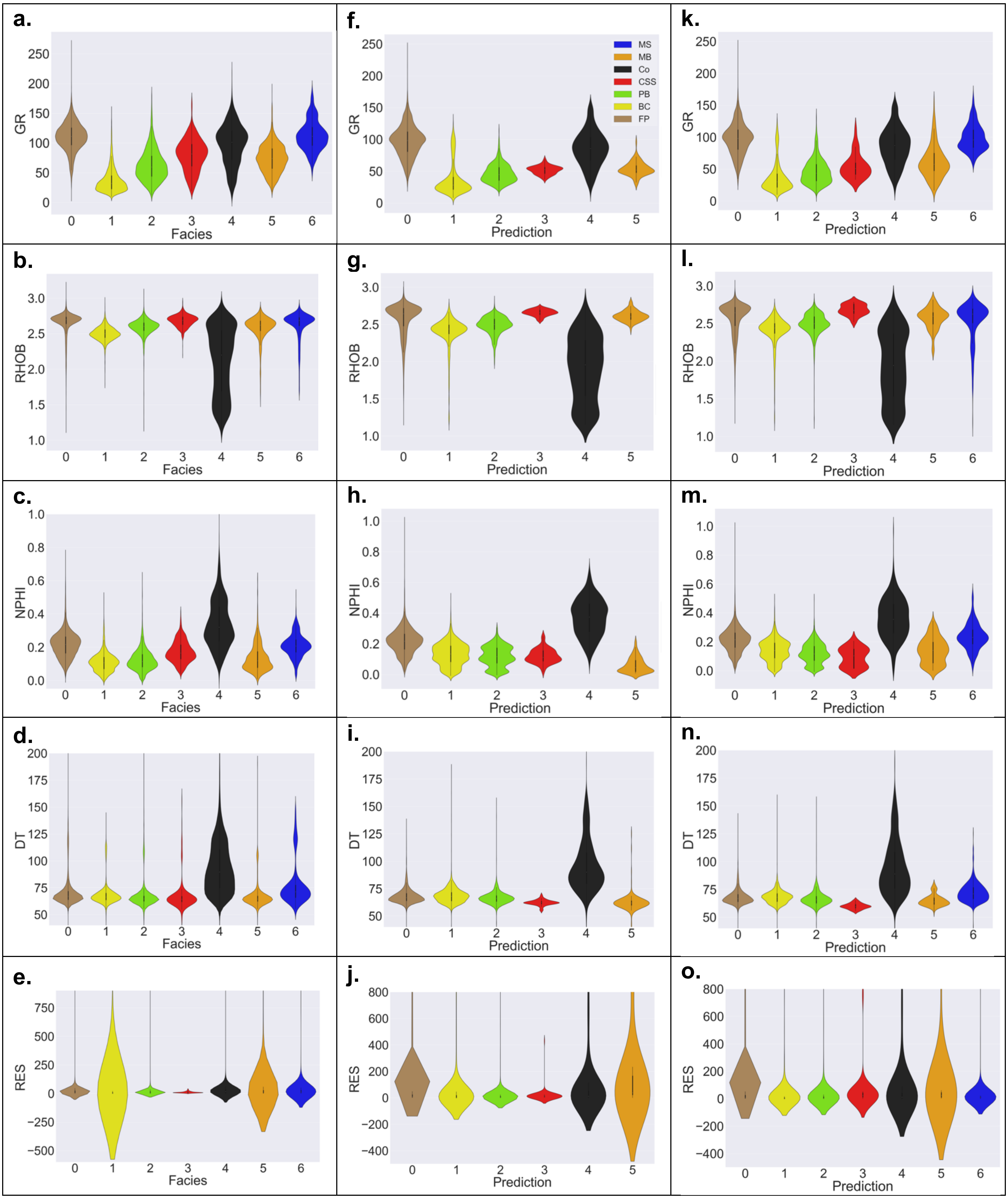

Figure 26. Violin plots showing the statistical distribution of each facies with respect to each wireline log for the input data (a-e), the blind tests' prediction results using RNN without stratigraphic separation (f-j), and the blind tests' prediction results using RNN with stratigraphic separation (k-o).

4 Discussion

The wireline facies associations were reproducing the core lithofacies interpretations with an overall accuracy of 71%. This validation was limited to only 10% of the total downhole log length since core coverage was much shorter than wireline log coverage. Background floodplain and braided channels were more sampled in the core than other facies and thus could be more thoroughly validated. Both of these facies were the most accurately identified by wireline facies associations, where the accuracy of the background floodplain is 88%, and that of the braided channel is 81% (Table 5). On the other hand, the accuracy of mouth bar and marine shale wireline facies associations were less apparent since the cores only sampled mouth bars once and has not sampled marine shales at all. Mouth bar wireline facies associations within cored intervals often corresponded to crevasse splays in the core, while marine shales corresponded to background floodplains. The overlap of mouth bars and crevasse splays can be attributed to the geomorphological termination of crevasse splays into these minor mouth bars. The marine shales and background floodplain overlap is due to the difficulties in identifying marine bands in the offshore data. Thus, it is useful to also view the outputs of facies prediction with the seven facies regrouped into five.

What is referred to in literature as the *class imbalance* problem appears to play a role in this data set and in all classification trials [16][12][23]. Background floodplain facies are grossly overrepresented by comprising 66% of the total data, while other facies are underrepresented, crevasse splay sands 2%, mouth bars 4% and marine shale 2%. As observed, machine learning algorithms tend to focus on the abundant classes to maximize the total accuracy of the classifier [16], which in this case is the background floodplain.

For all three applied machine learning methods, SVM, MLP and RNN, the most occurring facies in the input data, which are the background floodplain, braided channel, point bars, and coal, were more likely to be predicted than the less occurring facies. None of the three methods made predictions for all seven facies. However, the F1 score of the background floodplain facies for all test runs was fixed between 0.88-0.89, but the recurrent neural network method has achieved the highest blind test overall accuracy of 80.9%, due to the higher F1 score values of the braided channel (0.88), point bar (0.60) and coal (0.53). These higher F1 scores for the sands mean that the RNN is better at predicting that an interval is a continuous braided channel or point bar interval instead of an interbedded reservoir units, which has implications on development plans.

To deal with imbalanced class distributions, precision and recall are useful for giving insight into the contribution of each class to the overall accuracy [12]. Numerous methods exist to improve the algorithms predictions abilities for minority classes [12][23]. There is work suggesting that the most favorable approach is to increase the size of the training data [12]. Since this is not always possible, imbalance correcting techniques can also be implemented such as under-sampling, over-sampling, a combination of the two, or ensemble learning [23].

Stratigraphically separating the data into Westphalian A, B and C and applying RNN on each unit independently has led to a lower overall accuracy of 75.6%. The results of this approach show lower F1 scores for the background floodplain (0.86), braided channel (0.81) and point bar (0.47) facies, because of the decrease in number of samples per class after unit separation, but higher F1 scores for mouth bar and marine shale facies. This approach was also able to make predictions for all seven facies. When adjacent facies were considered by grouping mouth bars with crevasse splays, and marine shale with background floodplain, the overall accuracy increased to 78.6%.

Applying RNN to the Westphalian A, B and C separately, appears to have served as a form of an imbalance correction method. This is especially visible in the Westphalian A where the background floodplain comprises 44% of the data and the marine shale comprises 15% resulting in an increase in the F1 score of marine shale from zero to 0.17. Further refinement of these results in future work can apply under-sampling for the background floodplain and over-sampling of the crevasse splay, mouth bar and marine shale facies. The chosen imbalance correcting algorithm must be one that accounts for the dataset's overlapping classes and high dimensionality [24]. The appropriate imbalance correction method has the potential to help eliminate the overshadowing effect of the background floodplain and improve the classifier's predictions of other facies.

Using wireline facies associations can provide the advantage of alleviating data shortage in facies prediction by providing a more extensive input dataset compared to only using core data. However, wireline facies associations are inherently less accurate than core facies associations since they are assigned using measured rock properties, compared core facies associations which are assigned by direct rock examination. When using these wireline facies associations as an input for facies prediction with machine learning, it is essential to bear in mind the added layer of uncertainty this introduces to the results, especially for facies that are less extensively validated or not validated by core data. In the case of the Carboniferous of the Southern North Sea, machine learning with wireline facies associations was shown to be effective in picking the non-reservoir background floodplain units, the coals, and the two best reservoir facies of braided channels and point bars [25]. Applying the approach described in this project to other datasets has the potential of automating a portion of the process of facies picking on well logs. This can be followed by secondary steps of manually refining the results, which can be customized according to each dataset's unique characteristics.

5 Conclusion

Using wireline facies associations as an input for machine learning can provide a more extensive facies prediction training dataset since log coverage is always more plentiful than core data. However, since wireline facies associations are assigned using measured rock properties instead of directly on rocks, the accuracy of this data needs to be quantified with cores before using it as an input for machine learning. Wintershall has manually assigned wireline facies associations to well logs in the Carboniferous of the southern North Sea following a facies scheme comprised of seven facies. The scheme links wireline log characteristics of facies to sediment grain size, body geometry, upper and lower boundaries and sedimentary structures.

The Carboniferous of the southern North Sea has been determined to have untapped exploration and development potential. Facies prediction can be an aid by providing an understanding of the distribution of facies away from cored wells and thus developing a refined understanding of the architecture of the subsurface, fluid volumes and flow. This project was focused on evaluating the accuracy of these wireline facies associations compared to core data, and determining which of the three machine learning algorithms, support vector machine (SVM), multilayer perceptron (MLP) and recurrent neural networks (RNN), would yield the best results for facies prediction.

The wireline facies associations were validated with core facies associations for nine wells resulting in an overall accuracy of 71%. The background floodplain and braided channel were the most accurately validated facies, while the mouth bars and the marine shales were harder to validated because of insufficient core coverage. During the application of facies predictions algorithms, it's important to account for the uncertainty this type of input adds to the results, especially for facies that are less validated or not validated at all by core data.

When these wireline facies associations were used as an input to build SVM, MLP and RNN classifiers, RNN was the most effective in predicting continuous reservoir units and it achieved the highest overall accuracy of 80.9% with the highest F1 scores for braided channels (0.88), point bars (0.60) and coal (0.53). The effect of the class imbalance problem is evident for this data set where the machine learning algorithms are making more predictions for the abundant classes of background floodplain, braided channels, point bars and coals, and little to no predictions for the underrepresented classes of crevasse splays, mouth bars and marine shales. Applying the best performing machine learning algorithm, RNN, to the Westphalian A, B and C separately appears to have performed as a form of imbalance correcting technique that increased the F1 score of the underrepresented facies. Further imbalance correction can be applied in future studies by under-sampling the background floodplain facies and over-sampling the crevasse splay. Doing so has the potential of enhancing the prediction accuracy for the under-represented facies and reducing the dominance of the over-represented floodplain facies. The approach described in this project can be tested on other datasets, which can help in automating part of the process of facies picking on well logs. Depending on the characteristics of each dataset, this process can be followed by post-processing steps to enhance the results.

Bibliography

[1] D. Cameron, J. Munns and S. Stoker, "Remaining hydrocarbon exploration potential of the Carboniferous fairway, UK southern North Sea," in Carboniferous hydrocarbon geology: the southern North Sea and surrounding onshore areas, Yorkshire Geological Society, 2013, pp. 209-224.

[2] Y. Z. Ma, “Facies and Lithofacies Classifications from Well Logs,” in Quantitative Geosciences: Data Analytics, Geostatistics, Reservoir Characterization and Modeling, Denver, CO: Springer, 2019, pp. 231-254.

[3] J. H. Doveton, Principles of mathematical petrophysics. Oxford: Oxford University Press, 2014.

[4] J. M. Cole, M. Whitaker, M. Kirk and S. Crittenden, "A sequence-stratigraphy scheme of the Late Carboniferous, southern North Sea, Anglo-Dutch sector," in Carboniferous hydrocarbon geology: the southern North Sea and surrounding onshore areas, Vols. 7, J. D. Collinson, D. J. Evans, D. W. Holliday and N. S. Jones, Eds., Yorkshire Geological Society, 2005, pp 75-104.

[5] P. T. O'mara, “Correlation, facies distribution and sequence stratigraphic analysis of the Westphalian B coal measures in quadrant 44 of the southern North Sea,” Durham theses, Durham University E-Theses Online: http://etheses.dur.ac.uk/5359/, 1995.

[6] D. Cameron, J. Munns, and S. Stoker, “Remaining exploration potential of the Carboniferous fairway, UK Southern North Sea,” in Carboniferous hydrocarbon geology: the southern North Sea and surrounding onshore areas, vol. 7, Yorkshire Geologic Society, 2013, pp. 209–224.

[7] S. Learn, "Compare the effect of different scalers on data with outliers," 2007-2020. [Online]. Available: https://scikit-learn.org/stable/auto_examples/preprocessing/plot_all_scaling.html#sphx-glr-auto-examples-preprocessing-plot-all-scaling-py.

[8] Scikit Learn, "Support Vector Machines," 2007-2020. [Online]. Available: https://scikit-learn.org/stable/modules/svm.html.

[9] J. Heaton, Introduction to Neural Networks for Java, Chestfield: Heaton Research, Inc, 2002-2015.

[10] B. Hall, “Facies classification using machine learning,” The Leading Edge, vol. 35, no. 10, pp. 906–909, 2016.

[11] E. Puskarczyk, “Artificial neural networks as a tool for pattern recognition and electrofacies analysis in Polish palaeozoic shale gas formations,” Acta Geophysica, vol. 67, pp. 1991–2003, Sep. 2019.

[12] D. Schaeffer and T. Maddix, "Xilinx," 2020. [Online]. Available: https://developer.xilinx.com/en/articles/exploring-support-vector-machine-acceleration-with-vitis.html.

[13] M. K. Dubois, G. C. Bohling, and S. Chakrabarti, “Comparison of four approaches to a rock facies classification problem,” Computers & Geosciences, vol. 33, pp. 599–617, 2007.

[14] Scikit Learn, "Neural Netwrok Models (supervised)," 2007-2020. [Online]. Available: https://scikit-learn.org/stable/modules/neural_networks_supervised.html.

[15] I. Farley, "SEG Wiki," Society of Exploraiton Geophysicists, 2017. [Online]. Available: https://wiki.seg.org/wiki/User:Ifarley/Facies_classification_using_Neural_Network_algorithm.

[16] J. Brownlee, "Machine Learning Mastery," 2018. [Online]. Available: https://machinelearningmastery.com/when-to-use-mlp-cnn-and-rnn-neural-networks/.

[17] J. Brownlee, "Machine Learning Mastery," 2016. [Online]. Available: https://machinelearningmastery.com/crash-course-recurrent-neural-networks-deep-learning/.

[18] R. Feng, "Lithos_GRU," GitHub, 2020. [Online]. Available: https://github.com/RhFeng.

[19] K. Cho, B. van Merrienboer, C. Gulcehre, D. Bahdanau, F. Bougares, H. Schwenk and Y. Bengio, "Learning Phrase Representations using RNN Encoder–Decoder for Statistical Machine Translation," Cornell University, vol. 1, 2014.

[20] D. Harlianto, S. Mardiyati and D. Lestari, "The comparison between recurrent neural network and grey model to predict Indonesia tuberculosis morbidity rate," Journal of Physics: Conference Serie, no. 1722, 2021.

[21] R. Prati, G. Batista and M. Carolina Monard, "Data Mining with Imbalanced Class Distributions: Concepts and Methods," in Indian International Conference on Artificial Intelligence, 2009.

[22] B. Juba and H. S. Le, "Precision-Recall versus Accuracy and the Role of Large Data Sets," in The Thirty-Third AAAI Conference on Artificial Intelligence, 2018.

[23] G. Lemaître, F. Nogueira and C. K. Aridas, "Imbalanced-learn: A Python Toolbox to Tackle the Curse of Imbalanced Datasets in Machine Learning," Journal of Machine Learning Research, vol. 7, pp. 1-5, 2016.

[24] S. Maldon, J. López and C. Vairetti, "An alternative SMOTE oversampling strategy for high-dimensional datasets," Applied Soft Computing Journal, vol. 76, pp. 380-389, 2019.

[25] R. Huis In't Veld, B. Schrijver and A. Salzwedel, "The Wingate Field, Blocks 44/23b, 44/24b and 44/19f, UK North Sea," in United Kingdom Oil and Gas Fields: 50th Anniversary Commemorative Volume, London, The Geological Society of London, 2020, pp. 1-16.

Appendices

Appendix A: Wireline Facies Associations Statistics

Figure A1. Statistics of the floodplain facies in the training data.

	GR	RES	DEN	NPHI	DT	POTA	THOR	URAN
count	33221	33221	33221	33221	33221	30077	30077	30077
mean	110.41	49.40	2.64	0.22	72.07	3.03	9.96	2.39
std	23.85	211.05	0.19	0.08	17.28	4.80	8.18	2.86
min	8.25	0.00	1.16	0.01	0.00	-0.38	-1.38	-137.59
25%	96.96	8.09	2.64	0.16	64.08	0.02	5.75	0.04
50%	111.25	13.93	2.70	0.22	67.12	1.45	10.97	2.67
75%	125.47	23.43	2.74	0.26	71.76	2.61	13.66	3.74
max	267.00	2341.85	3.18	0.77	288.74	34.03	574.00	13.49

Figure A2. Statistics of the braided channel facies in the training data.

	GR	RES	DEN	NPHI	DT	POTA	THOR	URAN
count	5710	5710	5710	5710	5710	5329	5329	5329
mean	37.31	290.15	2.50	0.11	68.57	0.77	3.85	0.88
std	20.24	1625.36	0.10	0.06	11.36	1.82	3.30	1.07
min	9.80	0.00	1.77	-0.01	0.00	-0.15	0.00	-1.91
25%	23.01	1.34	2.45	0.07	63.79	0.01	1.74	0.11
50%	31.93	2.94	2.50	0.11	66.40	0.13	2.95	0.74
75%	45.08	9.07	2.56	0.14	69.87	0.58	4.68	1.31
max	154.40	9993.02	2.98	0.51	140.96	15.67	22.27	16.63

Figure A3. Statistics of the point bar facies in the training data.

	GR	RES	DEN	NPHI	DT	POTA	THOR	URAN
count	4333	4333	4333	4333	4333	4006	4006	4006
mean	63.19	18.64	2.59	0.12	67.74	1.49	5.93	1.48
std	26.65	86.51	0.13	0.07	15.22	2.79	4.18	1.41
min	11.87	0.00	1.17	0.00	0.00	-0.24	0.00	-2.47
25%	44.15	4.29	2.54	0.08	62.55	0.01	2.67	0.21
50%	59.62	8.31	2.60	0.11	64.59	0.59	5.24	1.30
75%	78.07	16.84	2.65	0.16	67.33	1.27	8.40	2.32
max	184.60	2007.18	3.08	0.63	288.29	16.45	26.48	8.19

Figure A4. Statistics of the crevasse splay sands facies in the training data.

	GR	RES	DEN	NPHI	DT	POTA	THOR	URAN
count	874	874	874	874	874	853	853	853
mean	79.84	11.40	2.68	0.17	68.20	2.80	7.77	1.82
std	26.88	7.12	0.08	0.06	15.75	3.99	4.65	1.53
min	19.20	1.27	2.20	0.04	42.28	0.00	0.75	-1.20
25%	61.33	6.75	2.63	0.13	61.93	0.03	3.20	0.03
50%	81.85	9.50	2.69	0.16	64.36	1.19	8.02	1.89
75%	97.83	14.19	2.73	0.21	66.93	2.30	11.34	2.90
max	170.75	40.69	2.96	0.41	158.99	19.21	21.30	8.00

Figure A5. Statistics of the coal facies in the training data.

	GR	RES	DEN	NPHI	DT	POTA	THOR	URAN
count	2648	2648	2648	2648	2648	2491	2491	2491
mean	96.97	46.36	2.12	0.34	94.82	3.13	8.31	2.25
std	34.21	187.98	0.47	0.14	28.20	4.64	5.66	2.04
min	7.73	0.00	1.16	0.01	0.00	-0.05	0.00	-2.58
25%	72.50	11.01	1.69	0.24	74.86	0.04	2.74	0.03
50%	101.30	19.10	2.20	0.32	89.58	1.37	8.68	2.27
75%	120.31	29.85	2.54	0.44	110.37	2.69	12.76	3.76
max	222.25	2018.61	2.90	1.10	399.12	19.86	27.34	9.89

Figure A6. Statistics of the mouth bars facies in the training data.

	GR	RES	DEN	NPHI	DT	POTA	THOR	URAN
count	2113	2113	2113	2113	2113	1822	1822	1822
mean	74.26	107.77	2.58	0.14	66.88	1.93	6.91	1.81
std	23.53	771.44	0.18	0.08	13.87	3.67	4.48	1.54
min	18.24	0.00	1.55	0.01	0.00	0.00	0.00	-1.58
25%	57.52	6.38	2.54	0.08	62.39	0.02	2.80	0.18
50%	74.19	14.32	2.62	0.12	64.50	0.62	7.14	1.77
75%	90.38	27.48	2.68	0.17	67.20	1.35	9.69	2.85
max	189.40	9993.02	2.87	0.61	191.55	18.21	22.64	7.45

Figure A7. Statistics of the marine shale facies in the training data.

	GR	RES	DEN	NPHI	DT	POTA	THOR	URAN
count	1080	1080	1080	1080	1080	945	945	945
mean	112.80	62.58	2.62	0.21	78.07	1.13	8.33	3.05
std	25.24	246.76	0.20	0.07	20.25	1.18	5.68	2.53
min	48.52	0.00	1.66	0.03	55.36	0.00	0.00	-1.44
25%	96.20	9.41	2.61	0.17	65.94	0.02	3.02	0.00
50%	111.30	14.89	2.69	0.21	71.22	1.11	9.47	3.57
75%	126.47	26.14	2.73	0.24	77.37	2.05	12.46	4.86
max	192.80	2014.41	2.88	0.51	150.07	4.55	20.07	10.22

Appendix B: Tables Linking Core and Log Facies Associations

Table B1. Core description of facies in 44/12a-3. Core was described by Pilling Consultants Limited. Core description legend is in appendix C figure C1.

Core Facies Association	Description	Core Description	Wireline GR 0 200	Comparable Wireline Facies Association & Justification
Lacustrine Floodbasin	Red colored claystone and siltstones interbedded with fine to very fine sandstones with occasional rootlets. Has parallel laminations,	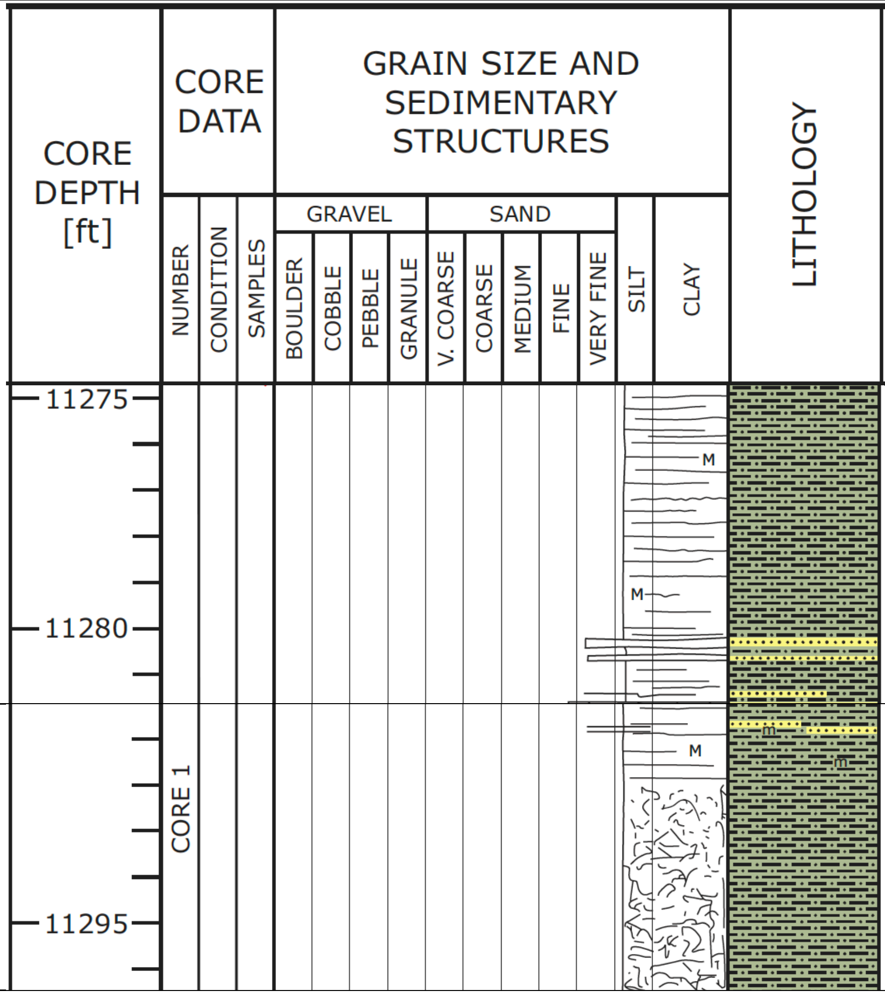	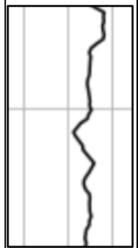	Background Floodplain
Floodbasin/ Interfluve Paleosols	Red colored claystone and siltstones interbedded with fine to very fine sandstones. Either parallel laminated or massive due to pedogenic modification by rootlets.		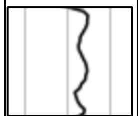	Background Floodplain

Floodbasin Lake	Red colored siltstones with rare interbedding of very fine sandstone.	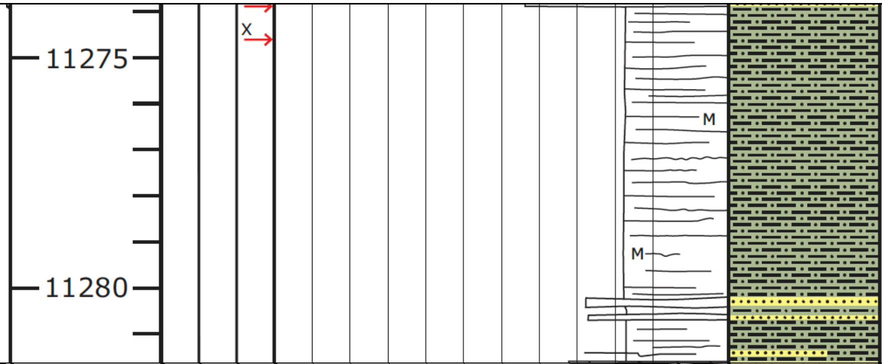	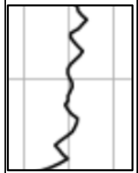	Background Floodplain
Minor Fluvial Channel	Purple to grey colored argillaceous sandstones with thin siltstone interbeds towards the top. Fine, medium and coarse grained, occasionally pebbly. Fining upwards. Moderate to well sorted. Has planar cross stratification and ripple cross-lamination.	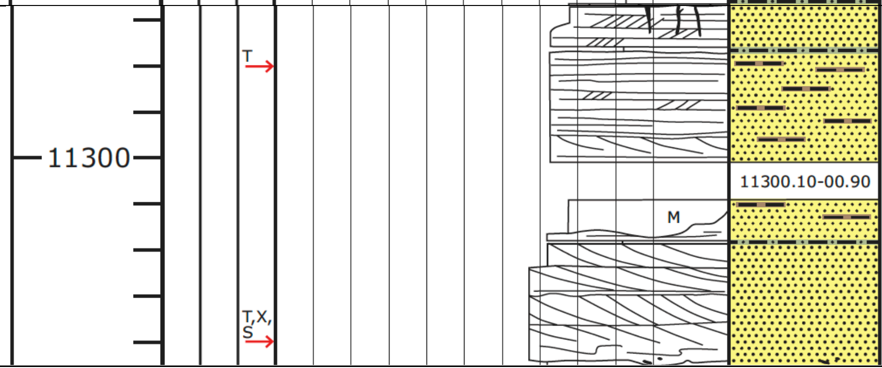		Point Bar: The term minor fluvial channel is used for meandering channels, which, similar to point bars, is composed of argillaceous sandstones as opposed to the clean sands of a braided channel.
Abandoned Channel Fill	Buff/purple colored sandstones or buff/red argillaceous sandstones and green/khaki siltstones. Fine with medium grained pebbles. Coarsening upwards. Sands are moderately to well sorted and have parallel laminations, ripple cross-laminations and trough cross-bedding. Silts are massive or parallel laminated. Contains hematite mottling.	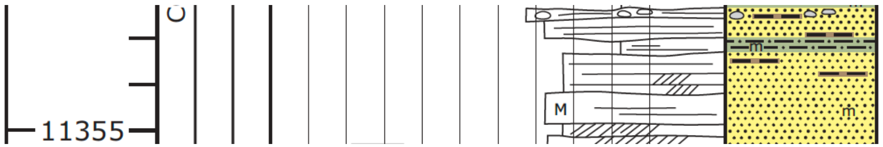	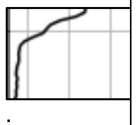	Braided Channel: In this core abandoned channel fills are always picked above fluvial channels where the top sharp gamma ray inflection occurs.

Fluvial Channel	Sandstone of medium to coarse pebbles and conglomerates. Fining upwards. Moderately sorted, with occasionally low angle planar cross-stratification.	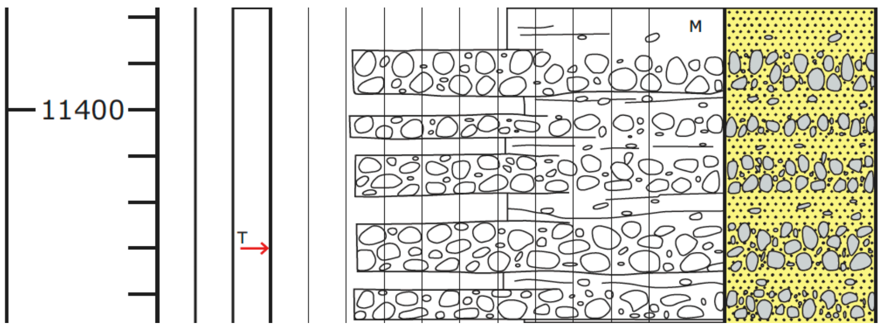	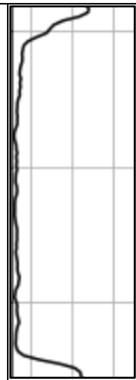	Braided Channel: These fluvial channels have clean, medium to conglomeratic sands with blocky gamma ray signatures, which is matches the definition of a braided channel in the log wireline facies association.
Channel Incision	Grey/buff colored sandstones. Medium grained and pebbly. Flat bedded to massive with hematite mottling.	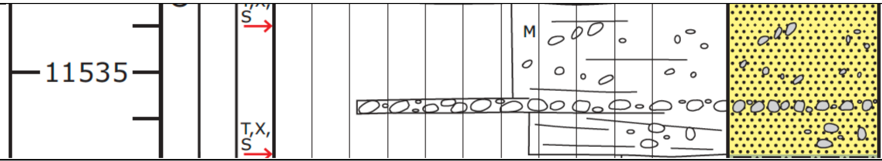	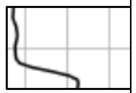	Braided Channel: This unit corresponds to the bottom of a braided channel where the bottom sharp gamma ray inflection occurs.

Table B2. Core description and log signatures of facies in 44/19a-8. Core was described by PanTerra. Core description legend is in appendix C figure C2.

Core Facies Association	Description	Core Description & Core GR	Wireline GR 0 250	Comparable Wireline Facies Association
Well-drained Floodplain	Claystones with rare to no rootlets. Varying from pale to dusky red due to hematite. Structureless or horizontally laminated. Have consistently high gamma ray with no clear pulses.	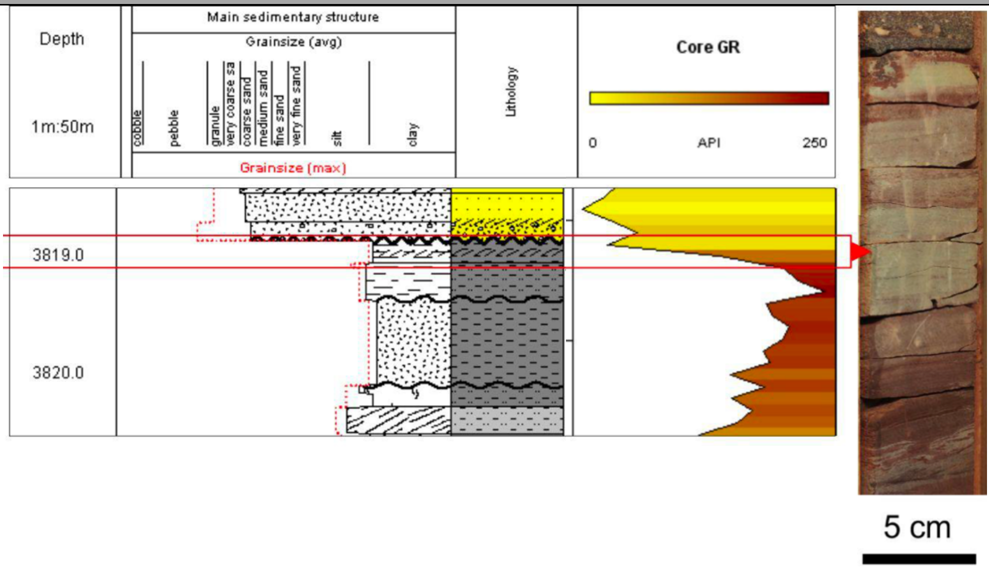	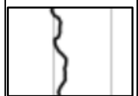	Background Floodplain

Well-drained Floodplain Soil (Rootlet dominated)	Differentiated from well-drained floodplain only by the presence of rootlets, where these intervals are rootlet dominate. Rootlet traces are filled with silt to very fine sand. If structures are present they are disrupted by rootletting. Reddened claystone cause mottling. Some areas are brecciated.	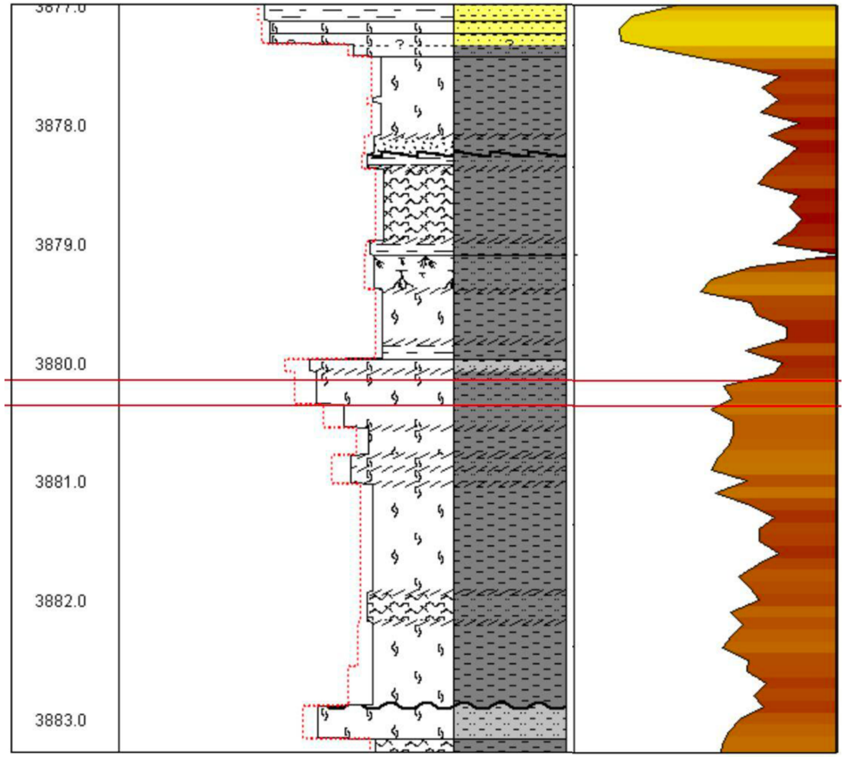 	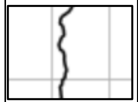	Background Floodplain
Well-Drained Floodplain Soil (some rootlets)	Differentiated from well-drained floodplain only by the presence of rootlets, where these intervals contain some rootlets.	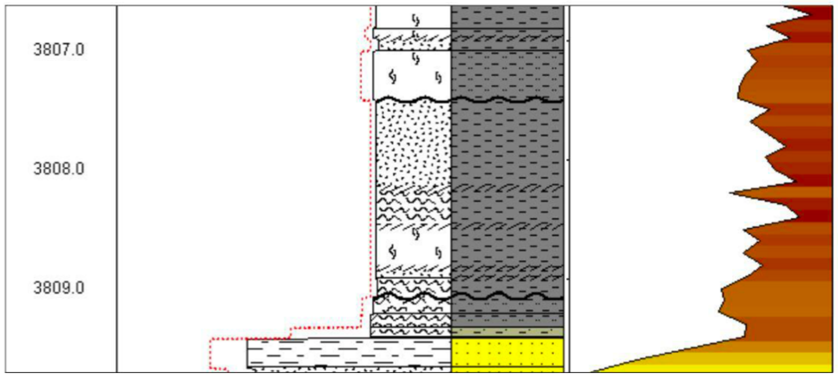	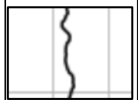	Background Floodplain

Crevasse Channel	Sandstone and claystone red in color due to hematite concretions. Fine grained with fining upwards sequence. Contain hematite cement and relatively high clay content, even in sandier deposits, making it a very poor reservoir. Mostly irregular or mottled but can contain horizontal laminations and cross-beddings. Has bell-shaped gamma ray, but smaller and less distinct than that of meandering channels.	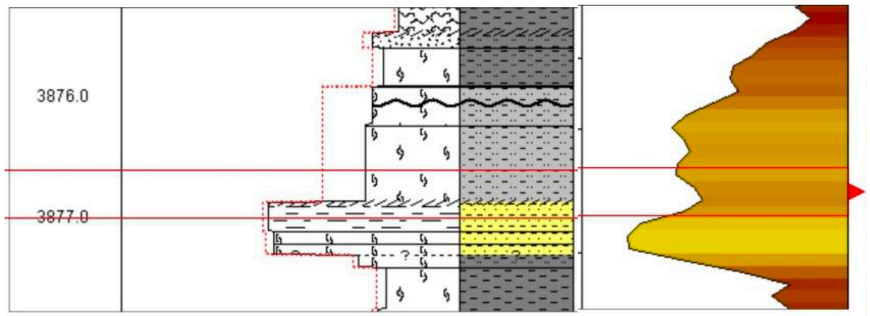		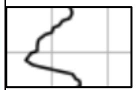	Crevasse Splay Sands

Braided Channel	Predominantly quartzite sandstone with less commonly claystone interclasts. Fine grains to conglomeratic pebbles exceeding 10 cm in diameter. Lacks continuous grading due to sand maturity. Cross-bedded, laminated or structureless. Has a blocky gamma ray.	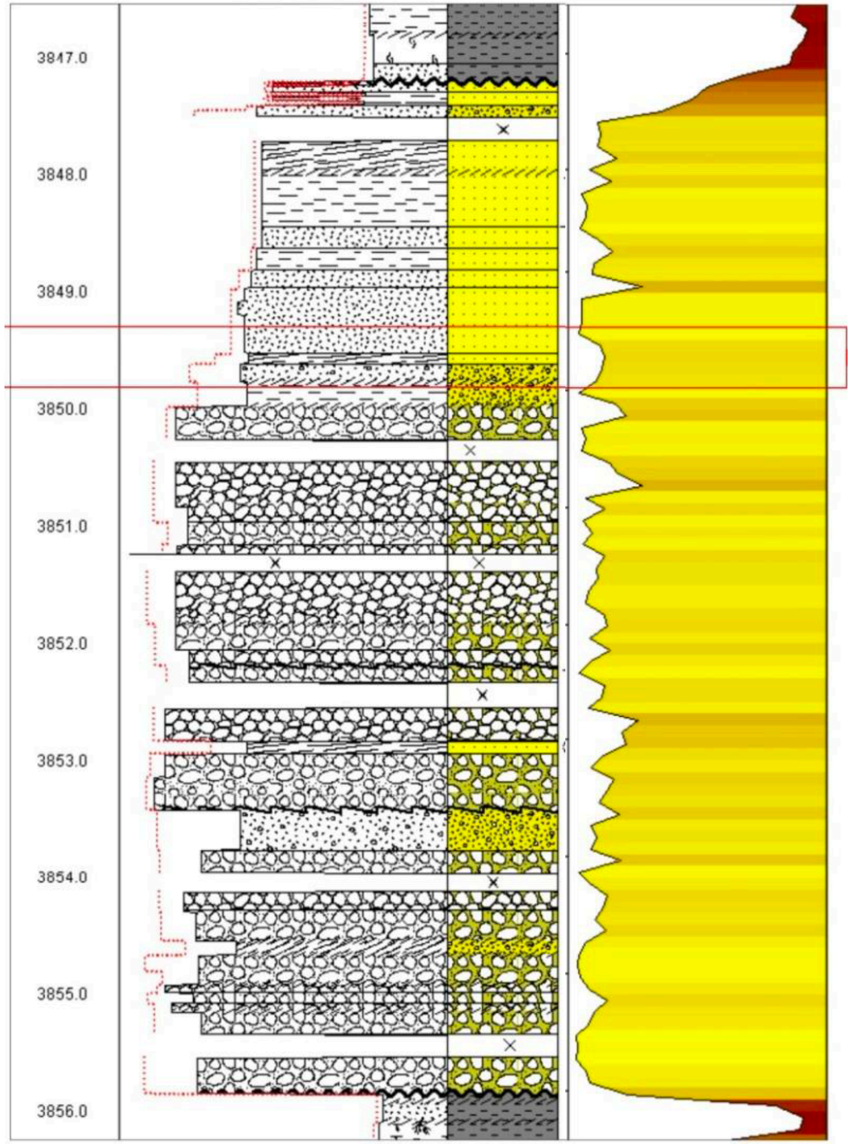		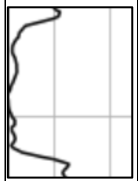	Braided Channel

Meandering Channel	Sandstones and clays. Erosional basal contact and increased clay content upwards. Conglomeritic to clay-dominated. Pebbles are rare and relatively small compared to braided channels. Typically fining upwards but grading is not always well-developed. Horizontal laminations, cross-bedding and structureless. Gamma ray is bell shaped.	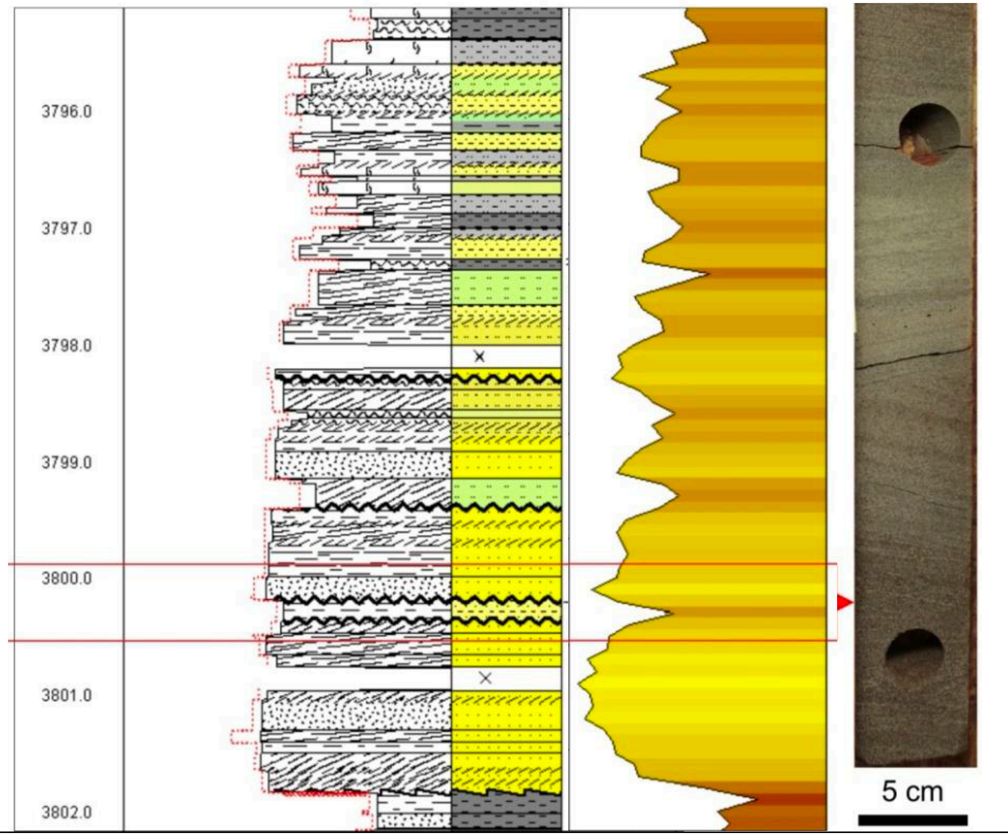	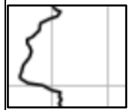	Point Bar

Table B3. Core description of facies in 44/23-9. Core was described by Poroperm Geochem Limited. Core description legend is in appendix C figure C3.

Core Facies Association	Description	Core Description	Wireline GR (0 – 150)	Comparable Wireline Facies Association
Seat Earth	Dark grey silty claystone with siderite and pyrite. Can contain thin coal streaks and rootlets. Has parallel laminations.	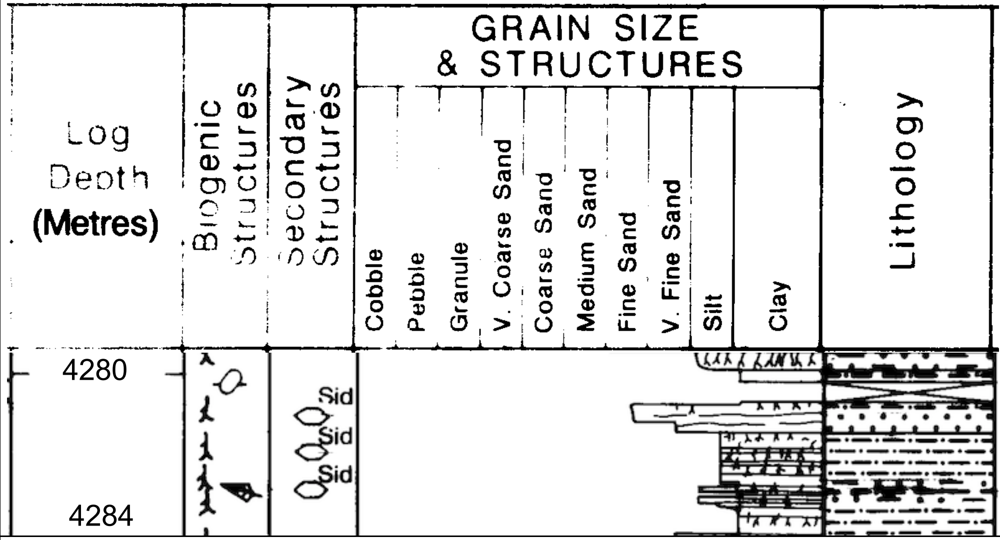	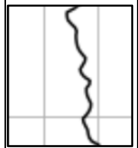	Background Floodplain
Crevasse Splay	Pale grey, mica-rich, argillaceous sandstones. Very fine to fine grains. Fining upwards. Moderate to well sorted. Contains ripples, cross laminations, parallel laminations, tabular and trough cross laminations.		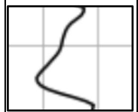	Crevasse Splay Sands
Lacustrine/ Inter-distributary Bay	Dark grey silt to very find sand and argillaceous siltstone with siderite. Parallel laminations and current ripple cross laminations.	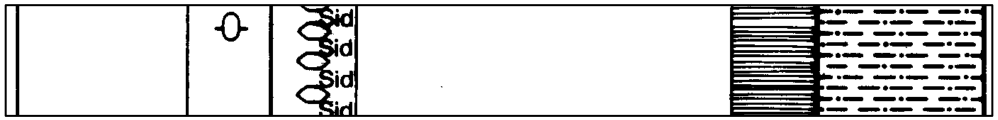	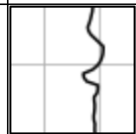	Background Floodplain
Swamp (Coal)	Alternating black bands of clarain and fusain and some layers rich in pyrite.		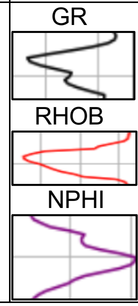	Coal

			DT 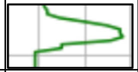	
Distributary Channel (low to moderate sinuosity) Multistory Fluvial Channel (low sinuosity)	Sandstone ranging from fine and medium grains to very coarse pebbles. Rip-up clasts at the base. Overall fining upwards. Moderate to well sorted. Horizontal and planar cross laminations, ripple cross laminations and parallel laminations.	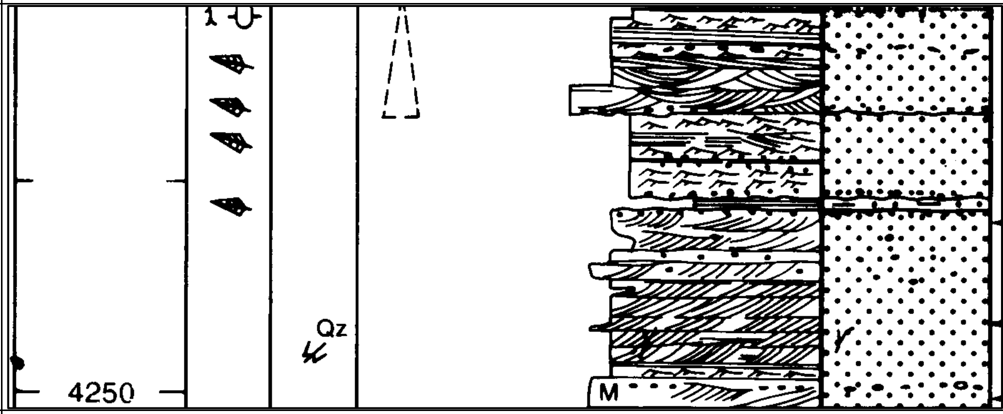	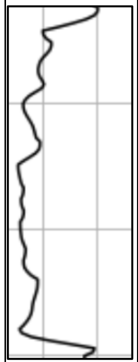	Braided Channel
Channel Abandon-ment	Buff/grey sandstone of fine to medium grains with pebbles at the base. Fining upwards. Well sorted. Cross lamination, trough cross lamination, sub-horizontal parallel laminations.	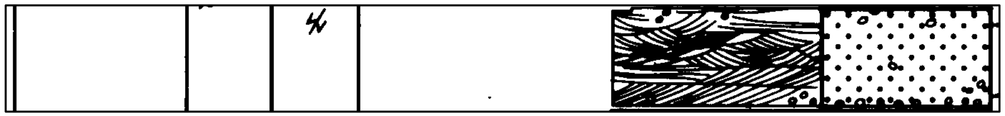		Braided Channel: In this core channel abandonments are always picked as the top of a braided channel where the sharp gamma ray inflection occurs.
Avulsion Unit	Sandstone ranging from fine and medium grains to very coarse. Upward fining profile. Poorly sorted. Tabular cross laminations and parallel laminations.		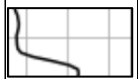	Braided Channel: Avulsion units are picked at the bottom of fluvial channels where the sharp gamma ray inflection occurs.

Table B4. Core description of facies in 44/24-4. Core was described by The Geochem Group. Core description legend is in appendix C figure C4.

Core Facies Association	Description	Core Description	Wireline GR 0 250	Comparable Wireline Facies Association
Fluvial Channel	Sandstone of fine, medium, coarse grains and pebble conglomerates. Poorly to moderately sorted. Horizontal and sub-horizontal laminations, cross stratification	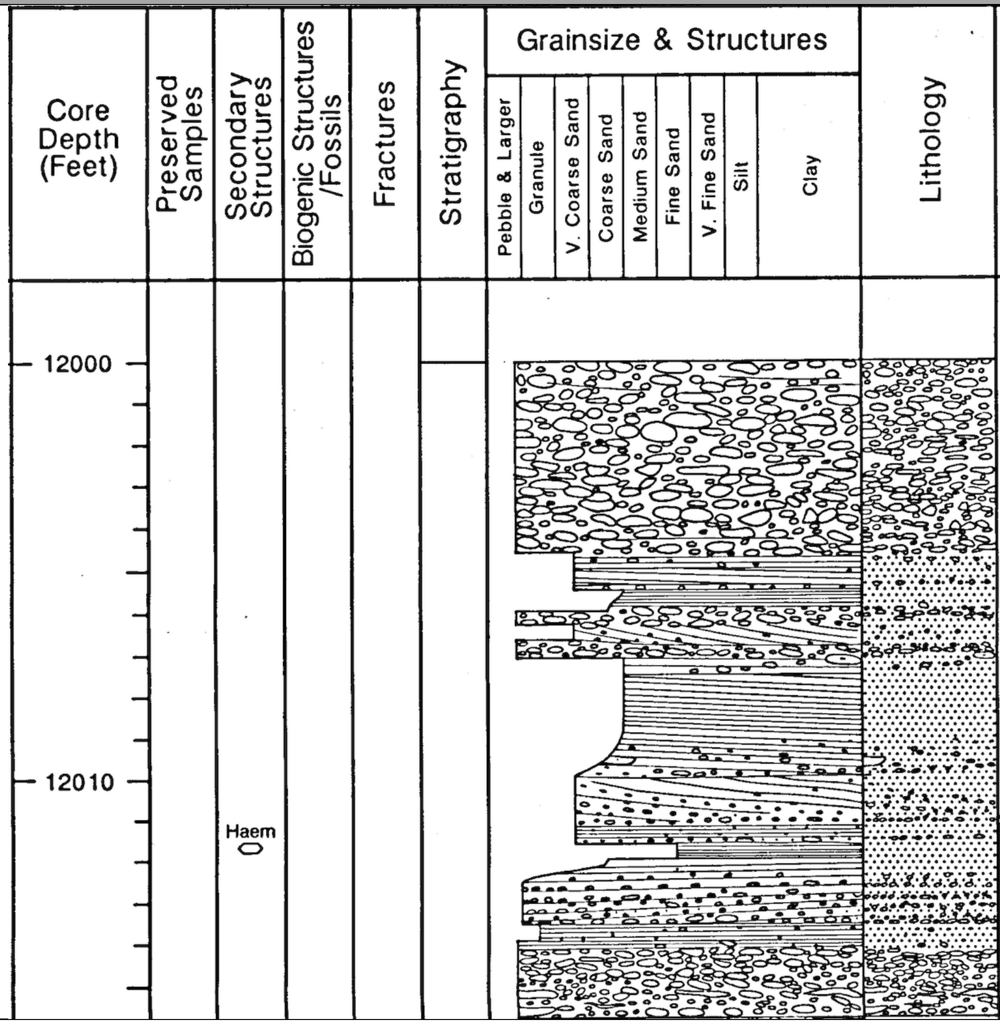	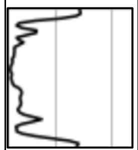	Braided Channel

Vegetated Floodplain Fines	Red-brown, grey-brown sandy siltstone. Moderately to poorly sorted. Can be mottled.	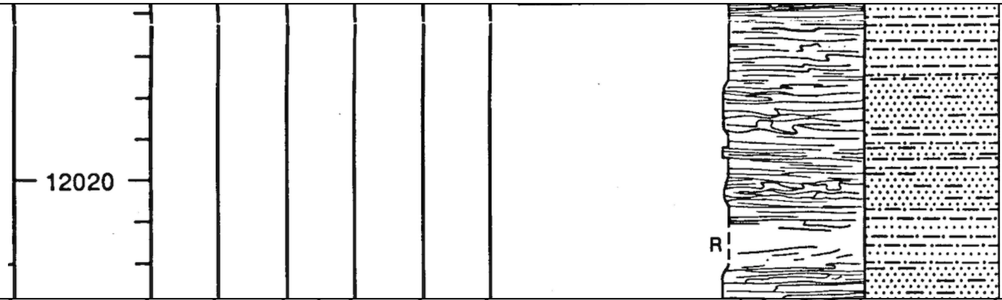		Background Floodplain
Well-drained Paleosols	Brown-red-purple sandy siltstone with rootlets. Can be mottled.	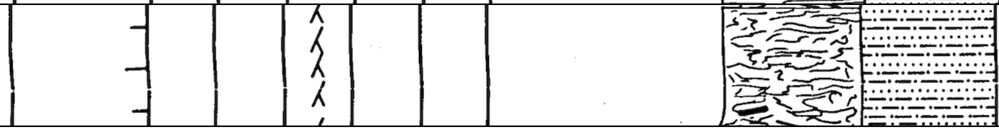		Background Floodplain
Crevasse Splay Sandstones	Purple/red/ brown sandstones with siltstone. Very fine, fine and medium grains. Moderately to poorly sorted. Horizontal laminations.		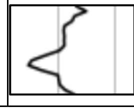	Crevasse Splay Sands

Table B5. Core description of facies in 44/27-1. Core was described by Poroperm Geochem Limited. Core description legend is in appendix C figure C5.

Core Facies Association	Description	Core Description	Wireline GR 0 200	Comparable Wireline Facies Association
Abandon-ment	Dark red hematite stained mudstones, sandy siltstones or purple-grey sandstone. Can be mottled, brecciated or bioturbated.	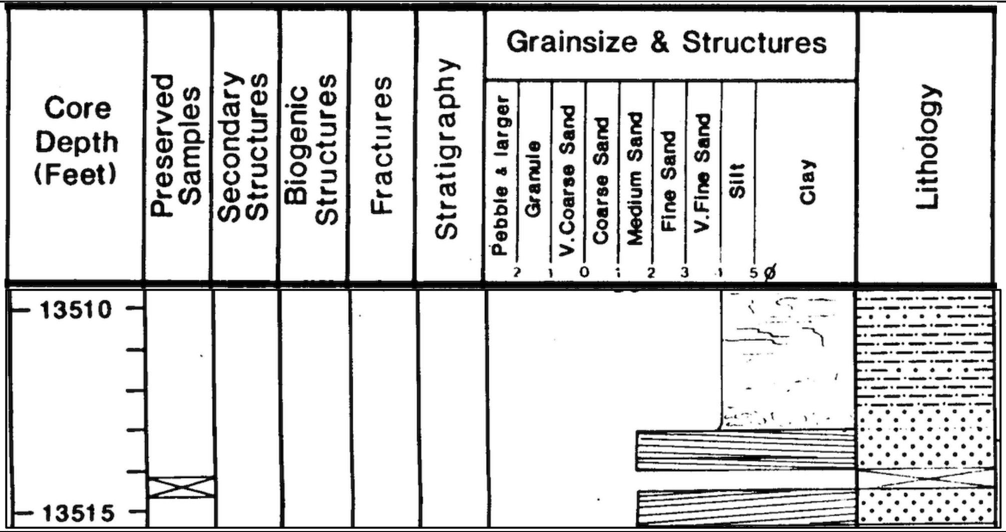	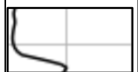	Braided Channel: Channel abandonments have been picked in the core as the top or bottom of a channel where gamma ray inflections occur.

Fluvial Channel (low sinuosity)	Sandstone of fine, medium, coarse and pebbly grains. Overall fining upwards. Poorly sorted. Planar cross-stratification	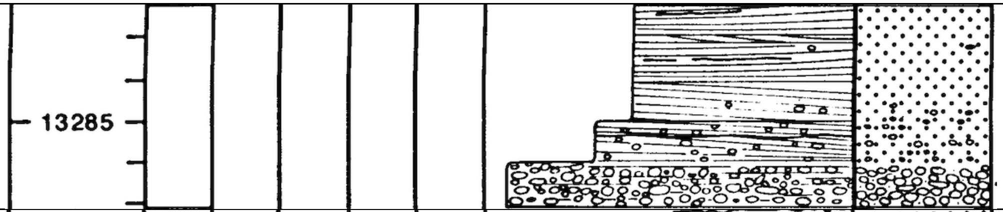	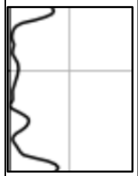	Braided Channel
Minor Fluvial Channel	Pink-grey fine sandstones. Deformed and diagenetically banded or with low-angle cross-stratification.	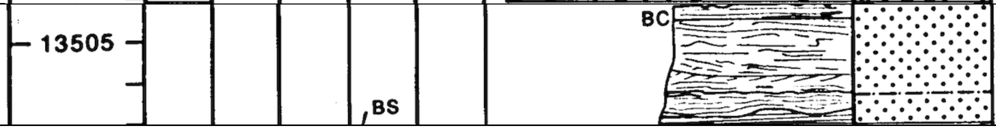		Point Bar: Corresponds to a bell shaped gamma ray characteristic of a point bar in a meandering channel.
Floodbasin	Sandstones, siltstones and claystone with rootlets. Clay-size and very fine grains. Can be leached and mottled.	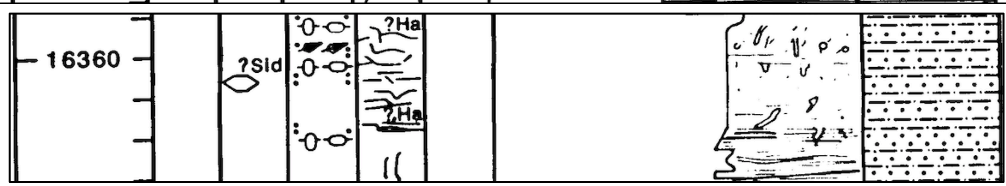	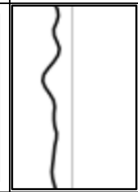	Background Floodplain
Low Energy Sheetfloods	Micaceous sandstones and siltstone. Very fine to fine. Generally flat bedded with some ripple lamination.	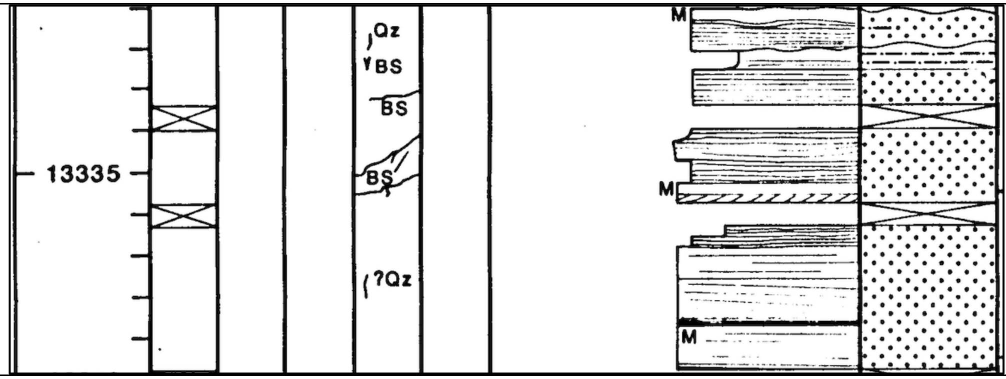		Crevasse Splay Sands: The core description shows low energy sheet floods as a series of fining upwards packages of silty sandstone where each has a bell-shaped gamma ray resembling those of crevasse splays.

Major Axis Sheetfloods (high energy)	Grey sandstones with siltstones. Fine to medium grains. Well sorted. Horizontal stratification.	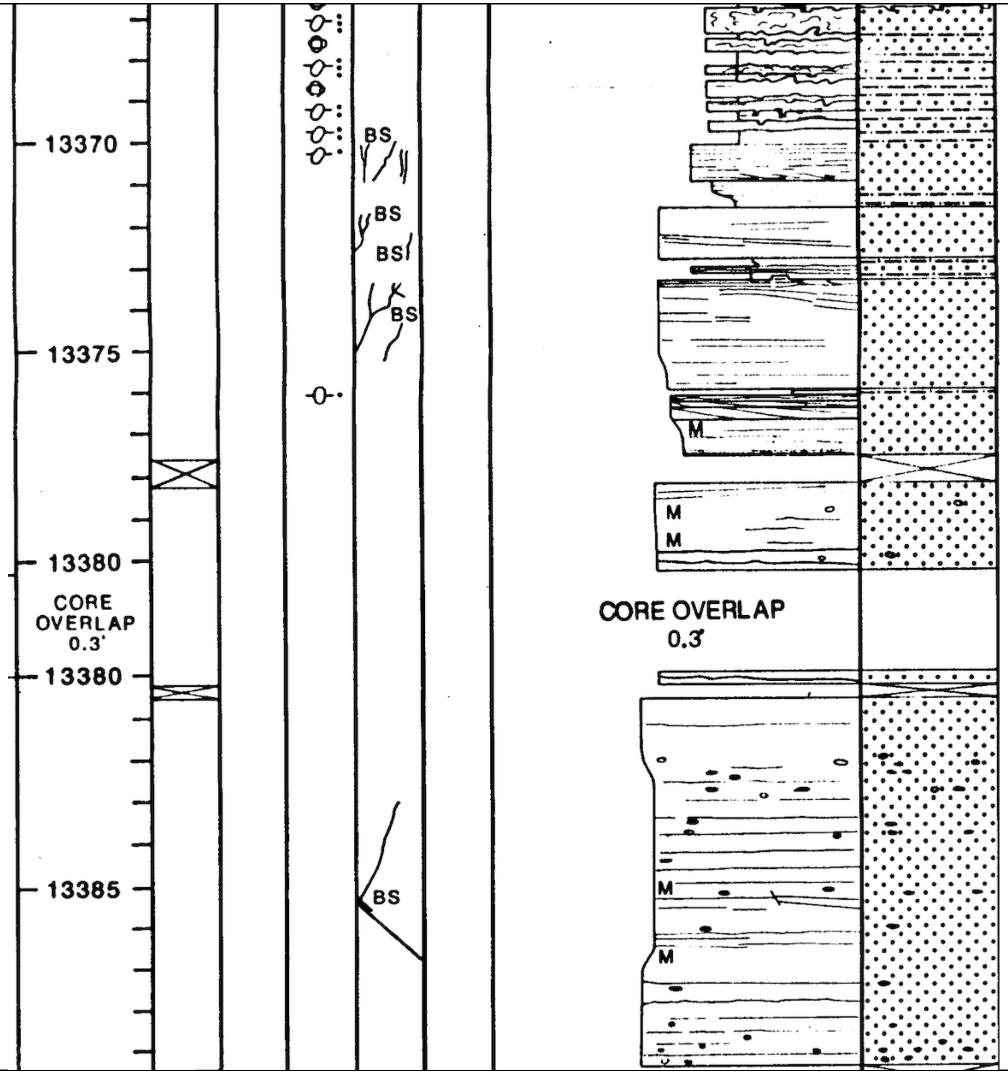	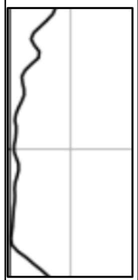	Crevasse Splay Sands: This sheet flood is composed of a series of stacked crevasse splays with a bell shaped gamma ray profile.
Lake	Black and dark grey siltstones and sandstones with plant debris. Very fine grains.	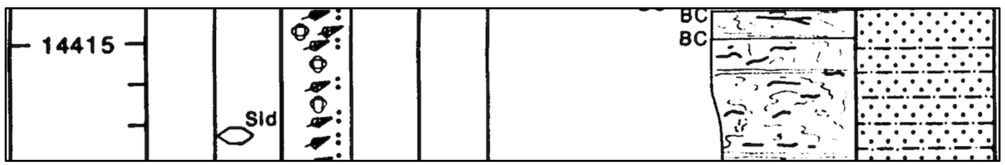	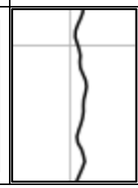	Background Floodplain

Crevasse Splay	Grey sandstone. Very fine and fine. Ripple-laminated.	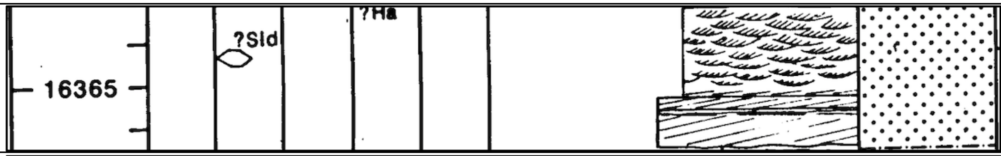		Crevasse Splay Sands
Seat Earth	Mid grey sandstone with probable roots and burros. Very fine grains. Churned texture.	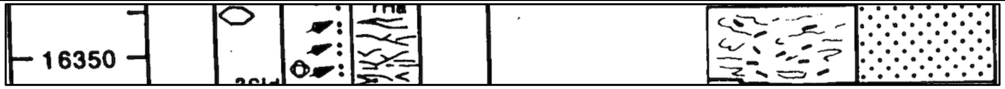		Background Floodplain

Table B6. Core description of facies in 49/1-3. Core was described John Collinson Consulting. Core description legend is in appendix C figure C6.

Core Facies Association	Core Description	Core Description	Wireline GR 0 250	Comparable Wireline Facies Association
Channel	Sandstone of fine to very coarse pebbles. Poor to well sorted with cross bedding.	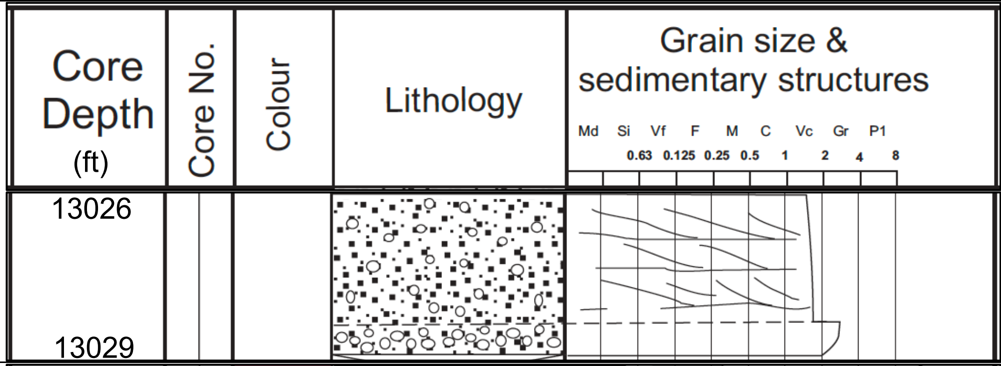	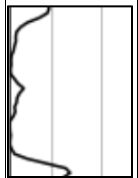	Braided Channel
Lake (Dysoxic)	Mudstone and siltstone with rootlets. Horizontal laminations and bioturbations.	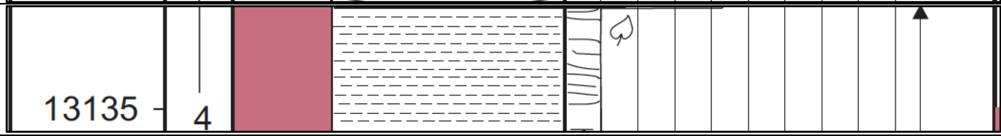	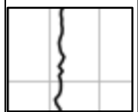	Background Floodplain
Paleosols /Floodplains	Dark red mudstone and siltstones with rootlets. Can have an evolved pedogenic texture and grey mottles.	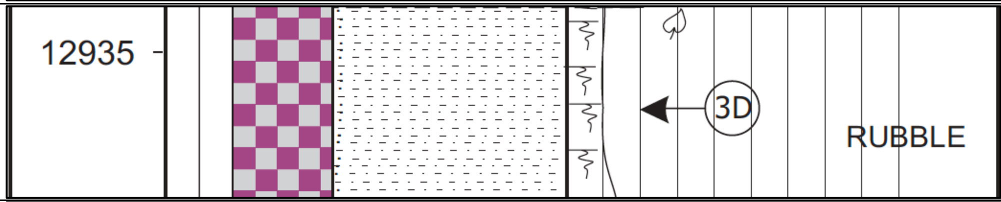	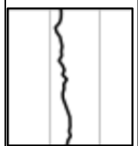	Background Floodplain
Crevasse Splay	Sandstone and mudstone. Very fine to fine. Moderate to well sorted. Ripple cross laminations.	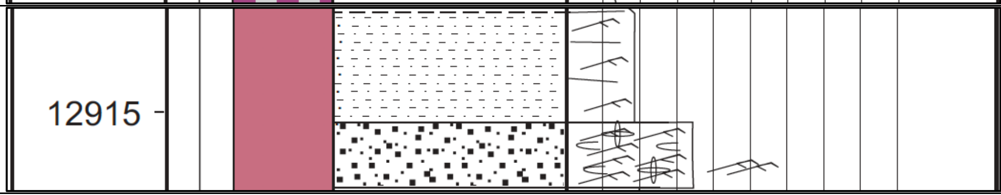	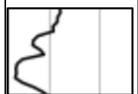	Crevasse Splay Sands.

Mouth Bar	Sandstone and mudstone. Very fine grains. Moderate to well sorted. Sandstones have ripple cross lamination. Mudstones have and wavy lamination and ripple cross laminations. Both contain bioturbations.	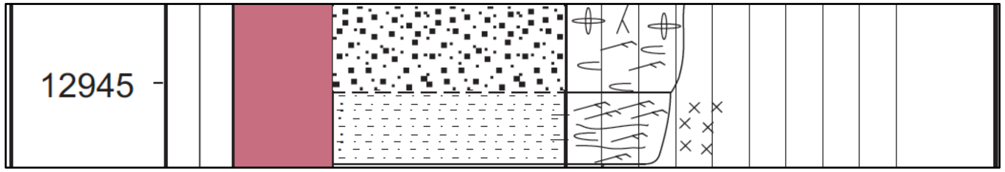		Mouth Bar

Table B7. Core description of facies in E10-3 as described by PanTerra. The core in well D15-FA101 was also described by PanTerra with the same classification. Core description legend is in appendix C figure C7.

Core Facies Association	Description	Core Description	Wireline GR 0 200	Comparable Wireline Facies Association
Well Drained Floodplain	Overall reddish sandy claystone thoroughly rouletted. Mottled. May have a brecciated appearance.	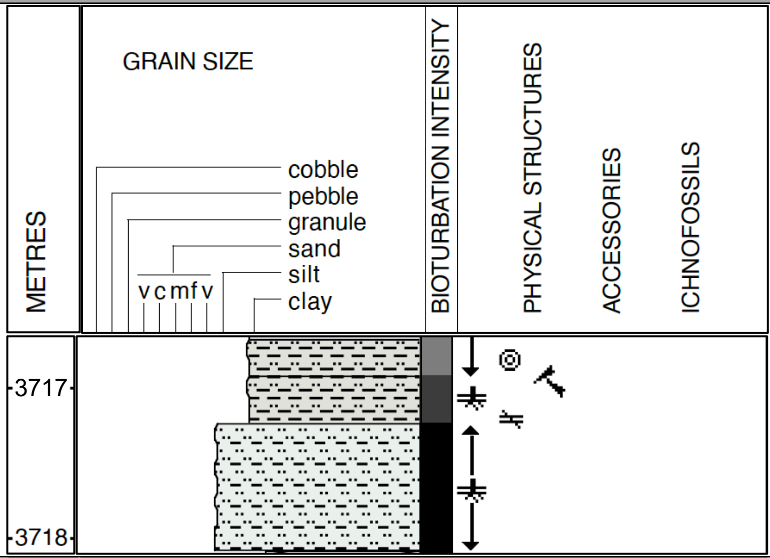	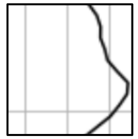	Background Floodplain
Poorly Drained Floodplain	Dark grey to black claystone with rootlets and siderite nodule and organic matter.	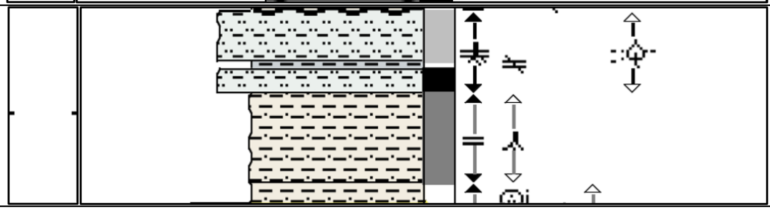	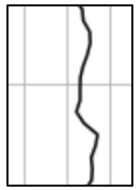	Background Floodplain

Crevasse Splay	Sandstone with clay. Very fine to fine grains. Poorly to moderately sorted. Ripple laminations.	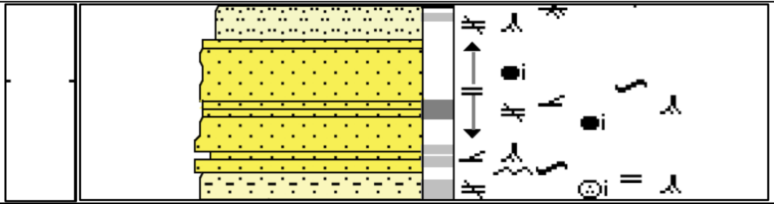	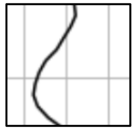	Crevasse Splay Sands
Inter-distributary Bay	Dark grey claystone with few silt and sand. May contain yellowish siderite cement. Parallel laminations.	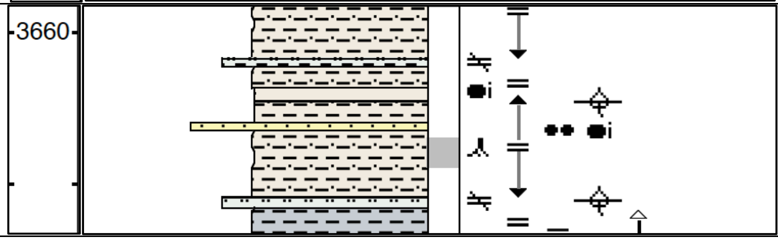	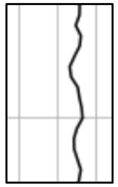	Background Floodplain
Braided Channel Complex	Sandstone of fine, medium and pebble size. Generally fining upwards. Very poor to moderate. Alternations of massive, cross beddings, horizontal laminations and ripple laminations.	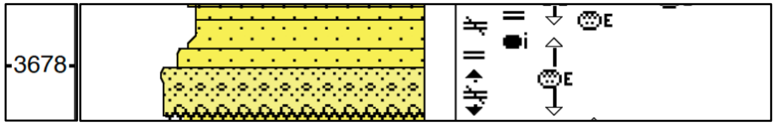	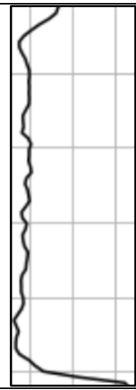	Braided Channel
Coal	Abundant in organic material. Associated with the poorly drained floodplain facies.	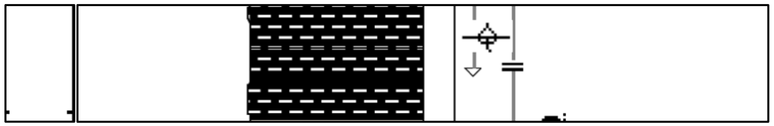	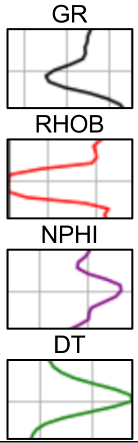	Coal

Table B8. Core description of facies in 44/29-3.

Core Facies Association	Description	Core Description	Wireline GR 0 150	Comparable Wireline Facies Association
Lacustrine	Claystone and siltstones. Structureless.	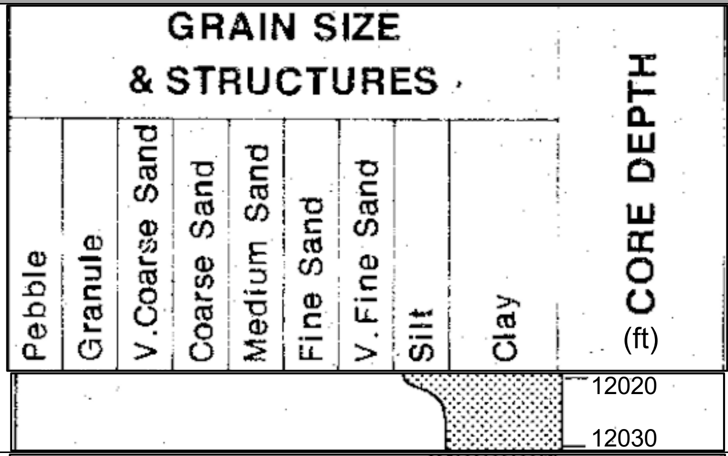	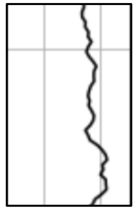	Background Floodplain
Crevasse Splay	Silt to very fine sand. Silt size to very fine. Ripple laminations and bioturbations.	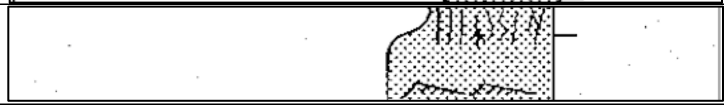	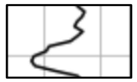	Crevasse Splay Sands
Fluvial Channel	Sandstone of fine to granular particle size. Trough cross bedding, horizontal laminations.	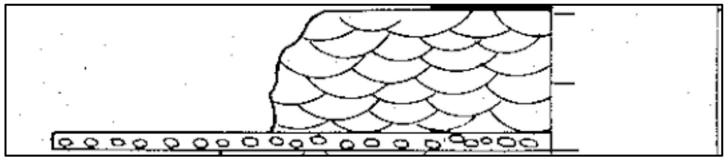	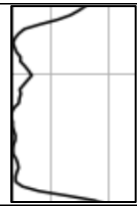	Braided Channel
Swamp	Claystone. Structureless or graded bedding.		high GR.	Background Floodplain
Coal	-	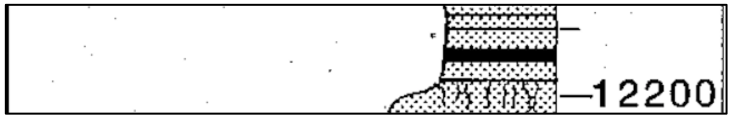	GR 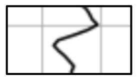 RHOB 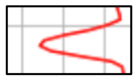 NPHI 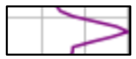 DT 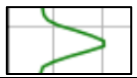	Coal

Appendix C: Core Description Legends

Figure C1. Core description legend for 44/12a-3.

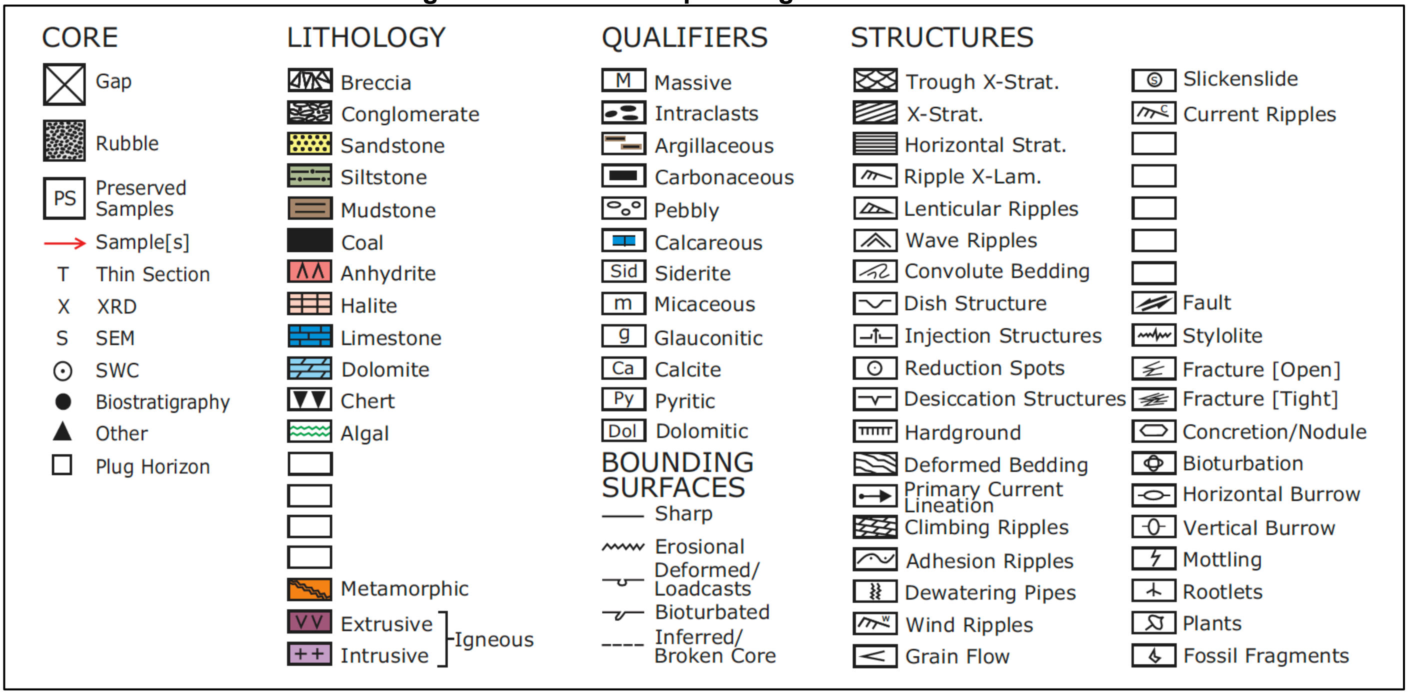

Figure C2. Core description legend for 44/19a-8.

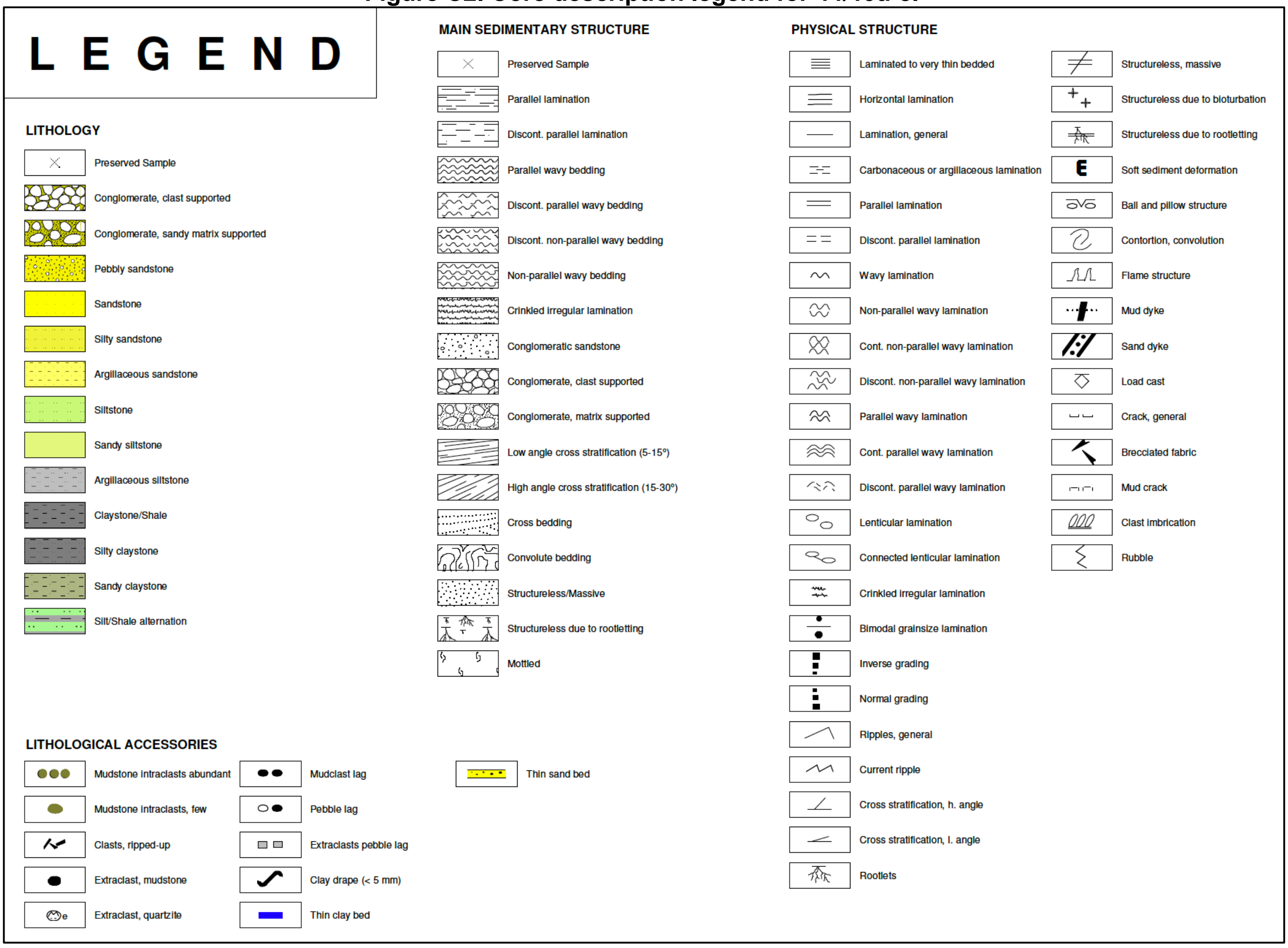

Figure C3. Core description legend for 44/23-9.

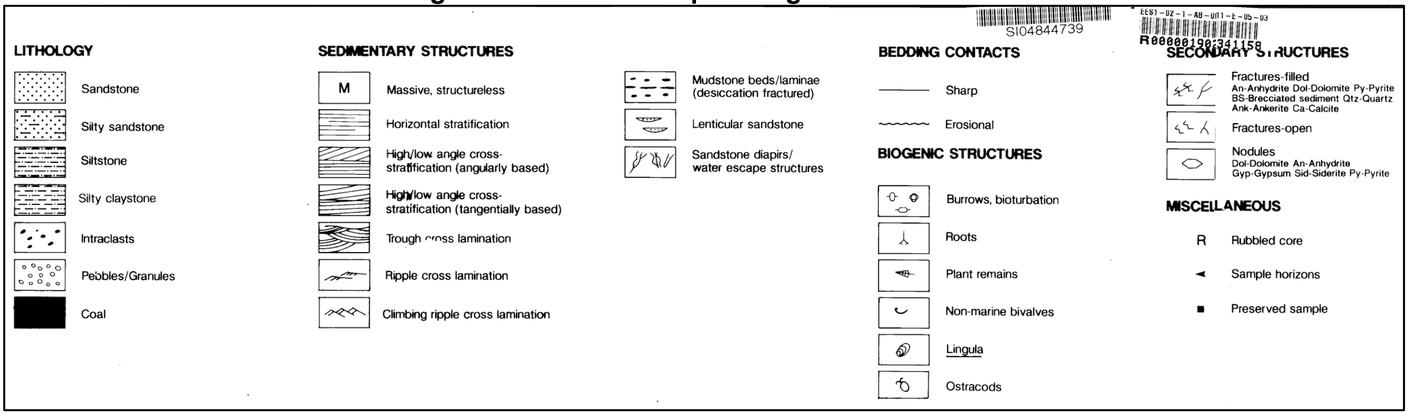

Figure C4. Core description legend for 44/24-4.

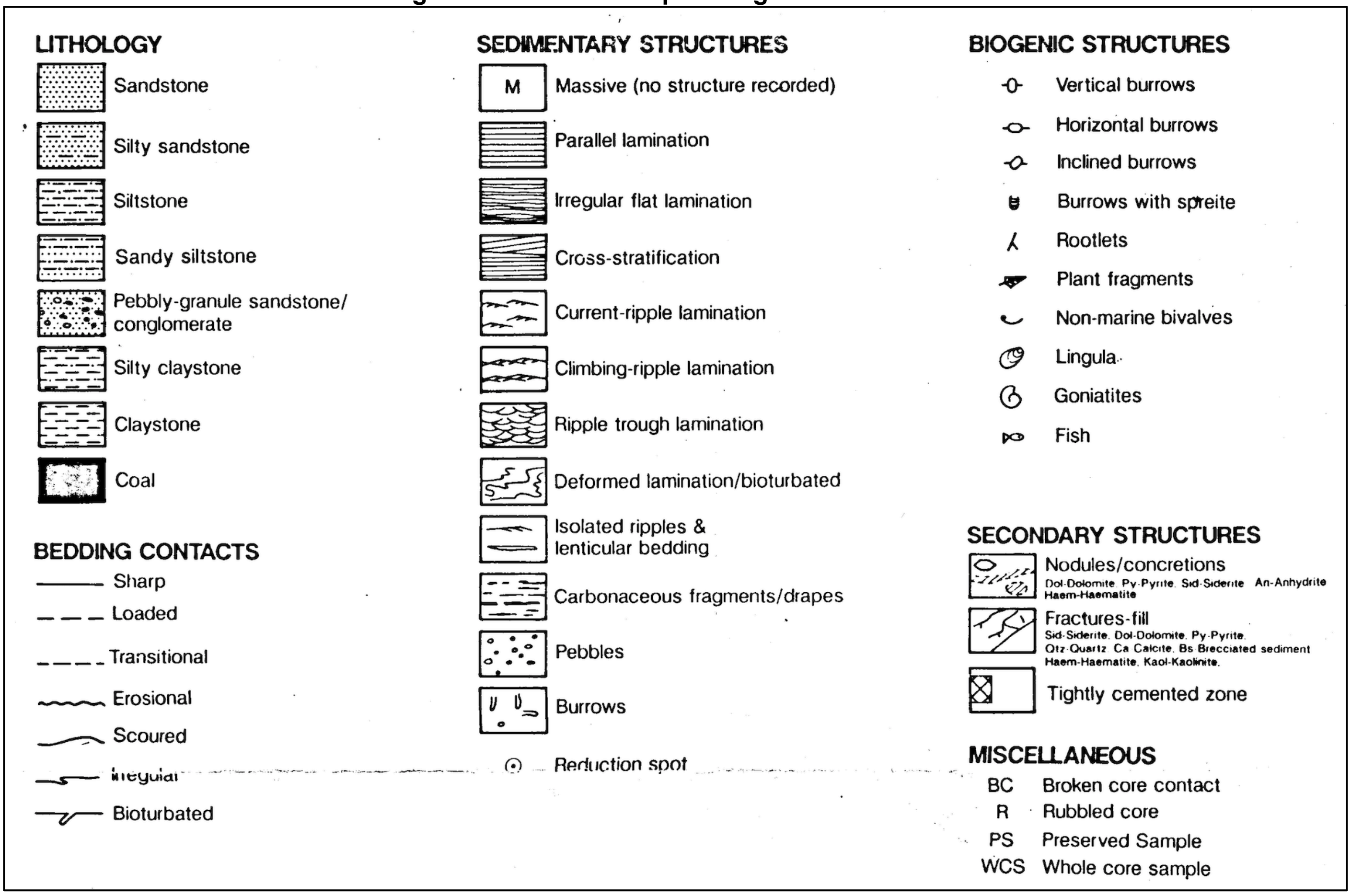

Figure C5. Core description legend for 44/27-1.

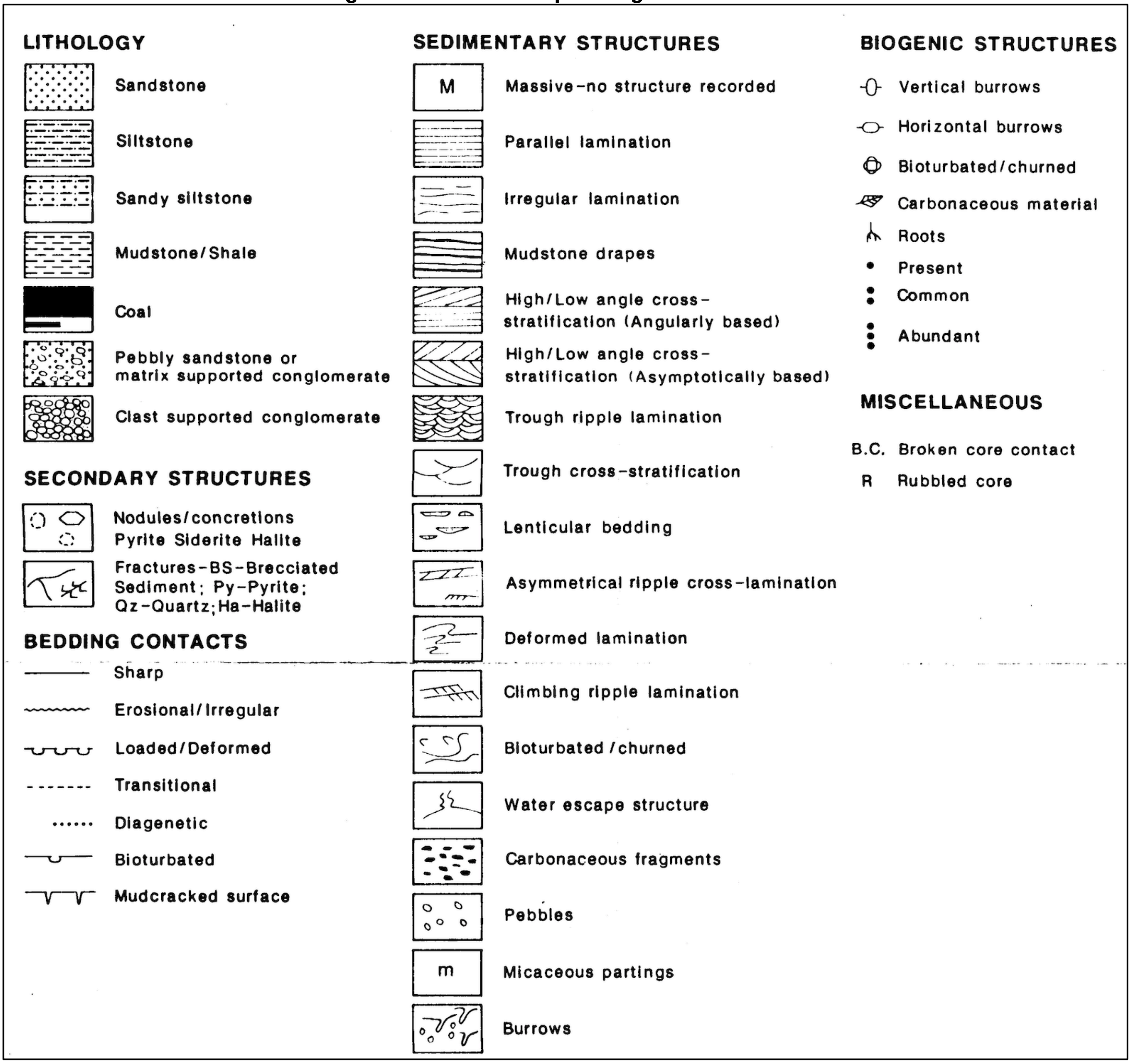

Figure C6. Core description legend for 49/1-3.

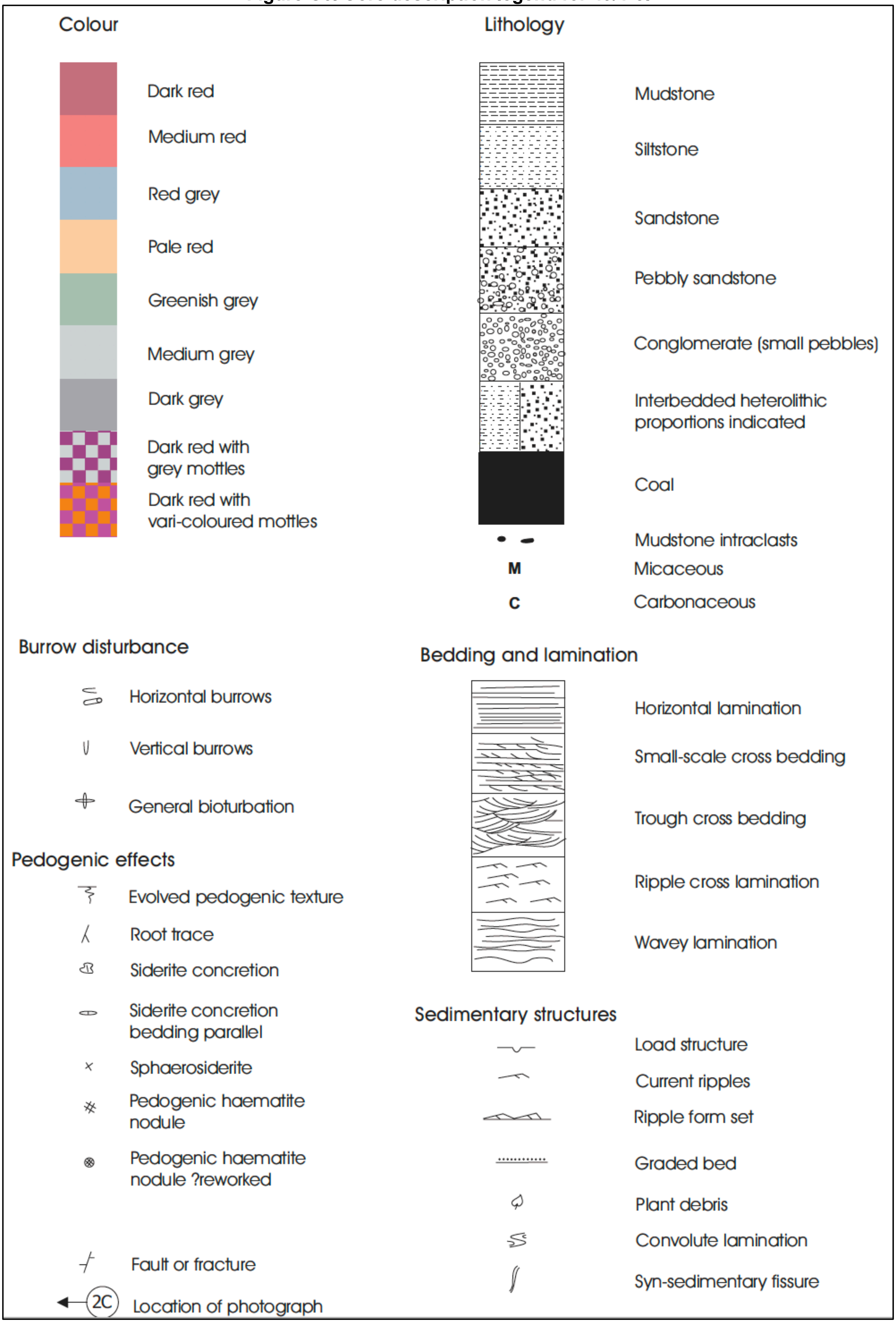

Figure C7. Core description legend for E10-3 and D15-FA101.

LITHOLOGY

SANDSTONE	SILTSTONE	CLAY/MUDSTONE/SHALE	organic clayst
silty sandst	sandy siltst	silty clayst	COAL
argil sandst	argil siltst	sandy clayst	pebbly sandst

CONTACTS

Scoured	Bioturbated	Undulating	Inclined

PHYSICAL STRUCTURES

rc current ripple	lp parallel lamination	wp parallel wavy lamination
dc contortion, convolution	d soft sediment deformation, general	ves scour
dl load cast	lndo discont. non-par. carbon. (organic matter) lamin.	lo carbonaceous (organic)
w wavy lamination	wn non-parallel wavy lamination	glpi mudclast lag
glpe extraclasts pebble lag	xl low angle cross-stratification (5-15˚)	xlr low angle internally rippled x-strat (5-15˚)
xh high-angle cross-stratification (15-30˚)	m structureless/massive, general	mr structureless due to rootletting
dd dish (and pillar) structure	di injection structure	dr syn-sedimentary (micro) fracture
vcb brecciated fabric	vd clay drape	or rootlets
xt tangential cross-bedding		

LITHOLOGIC ACCESSORIES

Gimu rip up clasts	Ggmc mica grain	Ggps pisoid
Gi intraclast, general	Gim mudstone intraclast	Gis sandstone intraclast
Geq quartzite extraclast	Ges sandstone extraclast	Gimr rounded mud intraclast

ICHNOFOSSILS

i ichnofossil/burow, general

FRACTURES

Dfsn normal shear fracture

DIAGENESIS

An nodule/concretion, general	Anan anhydrite concretion	Ando dolomite concretion
Anhe hematite concretion	Ansd siderite concretion	Amhe hematite cement
Amsd siderite cement		

Appendix D: Core Validation Plots

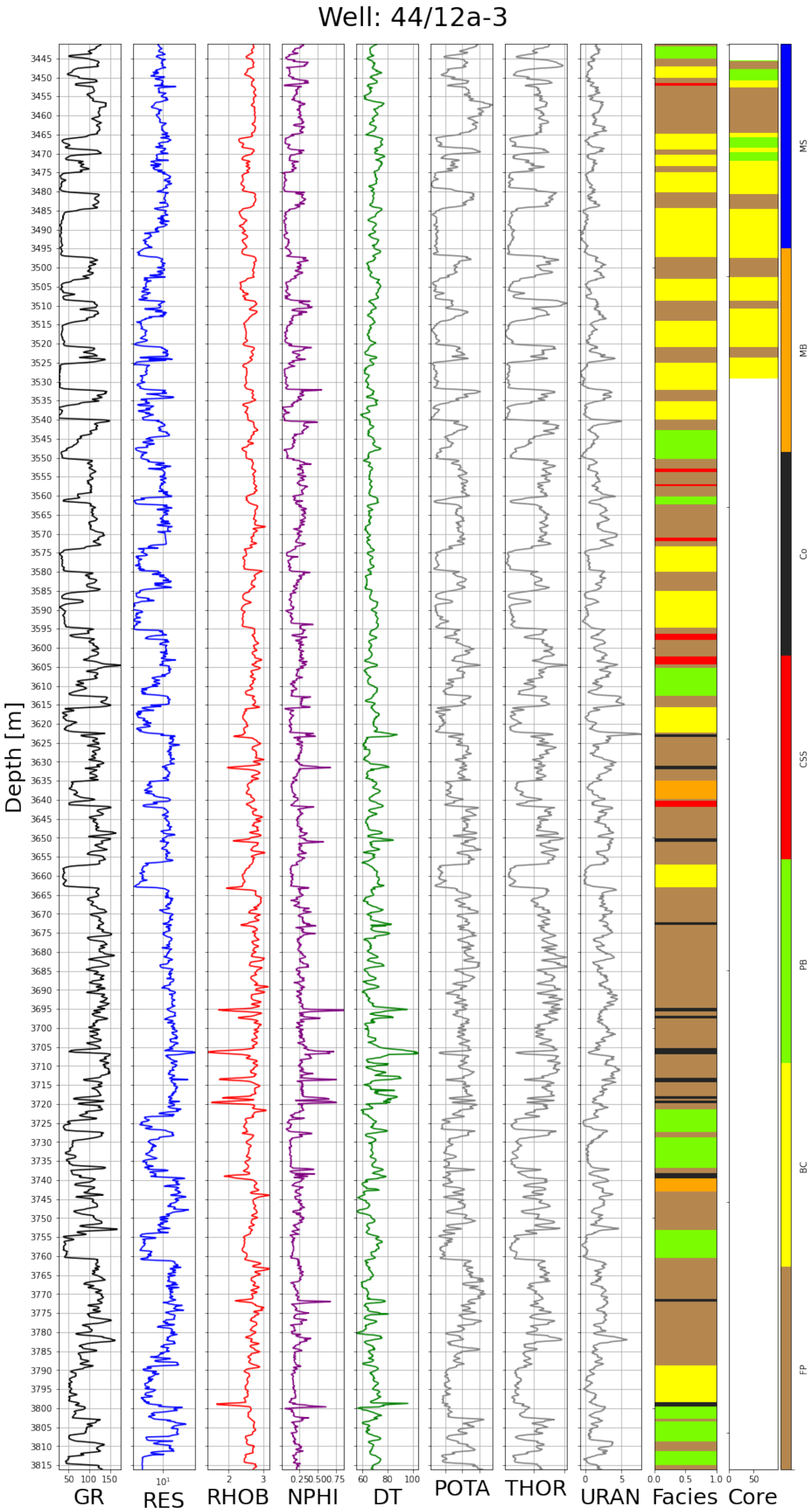

Figure 1D. Wireline logs, wireline facies associations and core for well 44/12a-3.

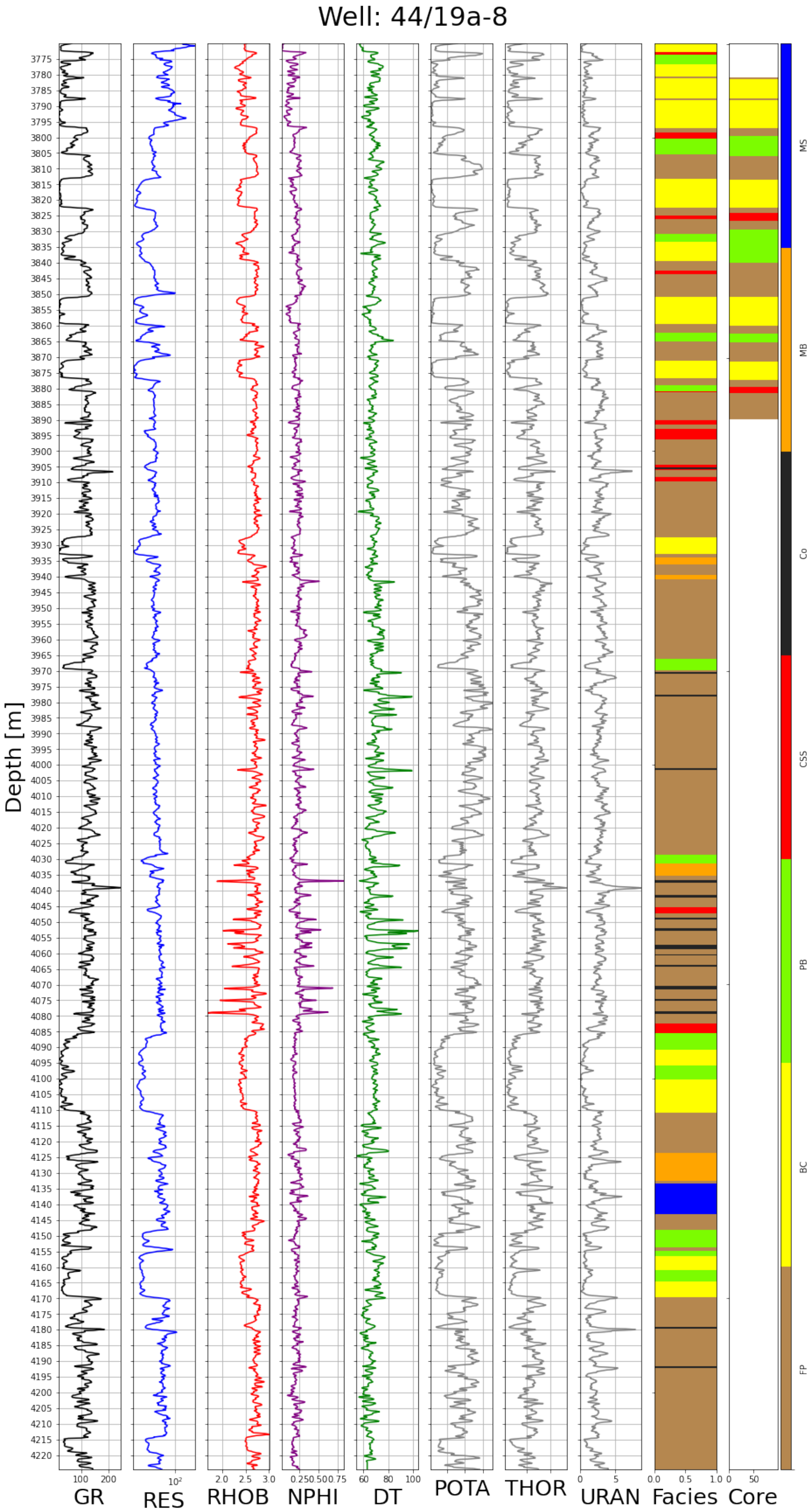

Figure 2D. Wireline logs, wireline facies associations and core for well 44/19a-8.

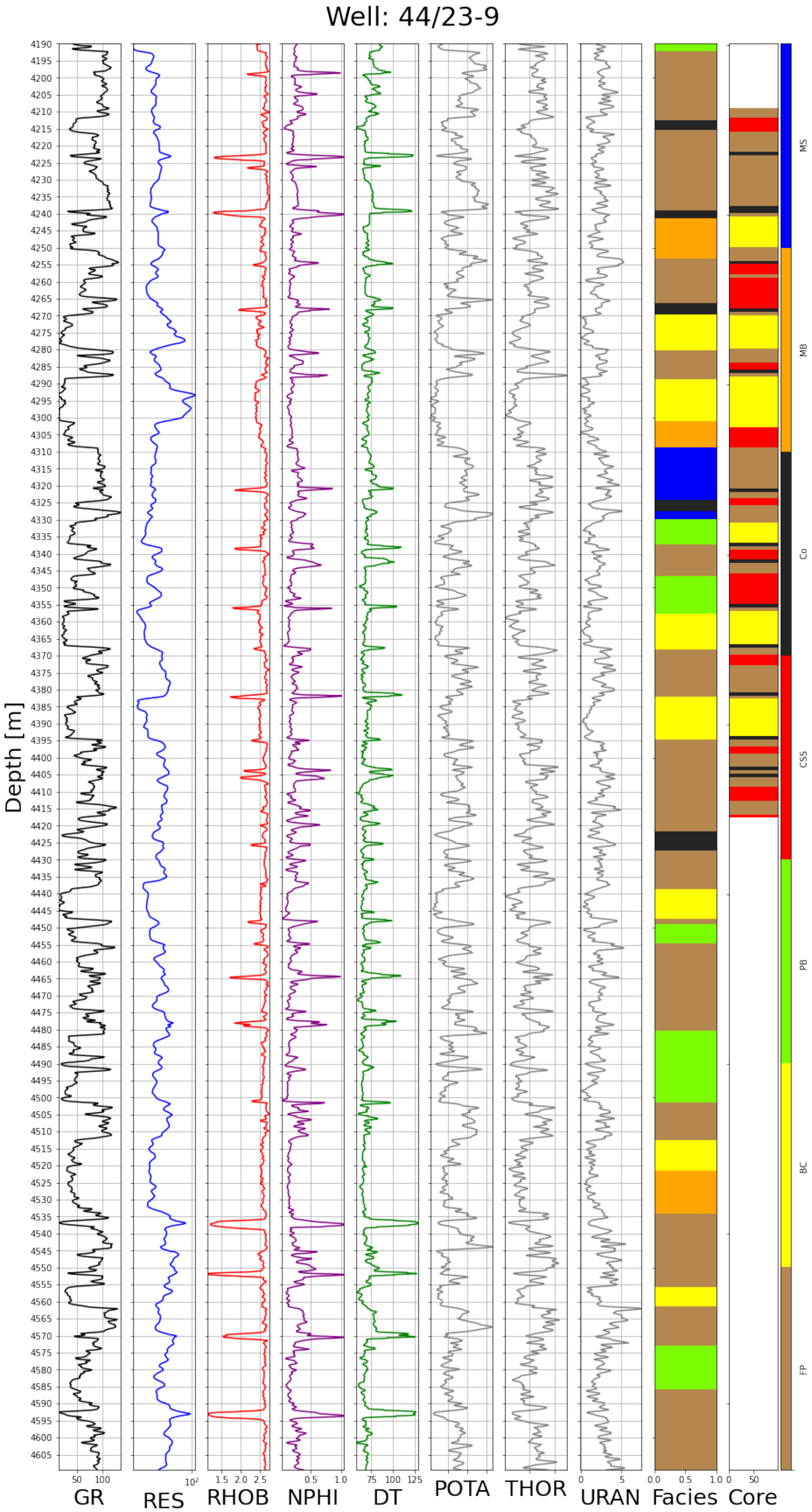

Figure 3D. Wireline logs, wireline facies associations and core for well 44/23-9.

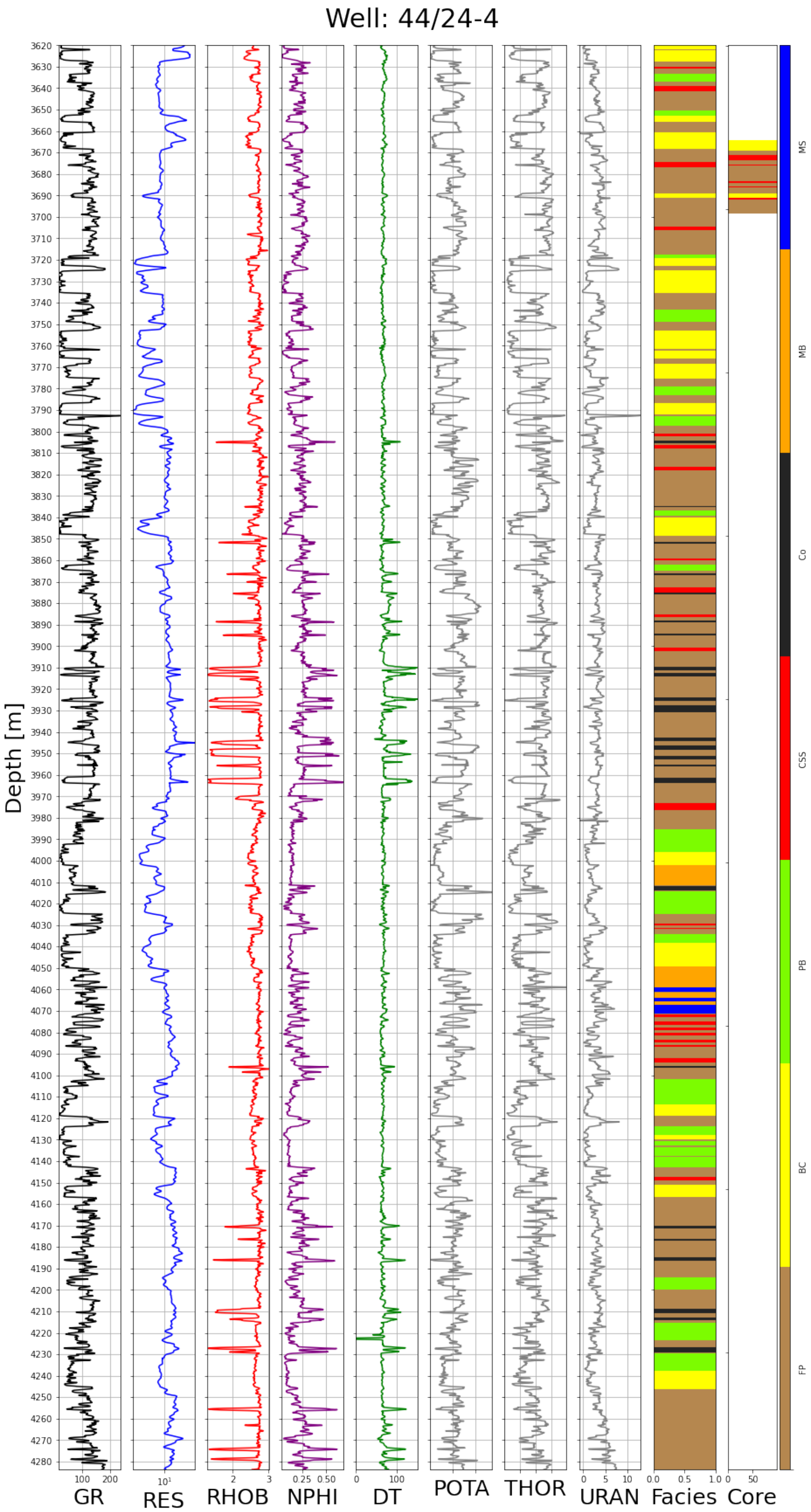

Figure 4D. Wireline logs, wireline facies associations and core for well 44/24-4.

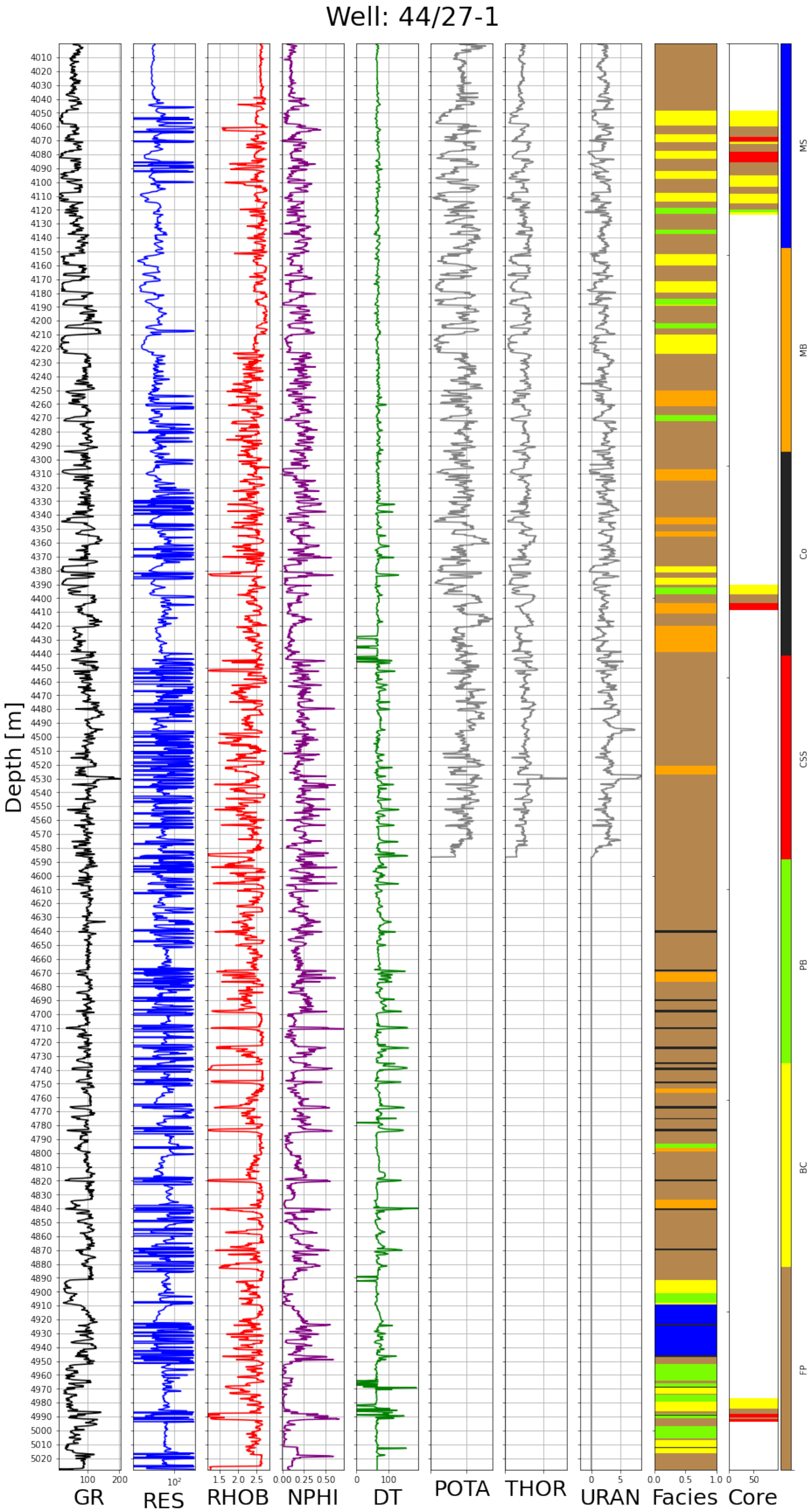

Figure 5D. Wireline logs, wireline facies associations and core for well 44/27-1.

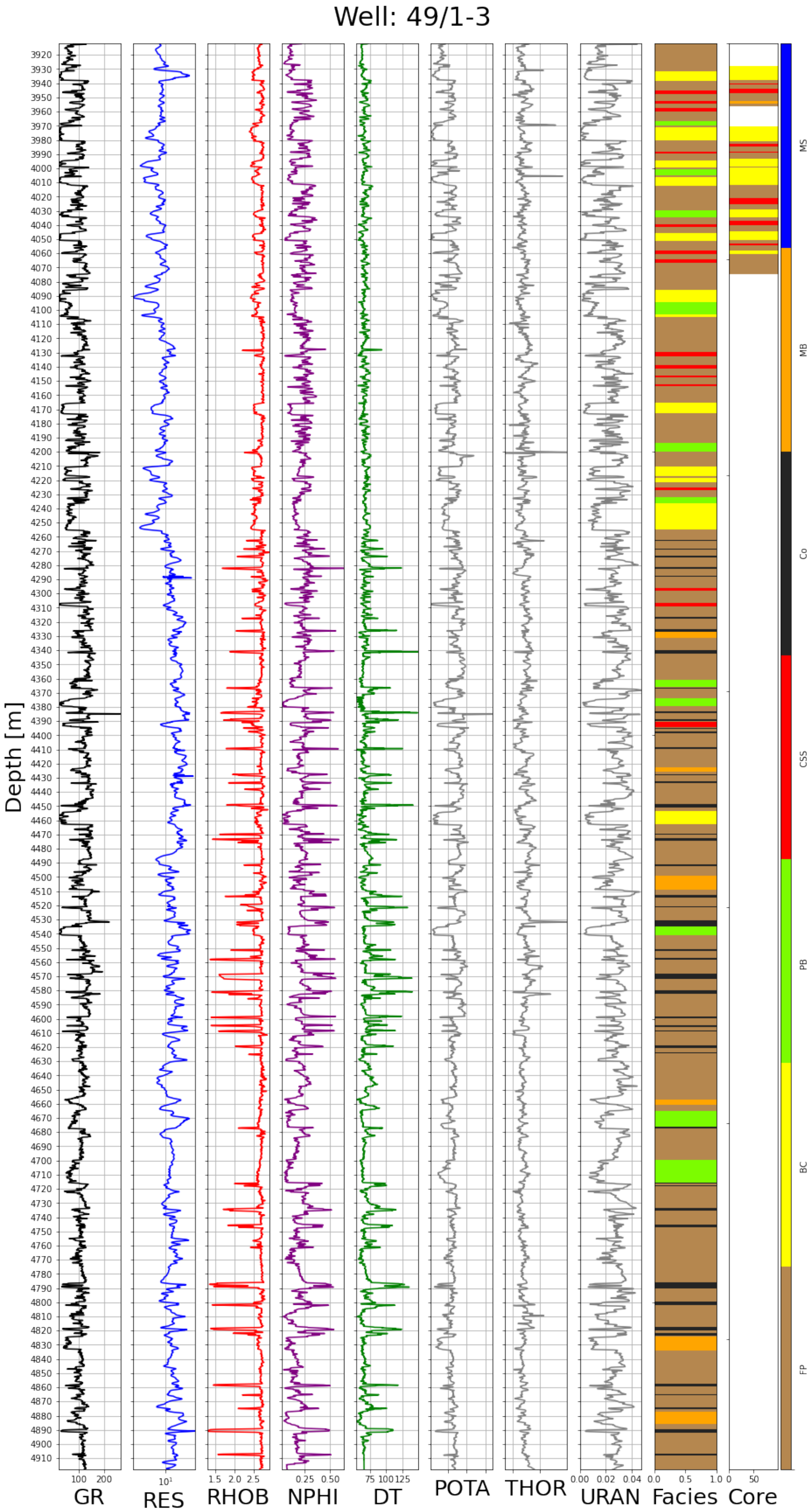

Figure 6D. Wireline logs, wireline facies associations and core for well 49/1-3.

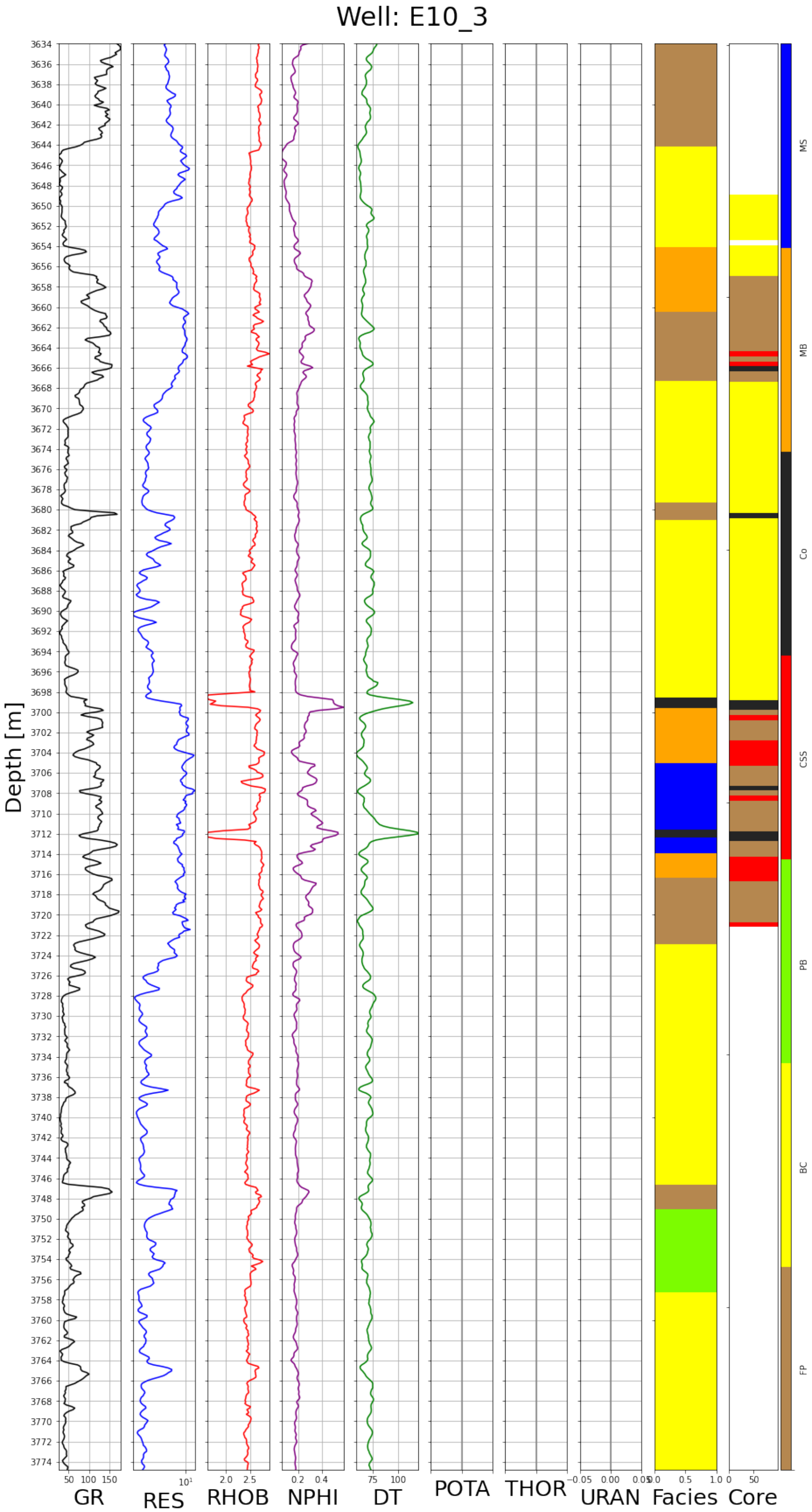

Figure 7D. Wireline logs, wireline facies associations and core for well E10-3.

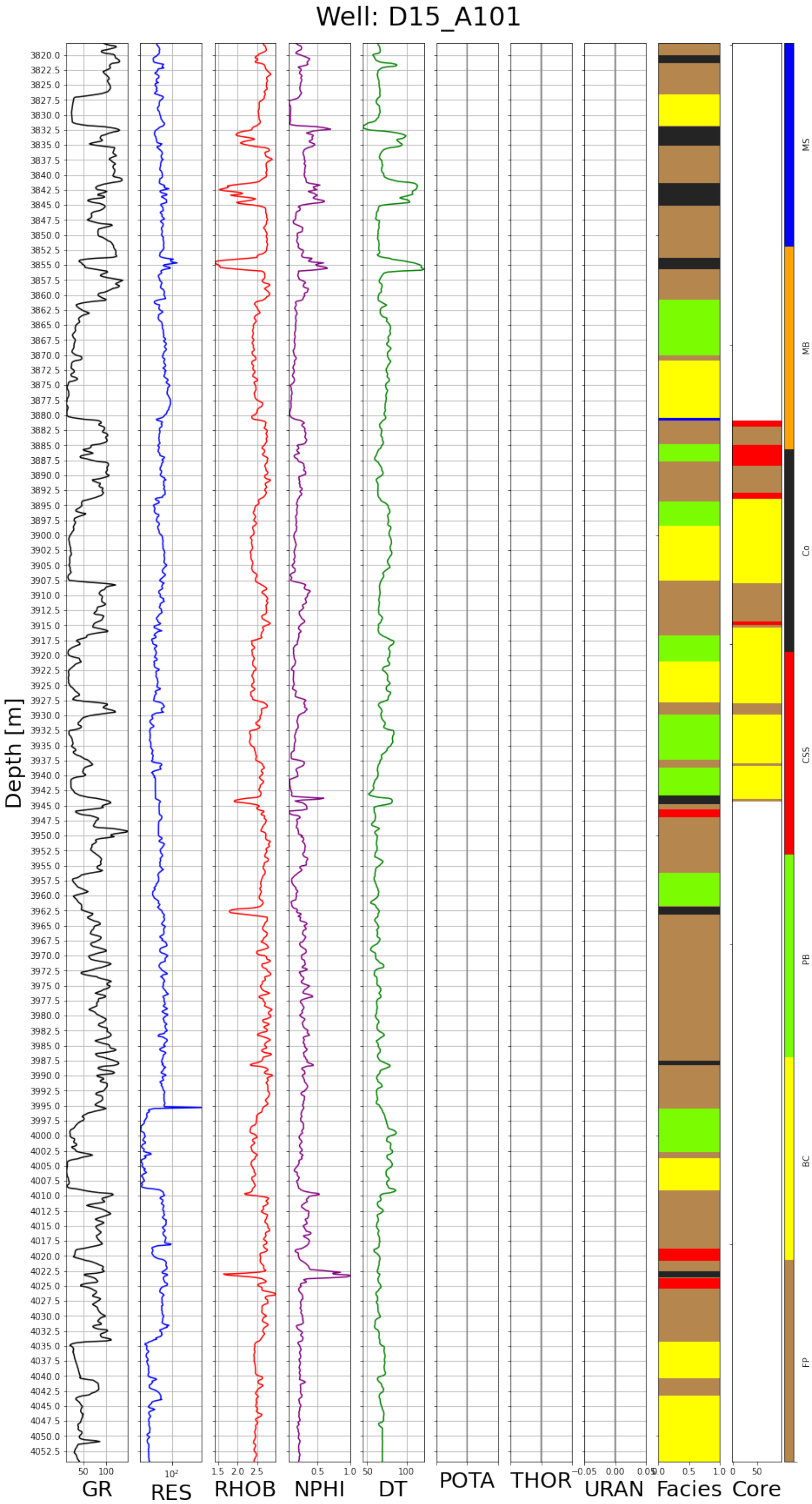

Figure 8D. Wireline logs, wireline facies associations and core for well D15-A101.

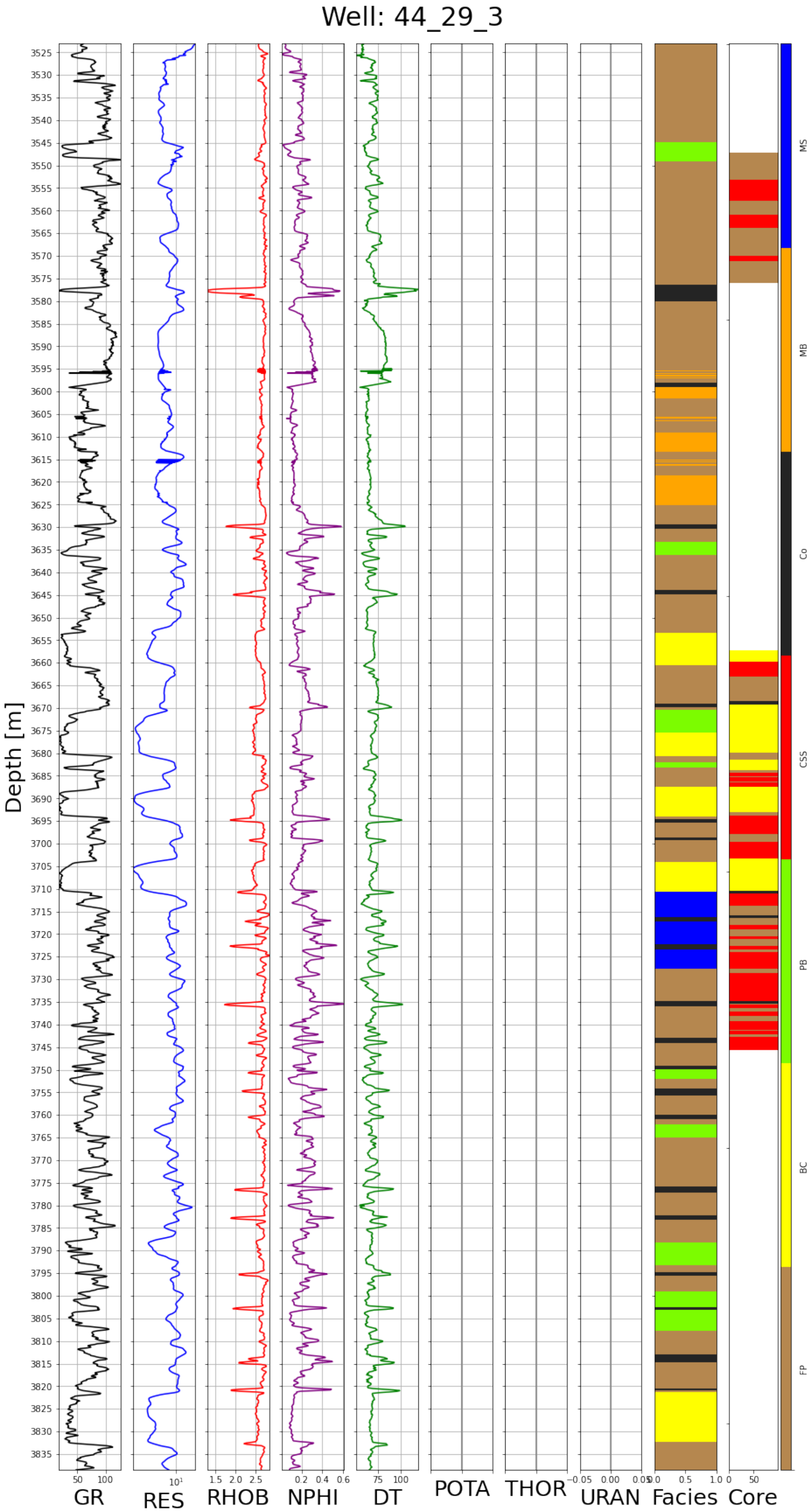

Figure 9D. Wireline logs, wireline facies associations and core for well 44/29-3.

Appendix E: Confusion Matrices

Table E1. Confusion matrix of SVM blind test on well 44/19a-8 after Yeo-Johnson power transformation.

Prediction / True	FP	BC	PB	CSS	Co	MB	MS	Total
Background Floodplain (FP)	1748	27	13		14			1802
Braided Channel (BC)	44	471	17		7			539
Point Bar (PB)	68	175	37					280
Crevasse Splay Sands (CSS)	96	1	13					110
Coal (Co)	57		2		19			78
Mouth Bar (MB)	83	2	22		3			110
Marine Shale (MS)	64							64
Precision	0.81	0.70	0.36	0.00	0.44	0.00	0.00	0.66
Recall	0.97	0.87	0.13	0.00	0.24	0.00	0.00	0.76
F1	0.88	0.78	0.19	0.00	0.31	0.00	0.00	0.70

Table E2. Confusion matrix of SVM blind test on well 44/19a-8 after quantile transformation (uniform PDF).

Prediction / True	FP	BC	PB	CSS	Co	MB	MS	Total
Background Floodplain (FP)	1747	3	37		15			1802
Braided Channel (BC)	28	467	25		19			539
Point Bar (PB)	65	106	108		1			280
Crevasse Splay Sands (CSS)	91		19					110
Coal (Co)	49		2		27			78
Mouth Bar (MB)	84		24		2			110
Marine Shale (MS)	64							64
Precision	0.82	0.81	0.50	0.00	0.42	0.00	0.00	0.7
Recall	0.97	0.87	0.39	0.00	0.35	0.00	0.00	0.79
F1	0.89	0.84	0.44	0.00	0.38	0.00	0.00	0.74

Table E3. Confusion matrix of MLP blind test on well 44/19a-8 after Yeo-Johnson power transformation.

Prediction / True	FP	BC	PB	CSS	Co	MB	MS	Total
Background Floodplain (FP)	1741	22	18		21			1802
Braided Channel (BC)	18	506	13		2			539
Point Bar (PB)	69	178	32		1			280
Crevasse Splay Sands (CSS)	99		11					110
Coal (Co)	40		4		34			78
Mouth Bar (MB)	86	4	18		2			110
Marine Shale (MS)	64							64
Precision	0.82	0.71	0.33	0.00	0.57	0.00	0.00	0.67
Recall	0.97	0.94	0.11	0.00	0.44	0.00	0.00	0.78
F1	0.89	0.81	0.17	0.00	0.49	0.00	0.00	0.71

Table E4. Confusion matrix of MLP blind test on well 44/19a-8 after quantile transformation (uniform PDF).

Prediction / True	FP	BC	PB	CSS	Co	MB	MS	Total
Background Floodplain (FP)	1752	18	21		11			1802
Braided Channel (BC)	31	478	20		10			539
Point Bar (PB)	89	114	75		2			280
Crevasse Splay Sands (CSS)	97		13					110
Coal (Co)	50		4		24			78
Mouth Bar (MB)	90	4	16					110
Marine Shale (MS)	64							64
Precision	0.81	0.78	0.50	0.00	0.51	0.00	0.00	0.69
Recall	0.97	0.89	0.27	0.00	0.31	0.00	0.00	0.78
F1	0.88	0.83	0.35	0.00	0.38	0.00	0.00	0.73

Table E5. Confusion matrix of RNN blind test on well 44/19a-8 after Yeo-Johnson power transformation.

True \ Prediction	FP	BC	PB	CSS	Co	MB	MS	Total
Background Floodplain (FP)	1737	24	24		15		2	1802
Braided Channel (BC)	16	501	9		13			539
Point Bar (PB)	49	149	79		2	1		280
Crevasse Splay Sands (CSS)	89	1	19				1	110
Coal (Co)	45	1	2		30			78
Mouth Bar (MB)	80	6	23		1			110
Marine Shale (MS)	64							64
Precision	0.84	0.74	0.51	0.00	0.49	0.00	0.00	0.70
Recall	0.96	0.93	0.28	0.00	0.39	0.00	0.00	0.79
F1	0.90	0.82	0.36	0.00	0.43	0.00	0.00	0.73

Table E6. Confusion matrix of RNN blind test on well 44/19a-8 after quantile transformation (uniform PDF).

True \ Prediction	FP	BC	PB	CSS	Co	MB	MS	Total
Background Floodplain (FP)	1743	2	41		16			1802
Braided Channel (BC)	21	460	46		12			539
Point Bar (PB)	54	63	161		2			280
Crevasse Splay Sands (CSS)	94		16					110
Coal (Co)	44		3		31			78
Mouth Bar (MB)	84		26					110
Marine Shale (MS)	64							64
Precision	0.83	0.88	0.55	0.00	0.51	0.00	0.00	0.72
Recall	0.97	0.85	0.58	0.00	0.4	0.00	0.00	0.8
F1	0.89	0.87	0.56	0.00	0.45	0.00	0.00	0.76